

AD-A070 633

INSTITUTE FOR ACOUSTICAL RESEARCH MIAMI FLA  
SEISMIC LOCALIZATION OF HOSTILE ARTILLERY.(U)  
JUL 78 D C FLETCHER, X ZABALGOGEAZCOA

F/G 17/10

UNCLASSIFIED

IAR-78002

N00014-77-C-0446

NL

1 OF 2  
AD  
A070633





MICROCOPY RESOLUTION TEST CHART  
NATIONAL BUREAU OF STANDARDS-1963-A



DA070633

DDC FILE COPY

LEVEL

18.51

**INSTITUTE FOR ACOUSTICAL RESEARCH**  
**MIAMI DIVISION PALISADES GEOPHYSICAL INSTITUTE**

**FINAL REPORT**

**SEISMIC LOCALIZATION OF HOSTILE ARTILLERY**

Dr. D.C. Fletcher  
Mr. Xavier Zabalgogezcoa  
Dr. James Dorman

DDC  
JUN 28 1979  
C

IAR 78002

This document has been approved  
for public release and sale; its  
distribution is unlimited.

**Miami, Florida 33130**

79 06 21 050

Institute for Acoustical Research  
Miami Div., Palisades Geophysical Institute  
615 S.W. 2nd Avenue  
Miami, Fla. 33130

⑨  
FINAL REPORT

⑥  
SEISMIC LOCALIZATION OF HOSTILE ARTILLERY

⑩  
Dr. D.C. Fletcher,  
Mr. Xavier Labalgogea  
Dr. James Dorman

DDC  
RECEIVED  
JUN 28 1979  
C

⑮  
N00014-77-C-0446

1473

⑭  
IAR-78002

This document has been approved  
for public release and sale; its  
distribution is unlimited.

⑪  
Jul 1978

⑫ 137p.

408141

79 06 21 050



## Abstract

↓ This report comprises the final statement regarding some initial exploratory research done by the Institute for Acoustical Research (IAR) on the Hostile Artillery Location (HAL) project. The objective of this research was to re-examine experimental data collected by Honeywell, Inc. and the Environmental Research Institute of Michigan (ERIM) during December 1975. The data collected comprised a series of digital tapes recording the response of a seismometer array to the firing of various howitzers at various ranges.

IAR's analysis of this data, though not considered technically complete, nevertheless is considered very successful at least with respect to bearing estimates at 5 km. The composite IAR estimate on three firings is within a few hundredths degree of true and the standard deviation is  $1\frac{1}{2}$  degrees. Range estimates can be improved with a larger array and a more sophisticated second stage. ←

This work was supported by the Office of Naval Research (ONR), Earth Physics Program (Code 463). The contract number is N00014-77-C-0446. *W*

## Section I

### Introduction

This report comprises the final statement regarding some initial exploratory research done by the Institute for Acoustical Research (IAR) on the Hostile Artillery Location (HAL) project. The objective of this research was to re-examine experimental data collected by Honeywell, Inc. and the Environmental Research Institute of Michigan (ERIM) during December 1975. The data collected comprised a series of digital tapes recording the response of a seismometer array to the firing of various howitzers at various ranges.

IAR's analysis of this data, though not considered technically complete, nevertheless is considered very successful at least with respect to bearing estimates at 5 km. The composite IAR estimate on three firings is within a few hundredths degree of true and the standard deviation is  $1\frac{1}{2}$  degrees. Range estimates can be improved with a larger array and a more sophisticated second stage.

Study of the 5 km events has led IAR to devise a processing scheme which is believed will be successful at 11 km and possibly at 17 km. The scheme has not yet been implemented.



The processing employed on the 5 km events is treated in great detail in sections II and IV. Section III supplies necessary background on the ERIM experiment. Processing to date on the 11 km events is presented in section V. Section VI gives the improved processing to be implemented on the long range events. Finally there are a series of Appendices giving necessary derivations and technical background to support the text.

This work was supported by the Office of Naval Research (ONR), Earth Physics Program (Code 463). The contract number is N00014-77-C-0446.

## Section II

### BASIC PROCESSING

This Section presents a brief though precise discussion of the mathematical procedure by which IAR has processed the Honeywell ERIM data. The mathematics is deliberately simple for this first approach to the problem and much has been learned to prepare the way for later studies. In particular, the approach to date has been to regard the Haar transform as a detector of local nonstationary behavior, and this seems valid. However, it has been noted as a result of these studies, that its success stems from its ability to whiten the background. The Haar transform is a fixed (in time) linear operator and thus works best on stationary or quasi stationary data. At great range, however, the S/N ratio is small enough that a detection system must contend as well with non stationary ambient noise; therefore, recently IAR has begun to focus on generalizations of the Haar transform which adapt to non stationarities in the background and still whiten them relative to the "signal". This broad class of operators are the adaptive autoregressive operators and they show great promise. As an example, the Haar transform detects a low frequency transient on 7 phones of event 39 at 11 km. This detection is sharpened by these operators. This processing is described in Section V.

The implemented IAR detection scheme is conceptually divided into two stages. Stage one obtains a set of arrival times of transients, and stage two processes these to determine whether they comprise a signal, and if so where did



it originate.

Explicitly the stages are as follows:

### First Stage

At a particular geophone, a time series  $x(t)$  is measured. It is then lowpass filtered (anti-alias) at some frequency  $F$  and sampled appropriately ( $\Delta t \leq \frac{1}{2F}$ )

Let the samples be denoted as:

$$x(n) = x_F(n\Delta t)$$

The discrete sequence  $x(n)$  is organized into blocks of length  $N$  (a power of two,  $N = 2^M$ ) samples each.

Let  $x(n): n = 0, \dots, N-1$  denote such a block, and let  $\hat{x}_m(k)$  denote its  $k^{\text{th}}$  Haar coefficient for some sequency group  $m$ :

$$\hat{x}_m(k) = \frac{1}{N} \sum_{n=0}^{N-1} x(n) H_m(k, \frac{n\Delta t}{N}) \quad \begin{matrix} k=0, \dots, 2^m-1 \\ m=0, \dots, M-1 \end{matrix}$$

where

$$H_m(k, t) = \begin{cases} H_0(0, t) = 1 & 0 \leq \frac{t}{T} \leq 1 \\ H_m(k, t) = \sqrt{2^m} & \frac{k}{2^m} \leq \frac{t}{T} \leq \frac{k+1/2}{2^m} \\ H_m(k, t) = -\sqrt{2^m} & \frac{k+1/2}{2^m} < \frac{t}{T} \leq \frac{k+1}{2^m} \\ = 0 & \text{elsewhere} \end{cases}$$

$$\text{and } k=0, \dots, 2^m-1$$

$$m=1, \dots, M-1$$

$$T = N\Delta t$$

The original sequence can be retrieved from the transform coefficients as

$$X_n = \sum_{m=0}^{M-1} \sum_{k=0}^{2^m-1} \hat{X}_m(k)$$

The Haar functions  $H_m(k, t)$  form an orthogonal set of functions:

$$\int_0^1 H_m(k, t) H_n(l, t) dt = \delta_{mn} \delta_{kl}$$

It is seen that the Haar transform (for  $n \neq 0$ ,  $k \neq 0$ ) effectively forms the difference between the pair of two mean values computed over adjacent subregions of the data block. Each local mean is computed over  $N/2^n$  samples. Consequently, each Haar coefficient (differenced local mean) is affiliated with a data sub-block whose center is located at time  $t = n\Delta t = T \cdot \frac{k+1/2}{2^m}$ . The index  $k$  is therefore, effectively, a decimated time index. For  $m = 0$  the value of the single Haar coefficient is the mean value of the time series.

The Haar transform therefore provides a way to examine the change in the mean value of a time series. Note, as well, that if the time series is squared before being transformed, then the coefficients of the transform will represent changes in the second moment of the original series. These operations could be done by other means, but an advantage of the Haar transform is that there exists a fast computer algorithm for the computation of the coefficients, based



upon the factorability of the matrix  $H_m(k, t)$ . For sequences of length 1024 pts the Haar transform is roughly 35 times faster than the FFT. Even greater speed advantage is attained if the digital computer utilized does not have floating pt. hardware, or if the sequences are longer.

If the input sequence is a sample of a stationary time series which is independently normally distributed with known parameters  $N(\mu, \sigma^2)$  then the Haar coefficients  $x_m(k)$  will be independent, normally distributed as  $N(0, \frac{\sigma^2}{2^{m+1}})$ . If the variance is unknown the Haar coefficients, normalized by the sample standard deviation, will be t-distributed with degrees of freedom  $\nu = \frac{2^{m+1}}{N} - 1$ .

We assume that the ambient seismological noise series is stationary so that the mean is constant. The above described t-statistic will then fluctuate about zero. Significant departures from zero will then be correlated with local non stationarity in some sequency group.

(Recall that there is a time dependent t-variable for each sequency group). We define such significant excursions of the t variable as designating the reception of a "transient" wave form within the data sub-block affiliated with the corresponding Haar coefficient. If the Haar coefficient is given by  $x_m(k^*)$ , then the sub-block is the one of length  $2N/2^m$  centered at  $t = \frac{R^* + 1/2}{2^m} T$ . We refer to this data sub-block as a "contender segment".

Let us now suppose that the above procedure has been carried out on all geophone channels. (Note that if a rough bearing estimate is known, the data on the horizontal geophone channels should be rotated to this bearing. This procedure allows approximate separation of the data into components transverse, longitudinal, and vertical to the incoming wave front, and thereby facilitates separation into Love and Rayleigh wave components).

We further suppose that transients are detected on several phones within some time window. That is, let  $\tau$  denote a maximum expected travel time across the array

$$\tau \approx A/c_{\min}$$

where  $A$  is the array aperture and  $c_{\min}$  is the minimum expected seismic wave group speed. And let  $T_i$  denote the center time of the contender segment on the  $i^{\text{th}}$  geophone. (These times should be drawn from channels of the same type).

We assume the times are within the window; that is:

$$\text{Let } T_{\max} = \max (T_i)$$

$$T_{\min} = \min (T_i)$$

$$\text{then } T_{\max} - T_{\min} < \tau$$

In this case, we further analyze this set of contender segments to determine whether a signal is present. Roughly speaking, a signal is present provided the relative times



between the transients allow the second stage (below) to obtain spatial positions whose covariance ellipse is small.

In order to obtain a more precise estimate of the relative times, cross correlation of the continuous Haar coefficients  $\hat{x}_m(s)$  is carried out for fixed  $m$  ( $m$  being the sequency index whose  $t$  variable indicated a transient). The variable  $s$  here indicates that the center of the Haar sub-block is varied continuously across the contender segment. This process can be visualized as Haar filtration of the contender segment (and its adjacent neighbors). Briefly then, each contender segment within the window is Haar filtered and then cross correlated with a reference segment.

Let the reference segment be chosen as the center phone of the array (this is not essential), then cross correlation of each remaining segment with this reference segment will give correlation diagrams which have a maximum at some point. Let us choose the relative time between the  $i^{\text{th}}$  phone and the central phone to be the lag value at which this maximum occurs on the  $i^{\text{th}}$  correlation diagram:

$$\max_{\tau} R_i(\tau) = R_i(T_i^*)$$

We therefore obtain relative arrival times between all phones and the central one. This procedure yields sharp

time estimates provided the correlation peak falls off sharply. The precision of this estimate is given approximately by the formula (confer Appendix A)

$$\sigma_{\Delta T} \approx \frac{1}{2.2w} (S/N)^{-1/2}$$

where  $S/N$  is the signal to noise peak power ratio and  $w$  is the bandwidth of the cross correlated signals. The bandwidth can be improved by carrying out the same procedure on higher sequency groups on the contender segment in the manner of a "protected t-test".

On the 5 km ERIM data, the  $S/N$  ratio is roughly 16 and the bandwidth  $w \approx 4$  Hz. This formula indicates that  $\sigma_{\Delta T} \approx .01$ , which is consistent with the result  $\Delta \phi \approx 2.5^\circ$  obtained from the second stage. If the relative arrival times are obtained by a procedure utilizing jointly all phones in the array (rather than pair wise as here) this precision can be expected to improve as the square root of the number of phones in array.



### Second Stage

A set of relative arrival times has been obtained by the first stage, and these times are now processed by the second stage to determine if they jointly indicate that their respective transients all came from the same location in space. The criterion as to whether this is, in fact, the case is given by the area of the  $x,y$  confidence ellipse. The definition of the  $x,y$  confidence ellipse is that elliptic contour within which we can be 95% certain that the transient wave front originated.

The equations that follow explicitly state how the  $x,y$  position is obtained from the relative arrival times, and how the confidence ellipse is determined. Also presented is the statistical means by which the various geophone channels are combined to obtain estimates which are more precise. The times  $T_i$  below are those obtained by the cross correlation procedure of the first stage. Note that the time  $T_i$  to the reference phone is zero.

The fundamental physical model is extremely simple, but is successful on the 5 km events. The program is not in any way committed to these equations and they will be made more sophisticated including, for example, dispersion and inhomogeneity.

As depicted in Fig. 2.1, suppose a source firing at time  $T$  is located at position  $x,y$ , and its seismic wave is received at times  $T_i: i = 1, \dots, N$ . Let the ranges to these sensors be denoted by  $r_i: i = 1, \dots, N$ . Then to first order (assuming straight line travel), we have the following equations:

$$T_i = T + \frac{1}{v} \left[ (x_i - x)^2 + (y_i - y)^2 \right]^{\frac{1}{2}}$$

These comprise  $n$  equations in 4 unknowns  $(x, y, t, v)$ , and if  $N = 4$  they can be solved exactly. However, the arrival times in fact contain random noise perturbations which will therefore introduce error into the solution. Consequently, many observations are made and the solution which maximizes the likelihood function is chosen.

The model thus becomes:

$$T_i = T + \frac{1}{v} \left[ (x_i - x)^2 + (y_i - y)^2 \right]^{\frac{1}{2}} + \epsilon_i$$

where the Gaussian random process  $\epsilon$  has zero mean and known covariance matrix  $\Lambda_{\epsilon}$ .

We choose  $x, y, T, v$  to minimize the form

$$Q(x, y, T, v) = \sum_{i,j}^N (T_i - h_i) \left[ \Lambda_{\epsilon}^{-1} \right]_{ij} (T_j - h_j)$$

where

$$h_i = T + \frac{1}{v} \left[ (x_i - x)^2 + (y_i - y)^2 \right]^{\frac{1}{2}} \quad i = 1, \dots, N$$

$\Lambda_{\epsilon}^{-1}$  denotes the inverse of  $\Lambda_{\epsilon}$

We now let:  $\underline{x} = (x, y, T, v)^T$

$$H_{ij}(\underline{x}) = \left. \frac{\partial h_i}{\partial x_j} \right|_{\underline{x}}$$



The normal equations for this problem become

$$-\sum_{ij}^N H_{ik} \left[ \Lambda_{\varepsilon}^{-1} \right]_{ij} (T_j - h_j) = 0 \quad k=1, \dots, 4$$

These non-linear equations are to be solved for the unknown vector  $\hat{x}$  estimating  $x$ .

The solution is obtained as the convergent limit of the Gauss-Newton iteration scheme

$$\hat{x}^{(n+1)} = \hat{x}^{(n)} + \left[ (H^T \Lambda_{\varepsilon}^{-1} H)^{-1} H^T \Lambda_{\varepsilon}^{-1} \right]_{\hat{x}^{(n)}} r^{(n)}$$

where:  $\hat{x}^{(n)}$  denotes the value of  $x$  at the  $n^{\text{th}}$  iteration

$$r^{(n)} = T - h(\hat{x}^{(n)})$$

$$T = (T_1, T_2, \dots, T_N)^T$$

$\hat{x}^{(0)}$  is an initial guess

The iterative scheme will converge for virtually any choice of  $\hat{x}^{(0)}$  to the same limit. In the program implemented the matrix  $\Lambda_{\varepsilon}$  is taken to be  $\sigma_{\text{RMS}}^2$  times the identity matrix.

$$\sigma_{\text{RMS}}^2 = \frac{N}{L} \left[ \sum_{i=1}^L \left( T_i - h_i (\hat{x}^{(n)}) \right)^2 \right]$$

The estimator  $\hat{\underline{x}}$  has a covariance matrix given by

$$\Lambda_{\hat{\underline{x}}} = (H^T \Lambda_{\epsilon}^{-1} H)^{-1}$$

The 1σ confidence ellipse about  $\hat{\underline{x}}$  is derived from this matrix.

The above method estimates a velocity which should be taken to represent the mean horizontal group velocity from the source to the array. To a great extent the method succeeds on real data because this mean velocity is a very stable physical parameter, and its value is not assumed known by the program

The equations governing the combination of observations are as follows:

Let  $\hat{\underline{x}}$  and  $\hat{\underline{y}}$  independently estimate a parameter  $\underline{g}$ . Let  $\Lambda_{\hat{\underline{x}}}$  and  $\Lambda_{\hat{\underline{y}}}$  denote their covariance matrices. Then the minimum variance unbiased composite linear estimator  $\hat{\underline{z}}$  is given by

$$\Lambda_{\hat{\underline{z}}}^{-1} \cdot \hat{\underline{z}} = \Lambda_{\hat{\underline{x}}}^{-1} \cdot \hat{\underline{x}} + \Lambda_{\hat{\underline{y}}}^{-1} \cdot \hat{\underline{y}}$$

$$\Lambda_{\hat{\underline{z}}}^{-1} = \Lambda_{\hat{\underline{x}}}^{-1} + \Lambda_{\hat{\underline{y}}}^{-1}$$



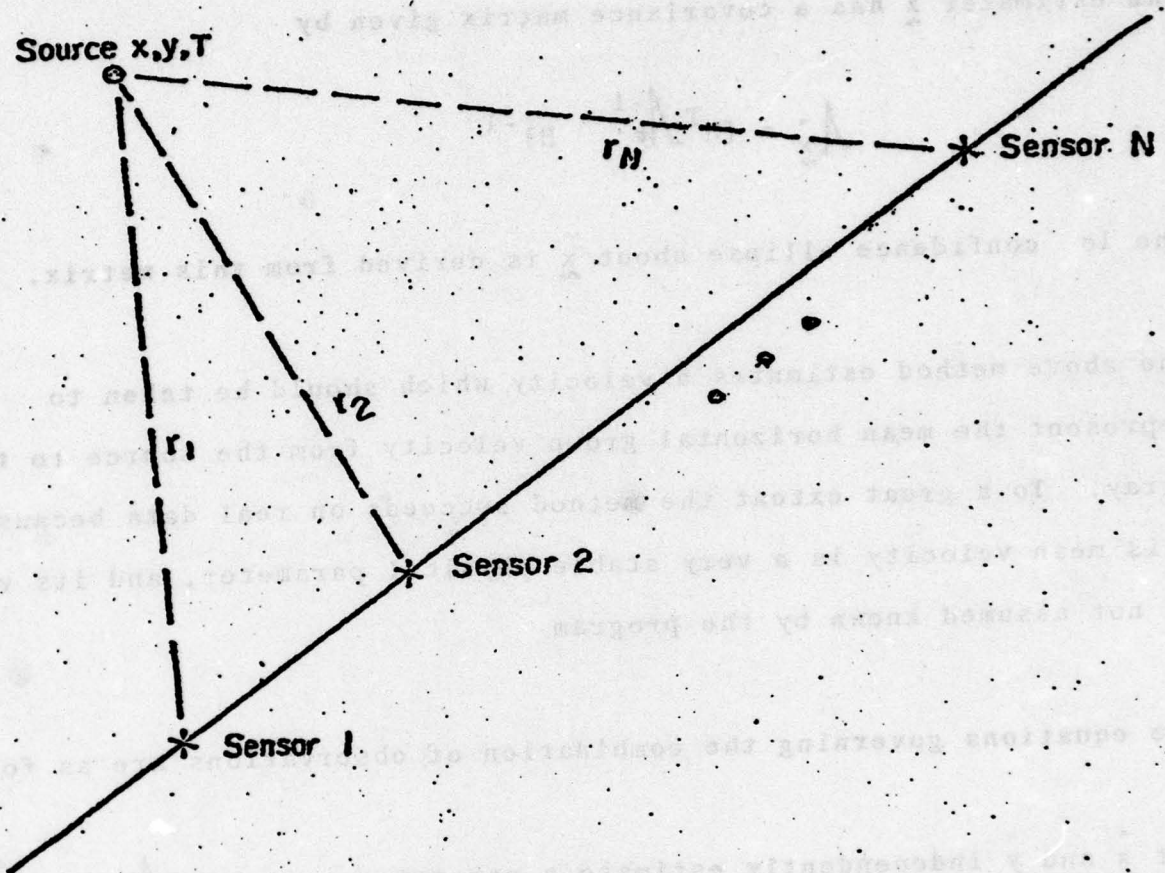


FIGURE 2.1

## SYSTEM GEOMETRY

### Section III

#### ERIM Experiment

This experiment was planned by Honeywell, Inc. and the Environmental Research Institute of Michigan (ERIM), and was carried out during December 1975. The weapon firings were done in the northwest corner of Anoka county, Minnesota, and the geophone arrays were located in Insanti and Sherbourne counties. The relative locations are depicted in Fig. 3.1.

The geology of the test region is given in Appendix C, but it is worth noting here that there were a number of frozen lakes between the firing site and the geophone arrays. There was significant snow cover, but some care was taken to ensure geophone contact with the ground.

The recording array consisted of nine 3-axis geophones arranged in a cross, as shown in Fig. 3.2. The geophone spacing along each leg of the cross was 75 meters. The legs were at right angles with the north-south leg aligned with true north. It is not known how precisely this configuration was surveyed.

The weapon was fired horizontally into a corrugated steel catcher backed by 20 feet of coarse sand between the steel and a 100 foot earth backstop. The azimuth relative to true north was  $268.5^{\circ}$  as shown in Fig. 3.1. All weapon shots were a charge 7 with a sand load.



There were a total of 88 firings. IAR has examined all 5 km recorded weapon firings, of which three were free of significant hardware problems (confer Appendix D). These 3 shots are fully discussed in section IV.

There remain 77 events consisting of forty 11 km. events and thirty-seven 17 km. events. Appendix B includes a transcription of the data logs. Regarding these events, IAR has taken the point of view that it is best to concentrate heavily on a single event at a given range until it is thoroughly understood before attempting further events at that range. Moreover it is though best to understand thoroughly the 11 km. events than to prematurely examine the 17 km. events.

There are very sound scientific and economic reasons for adopting this point of view. The scientific reasons are clear; and the economic reasons stem from the necessity to obtain computer generated plots of the raw data. This process is very time consuming, and consequently the IAR approach has been to generate these plots until an event is found which is free of hardware clipping and electronic noise. This event is then intensively studied as described above. Thereafter all other "hardware o.k." events at the same range are processed.

IAR has examined the raw data for the 17 km events 36, 37, 38 and has selected event #38 for study. The progress to

date on this event has been good. This matter is further described in section VI. The plotting of raw data for the 17 km. events was chosen to begin at event 36 because it is the first event with a 109 m.m. howitzer. This weapon was chosen by virtue of the fact that of the three processable 5 km events (#8, 9, 10), two of them were with the 109. It should be stressed again that "processable" refers only to freedom of the recording from hardware problems. Whether the 109 m.m. howitzer produces a larger seismic signal than other weapons, has not yet been examined.

Appendix B gives the correspondence between the data channel no. and the geophone - axis.

Fig. 3.1 Relative locations of recording sites and firing area (bearing angles are measured from due East)



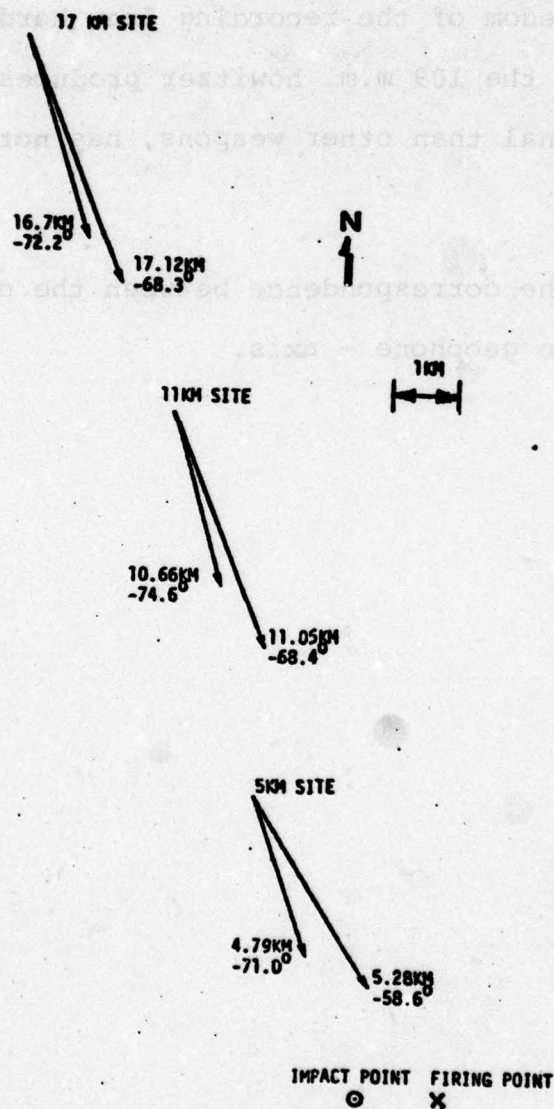


Fig. 3.1 Relative Locations of Recording Sites and Firing Area (Bearing Angles are Measured from Due East)

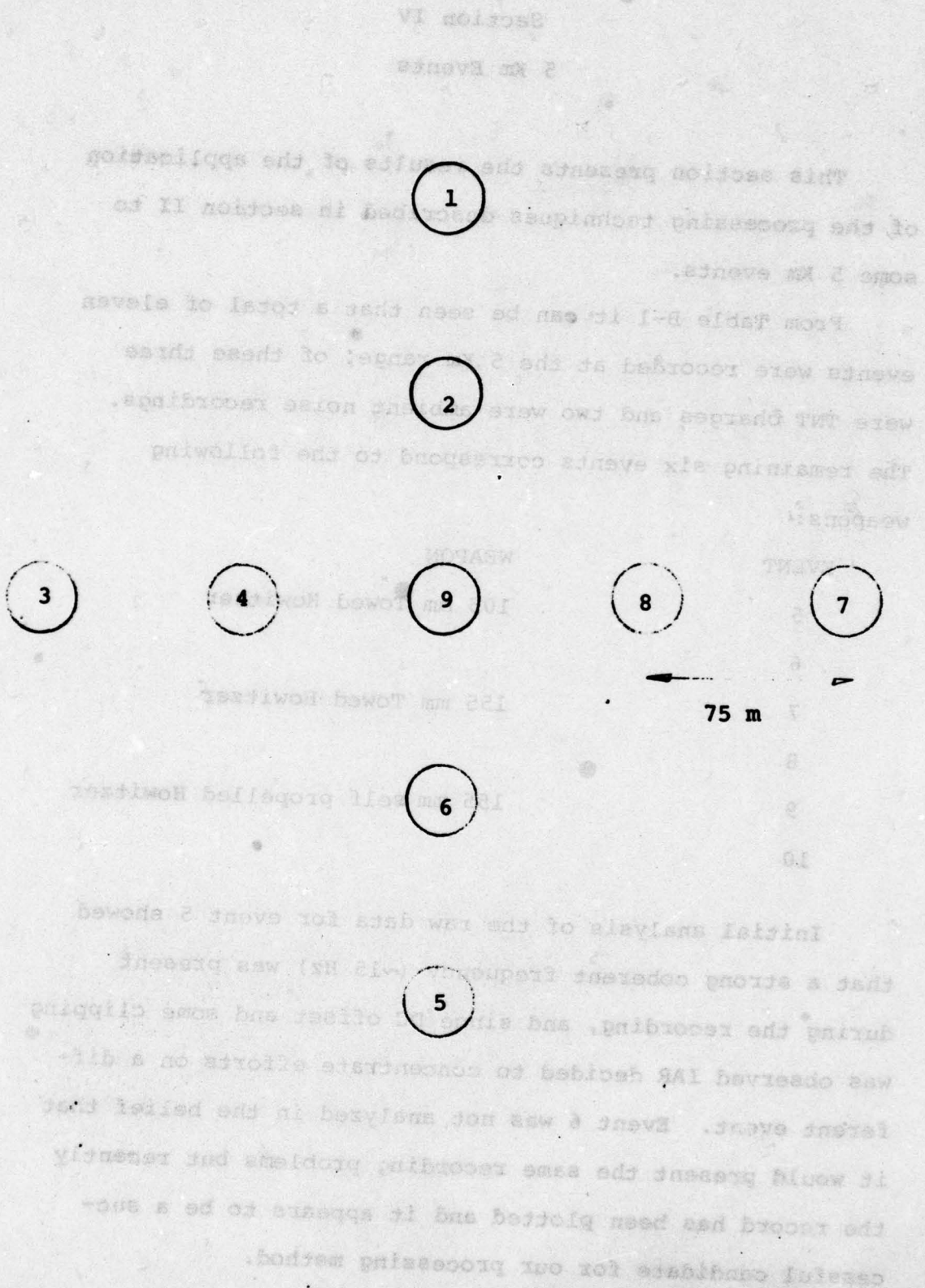


Fig. 3.2

## Section IV

### 5 Km Events

This section presents the results of the application of the processing techniques described in section II to some 5 Km events.

From Table B-1 it can be seen that a total of eleven events were recorded at the 5 Km range; of these three were TNT charges and two were ambient noise recordings. The remaining six events correspond to the following weapons:

EVENT	WEAPON
5	105 mm Towed Howitzer
6	
7	155 mm Towed Howitzer
8	
9	155 mm self propelled Howitzer
10	

Initial analysis of the raw data for event 5 showed that a strong coherent frequency ( $\sim 15$  Hz) was present during the recording, and since DC offset and some clipping was observed IAR decided to concentrate efforts on a different event. Event 6 was not analyzed in the belief that it would present the same recording problems but recently the record has been plotted and it appears to be a successful candidate for our processing method.



During the recording of event 7 some geophone lines appear to have been open since some records are characterized by hard clipped high frequency noise. The remaining three events 8, 9 and 10 were successfully processed and a brief description of the results follows.

Fig. 4.1(a) represents the Haar spectrum corresponding to the sequency group  $m=5$  for the N-S channels in event 8. A coherent seismic signal is detected about 7 seconds after the shot is fired. Fig. 4.1(b) is a plot of the raw data corresponding to this contender segment and Fig. 4.1(c) is the Haar filtered version. The filter used has an impulse response defined by the Haar function  $H_5(0,t)$ .

Figures 4.2 and 4.3 depict analogous processing for the E-W and vertical channels. Similarly event 9 is represented by Figs. 4.4, 4.5 and 4.6 and event 10 by Figs. 4.7, 4.8 and 4.9.

The filtered contender segments (continuous Haar spectrum) are then cross correlated with a reference channel to determine the initial estimates of relative arrival times (Fig. 4.10). As described in section II, the estimates of time differences can be improved by, based on the initial estimates, narrowing and cross-correlating the contender segments with higher sequency group Haar representations, but this technique was not followed for this first report and the results presented are based on initial time difference estimates.



The output of the position estimator for the three events is given in table 4.1. For each event two position estimates are recorded. The second one is a result of updating the measurement error covariance matrix with the residual errors obtained from the first estimate. Although simplistic in nature this method does improve the bearing estimation for two events. For the third event the bearing estimate is not in accordance with the simulation described in Appendix E; in this case refining the relative arrival time estimates by crosscorrelating higher frequency Haar spectra would have been in order.

Consistently range is underestimated by the position estimator. Initially this system was designed for surface waves and therefore the vector wave number associated with a signal wavefront was assumed to be horizontal. Given the geological stratification of the recording area (Appendix C) and the low frequency of the wave train detected it is logical to think about a "refraction arrival" coming into the receiving array at a certain critical angle ( $\sim 65^\circ$ ). The processing system had no capability of analyzing three-dimensional wave numbers and the range estimated is apparently the horizontal distance to the point of radiation to the upper strata. Finally a composite estimate of position, following the Gauss-Markov theorem, is given at the bottom of table 4.1. When the three events are considered, the bearing error is negligible. No doubt there is an element of luck here, but still the occurrence speaks strongly for the technique.

Table 4.1

Position Estimates\* for 5 Km

True Range:  $R_T = 5.280$  Km

True Bearing:  $\theta_T = 301.4^\circ$

Event	$R_E = \hat{R} - R_T$	$\Delta R$	$\theta_E = \hat{\theta} - \theta_T$	$\Delta \theta$
8	-4.98	.545	3.256	4.018
	-4.98	.438	1.357	2.5
9	-4.99	.394	1.717	2.82
	-5.	.28	1.2	2.25
10	-5.05	.35	-6.4	2.64
	-5.03	.32	-8.73	1.44

\* These estimates are based on initial (zero-iterates) relative arrival time measurements

COMPOSITE ESTIMATES

EVENTS 8 & 9

$$\begin{cases} R_E = -5.0 \\ \theta_E = 1.312 \end{cases}$$

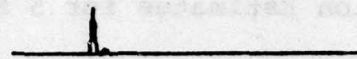
EVENTS 8,9 & 10

$$\begin{cases} R_E = -5.06 \\ \Delta R = .23 \\ \theta_E = -0.015 \\ \Delta \theta = 1.835 \end{cases}$$

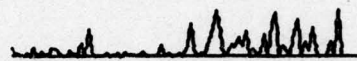
TIME (sec)

0 10

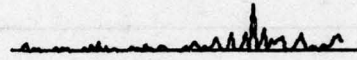
0



13



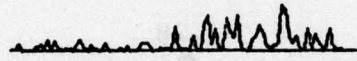
16



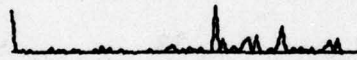
25



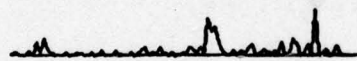
10



7



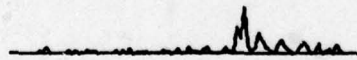
19



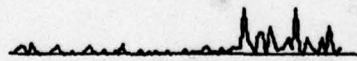
22



4



1



HAAR SPECTRUM

Sequency group 5

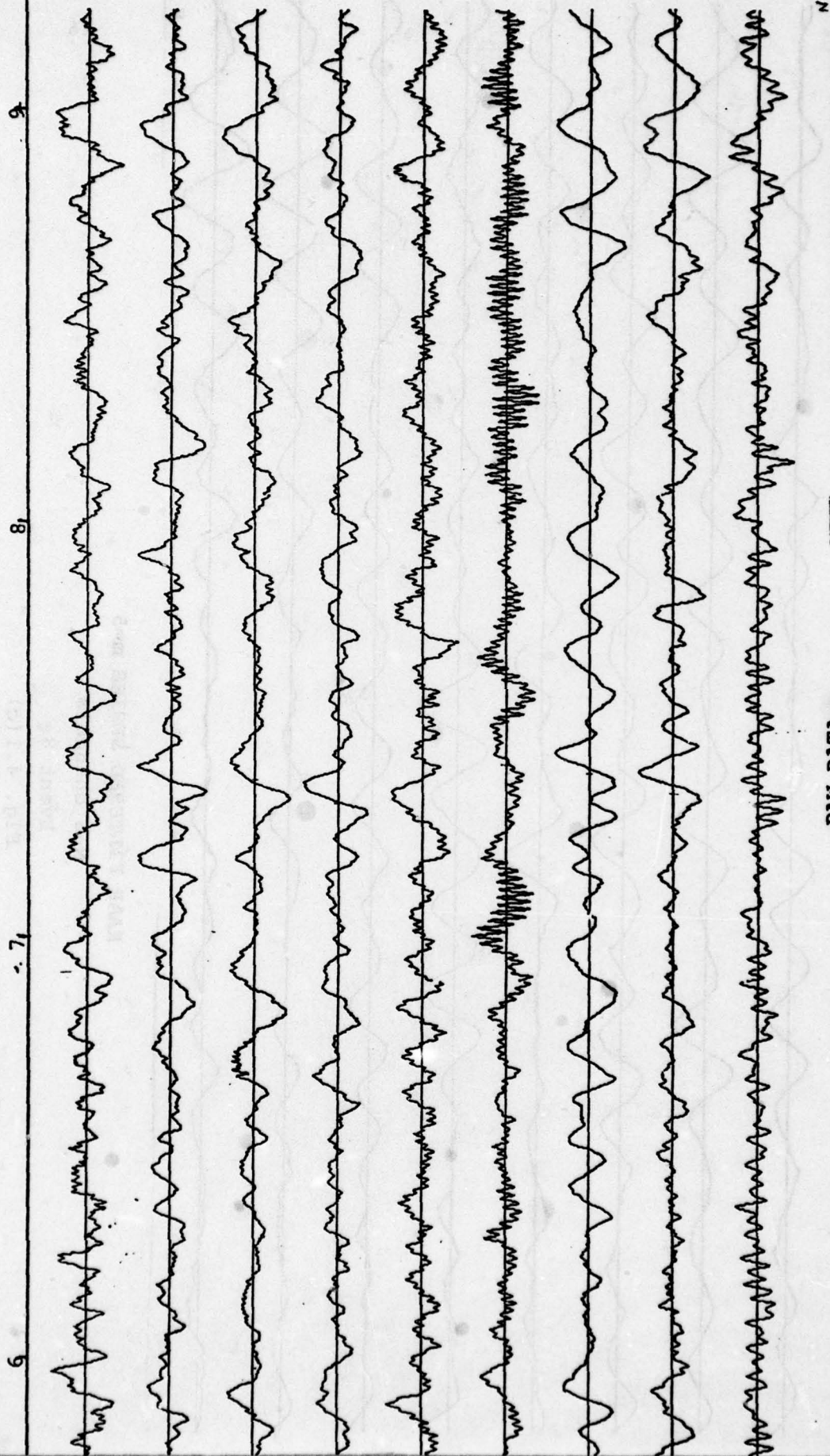
Event 8

Accelerometer on gun (ch 0)  
and N-S channels

Fig. 4.1(a)



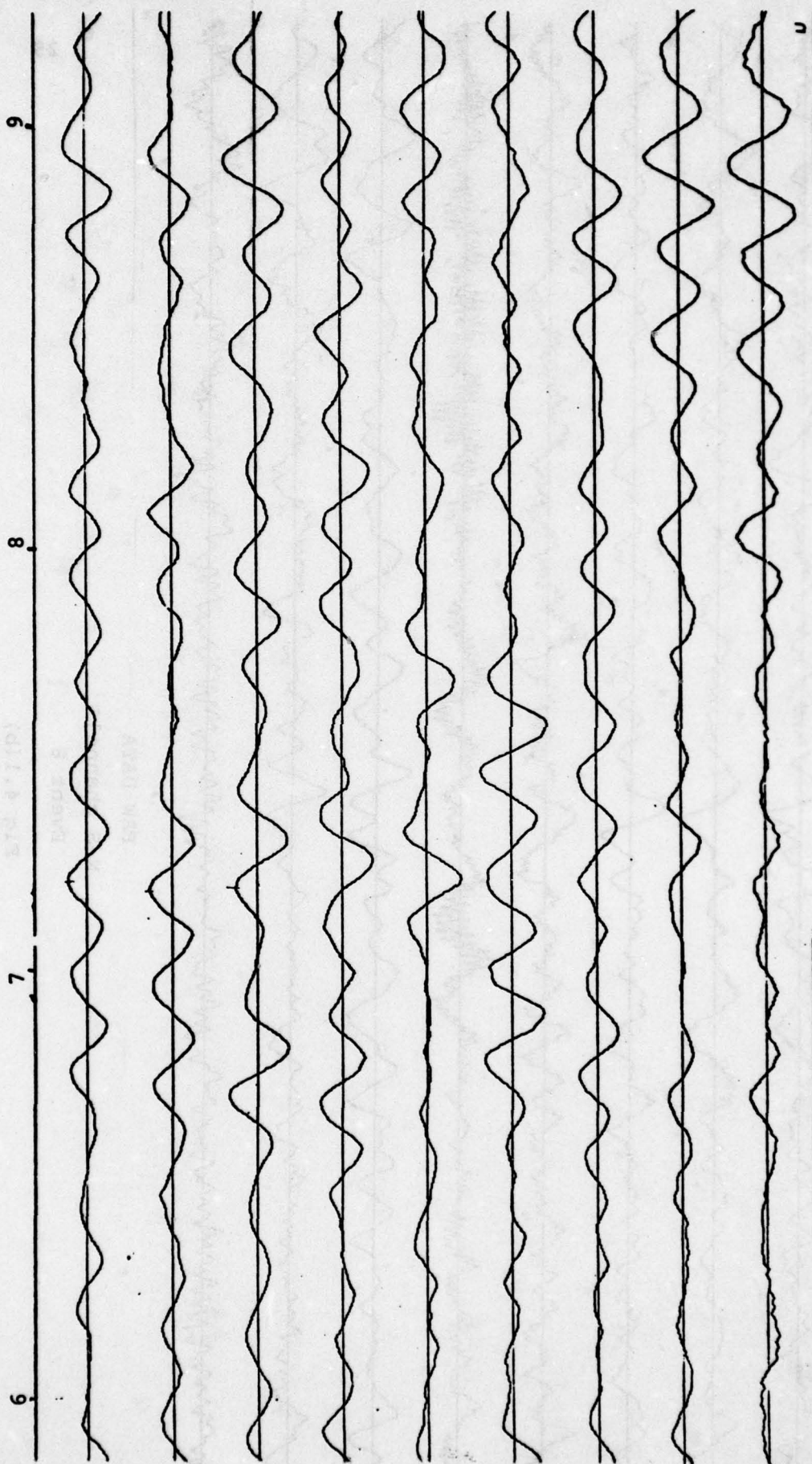
Time (sec.) elapsed after shot



RAW DATA  
N-S channels  
Event 8

Fig 4.1(b)

Time (sec.) elapsed after shot



HAAR FILTERED SERIES  $m=5$

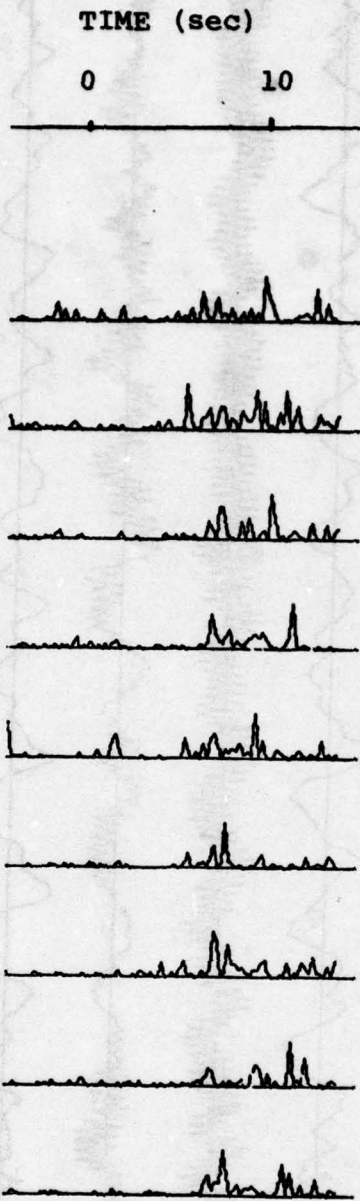
N-S channels

Event 8

Fig. 4.1(c)

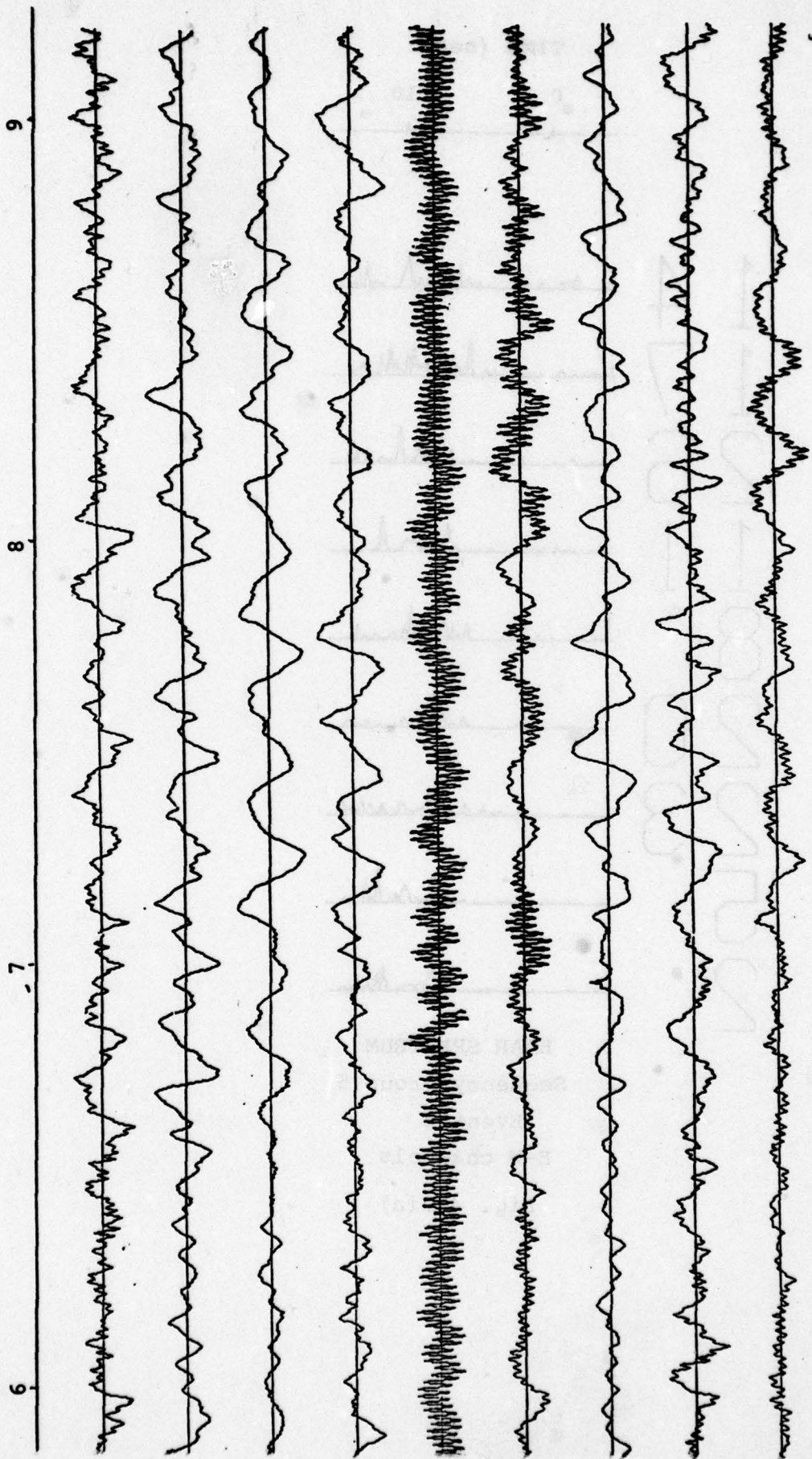


14  
17  
26  
11  
8  
20  
23  
25  
26  
27



HAAR SPECTRUM  
Sequency group 5  
Event 8  
E-W channels  
Fig. 4.2(a)

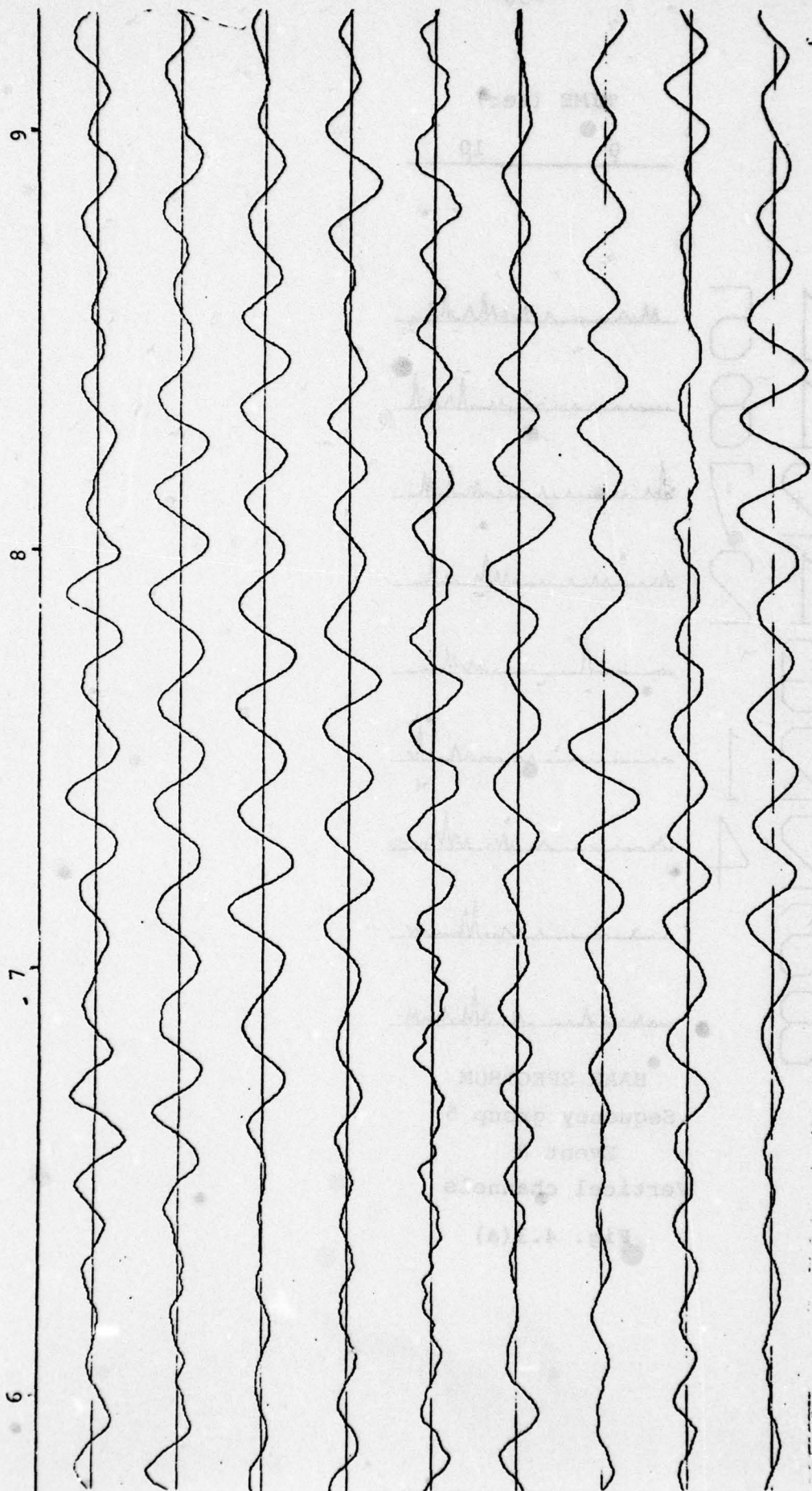
Time (sec.) elapsed after shot



RAW DATA  
E-W channels  
Event 8  
Fig 4.2(b)



Time (sec.) elapsed after shot



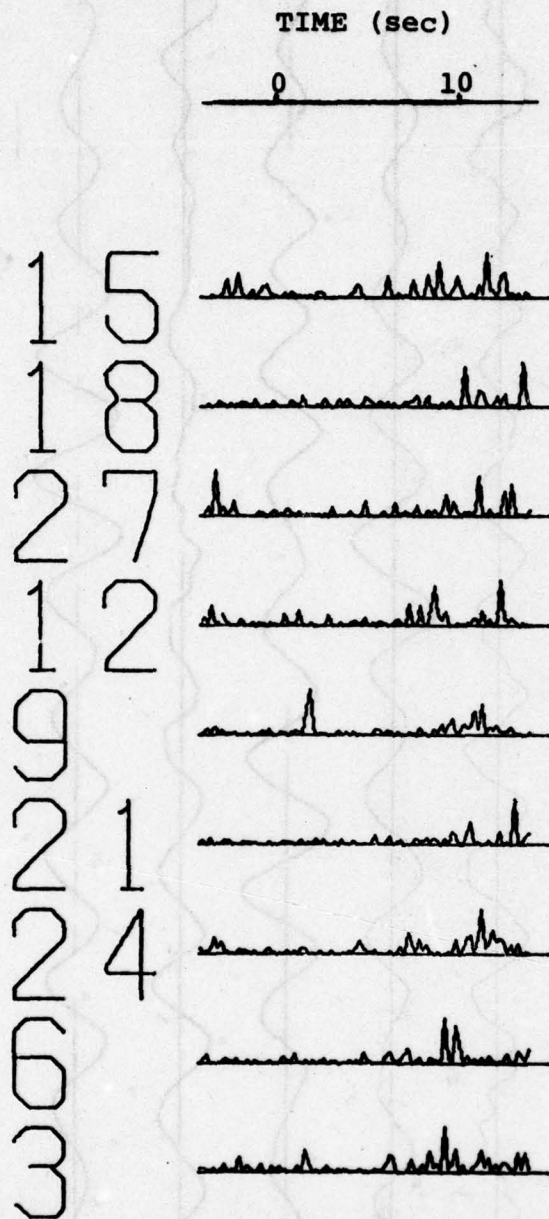
HAAR FILTERED SERIES  $m=5$

E-W channels

Event 8

Fig. 4.2(c)

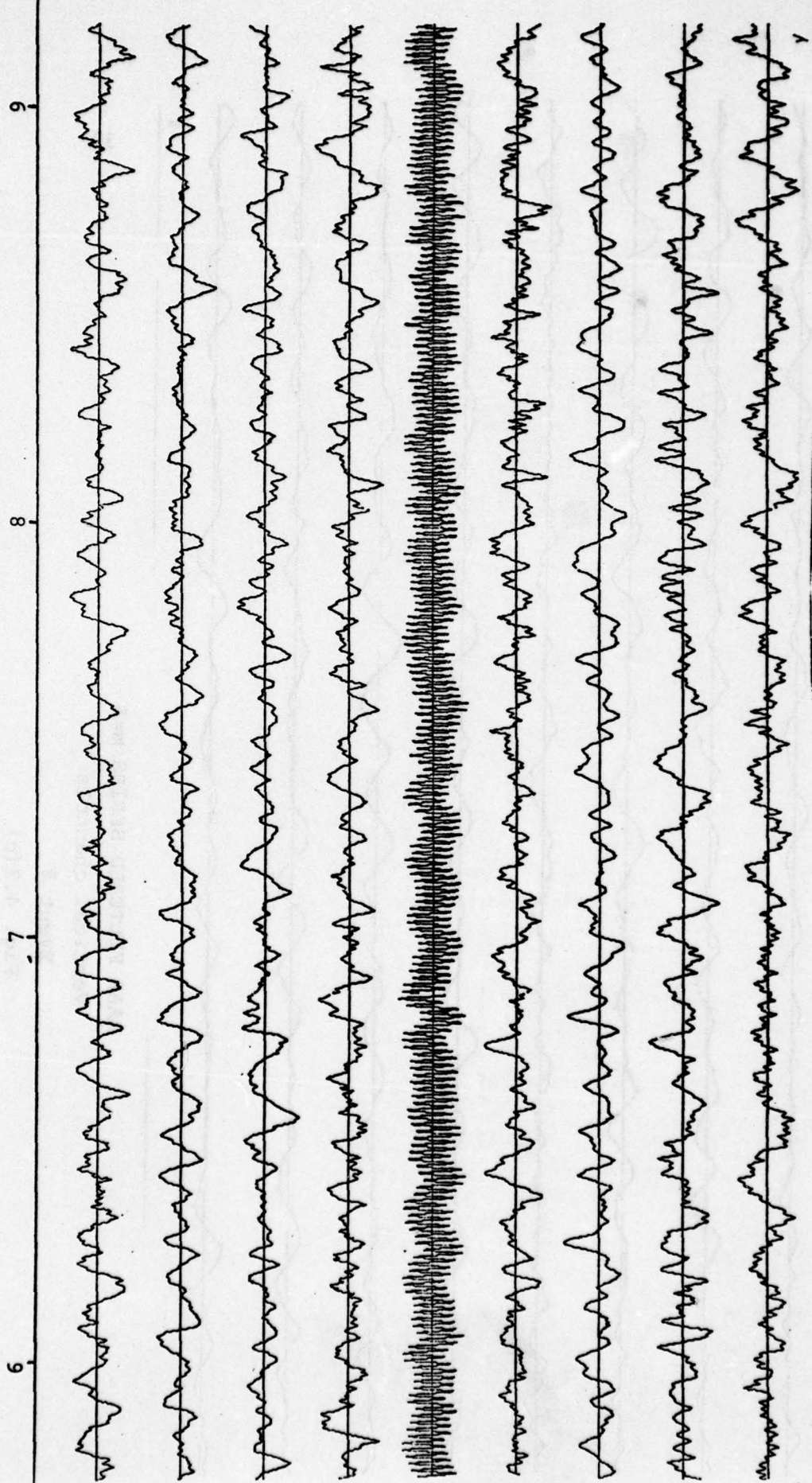




HAAR SPECTRUM  
Sequency group 5  
Event 8  
Vertical channels

Fig. 4.3(a)

Time (sec.) elapsed after shot



RAW DATA

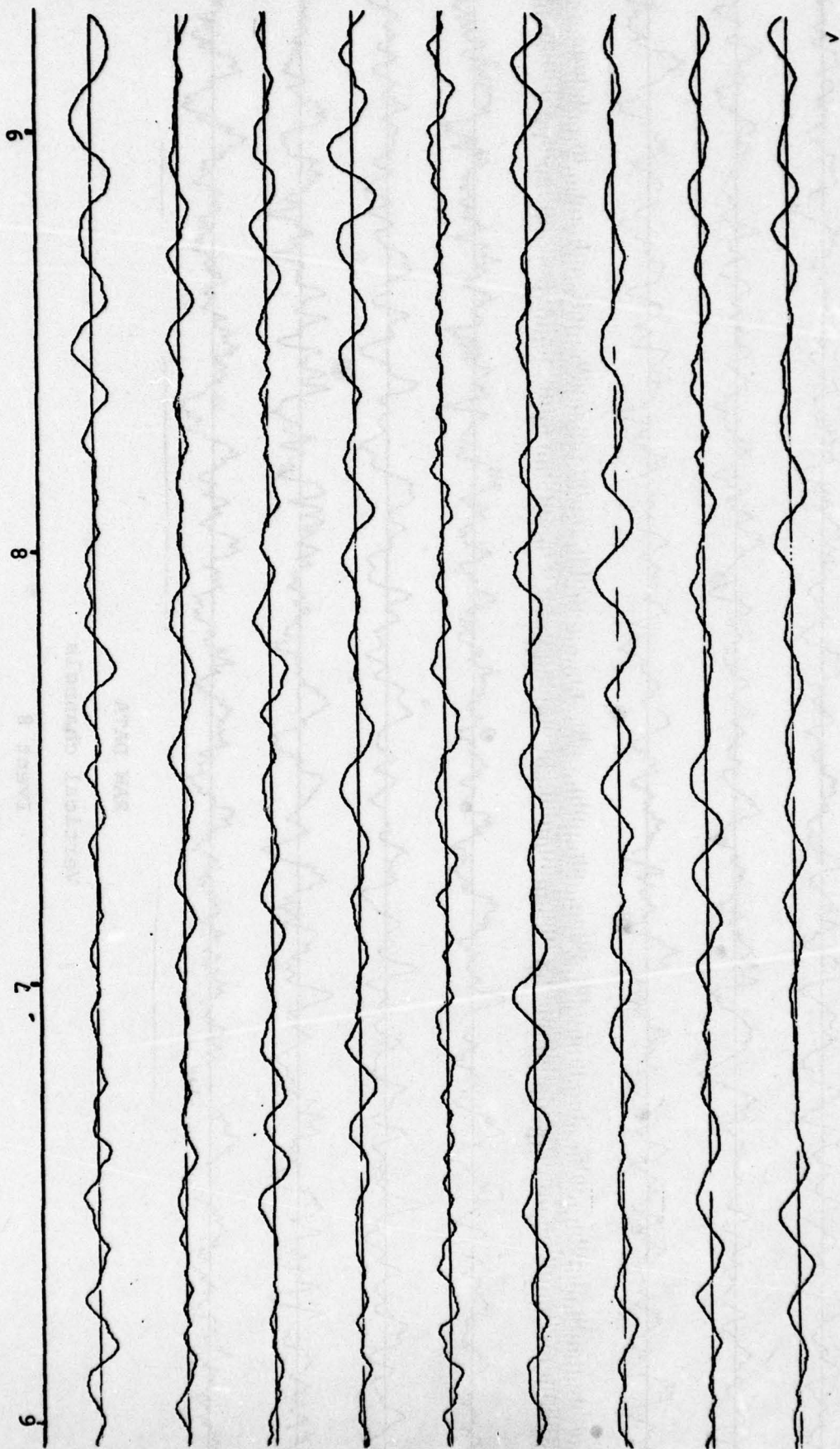
Vertical channels

Event 8

Fig. 4.3(b)



Time (sec.) elapsed after shot

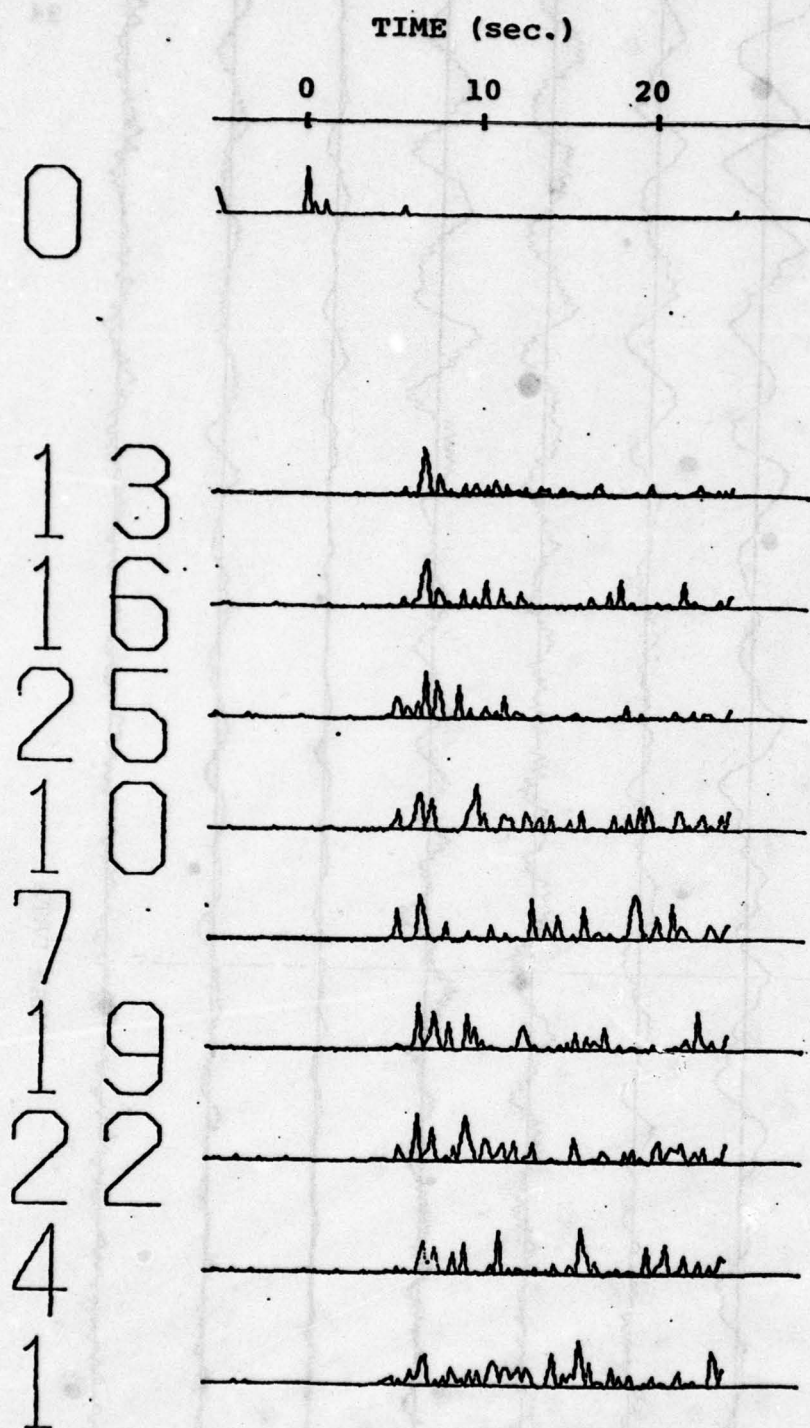


HAAR FILTERED SERIES  $m=5$

Vertical channels

Event 8

Fig. 4.3(c)

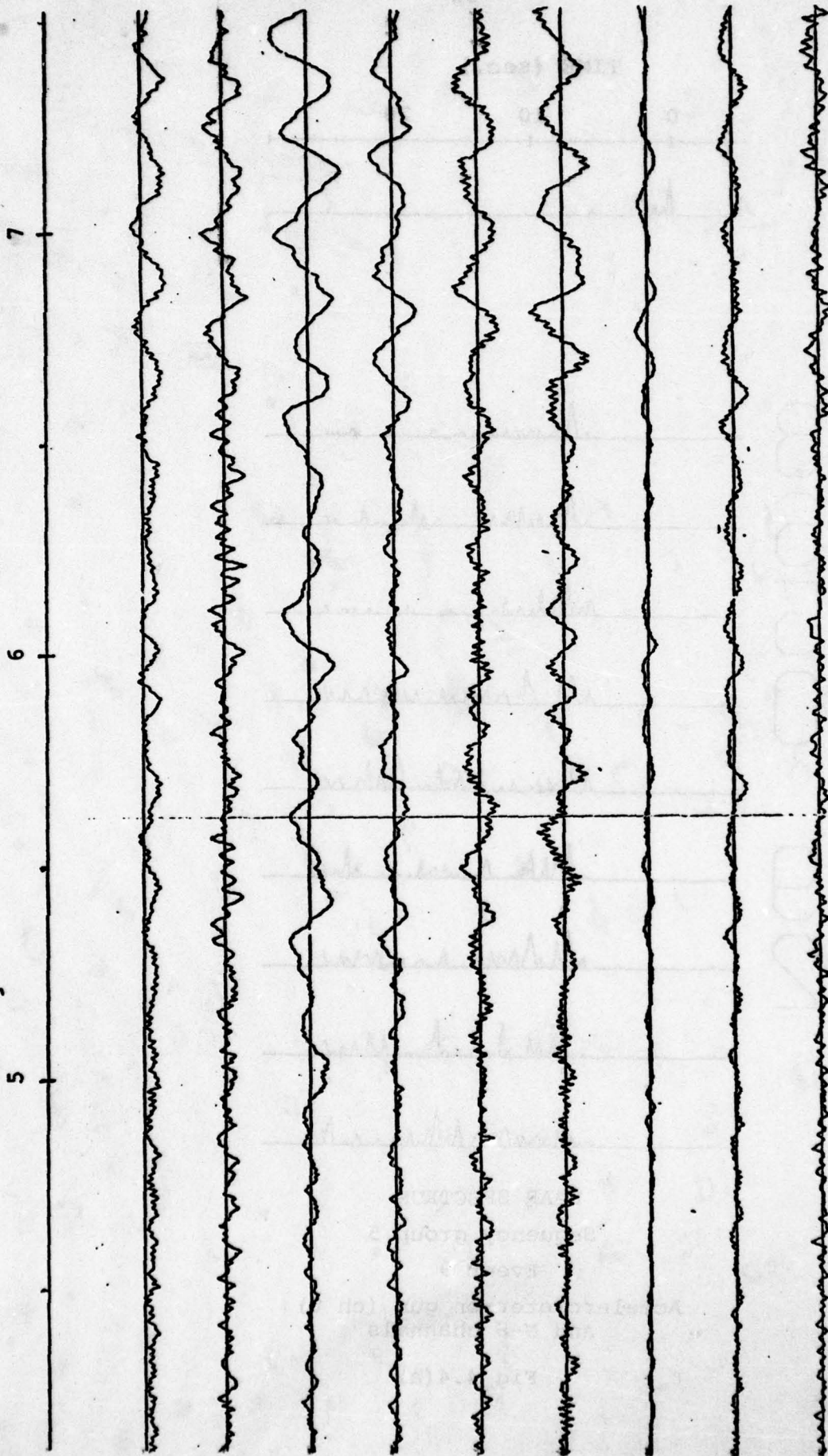


HAAR SPECTRUM  
Sequency group 5  
Event 9  
Accelerometer on gun (ch 0)  
and N-S channels

Fig 4.4(a)



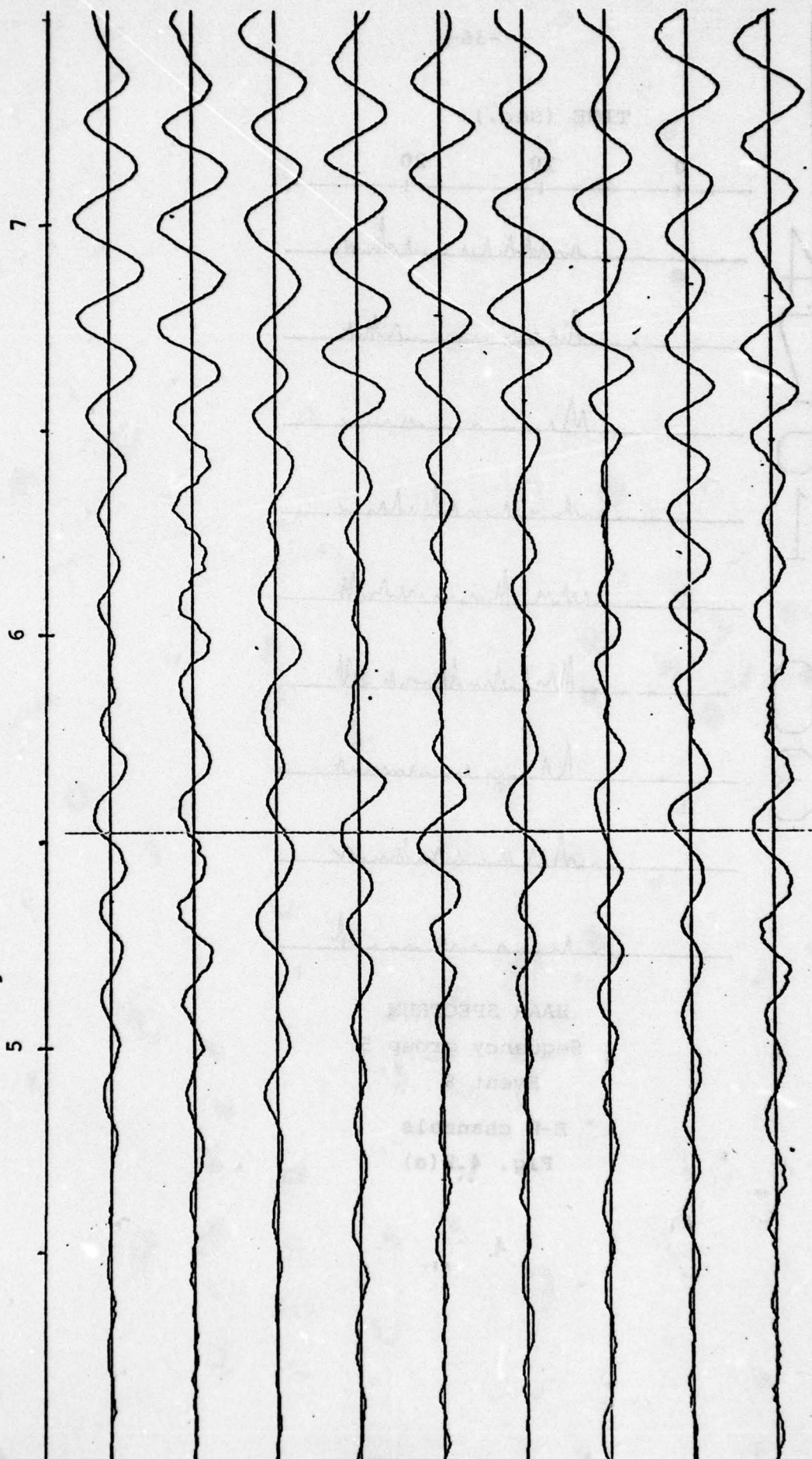
Time (sec.) elapsed after shot



Event 9

Fig. 4.4(b)

Time (sec.) elapsed after shot



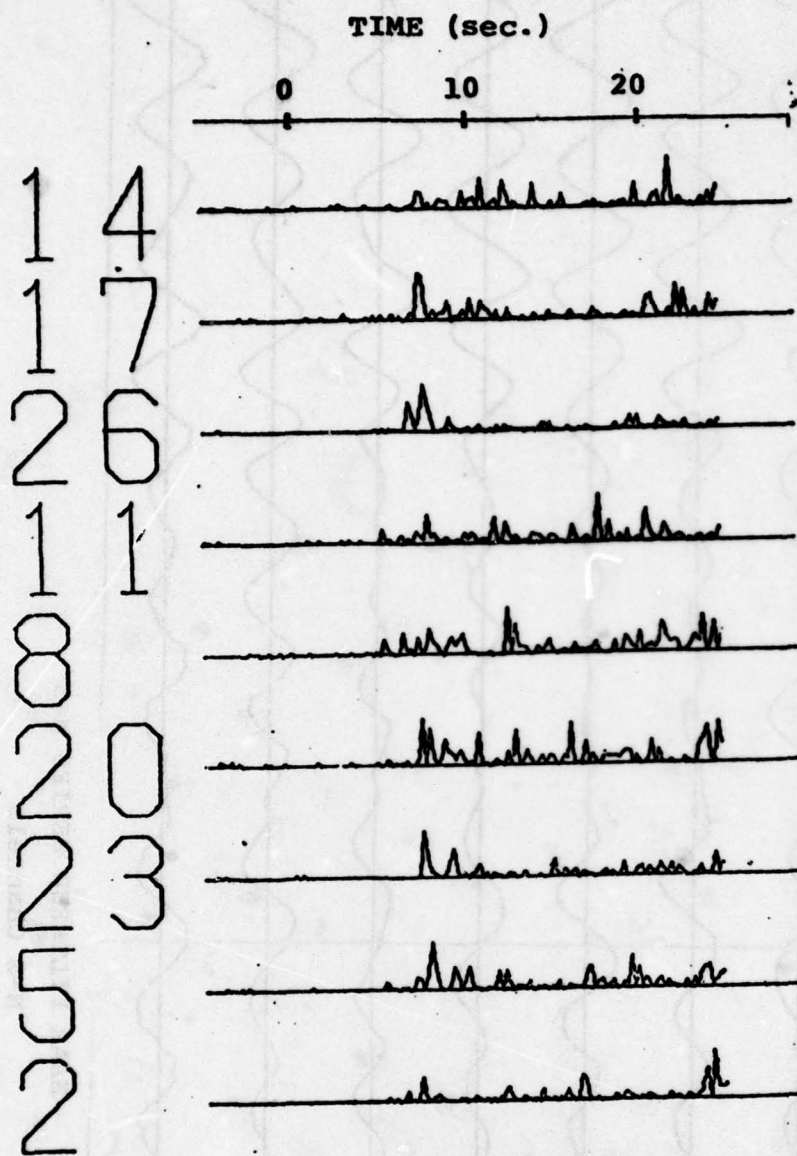
HAAR FILTERED SERIES  $m=5$

N-S Channels

Event 9

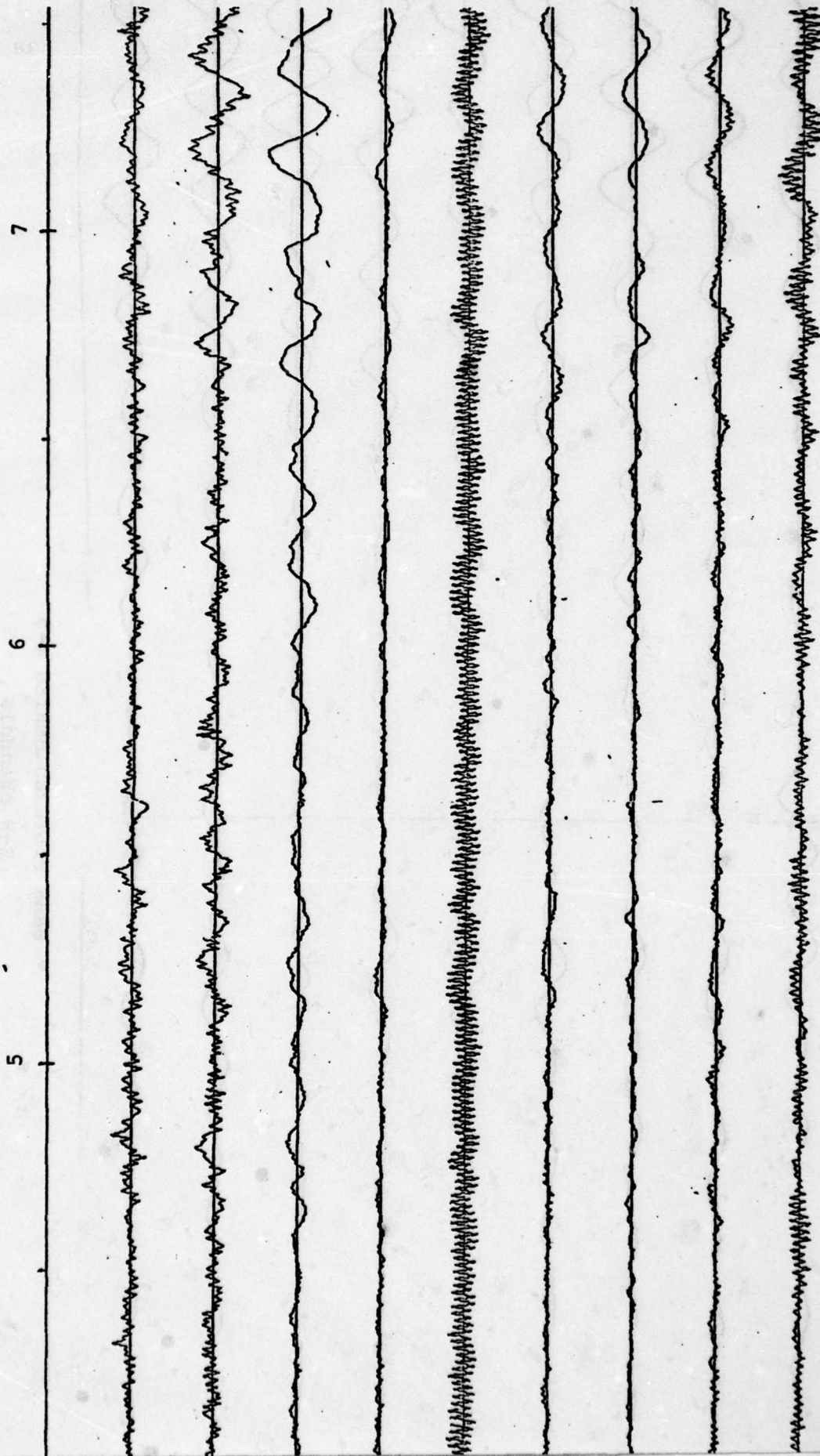
Fig. 4.4(c)





HAAR SPECTRUM  
Sequency group 5  
Event 9  
E-W channels  
Fig. 4.5(a)

Time (sec.) elapsed after shot



RAW DATA

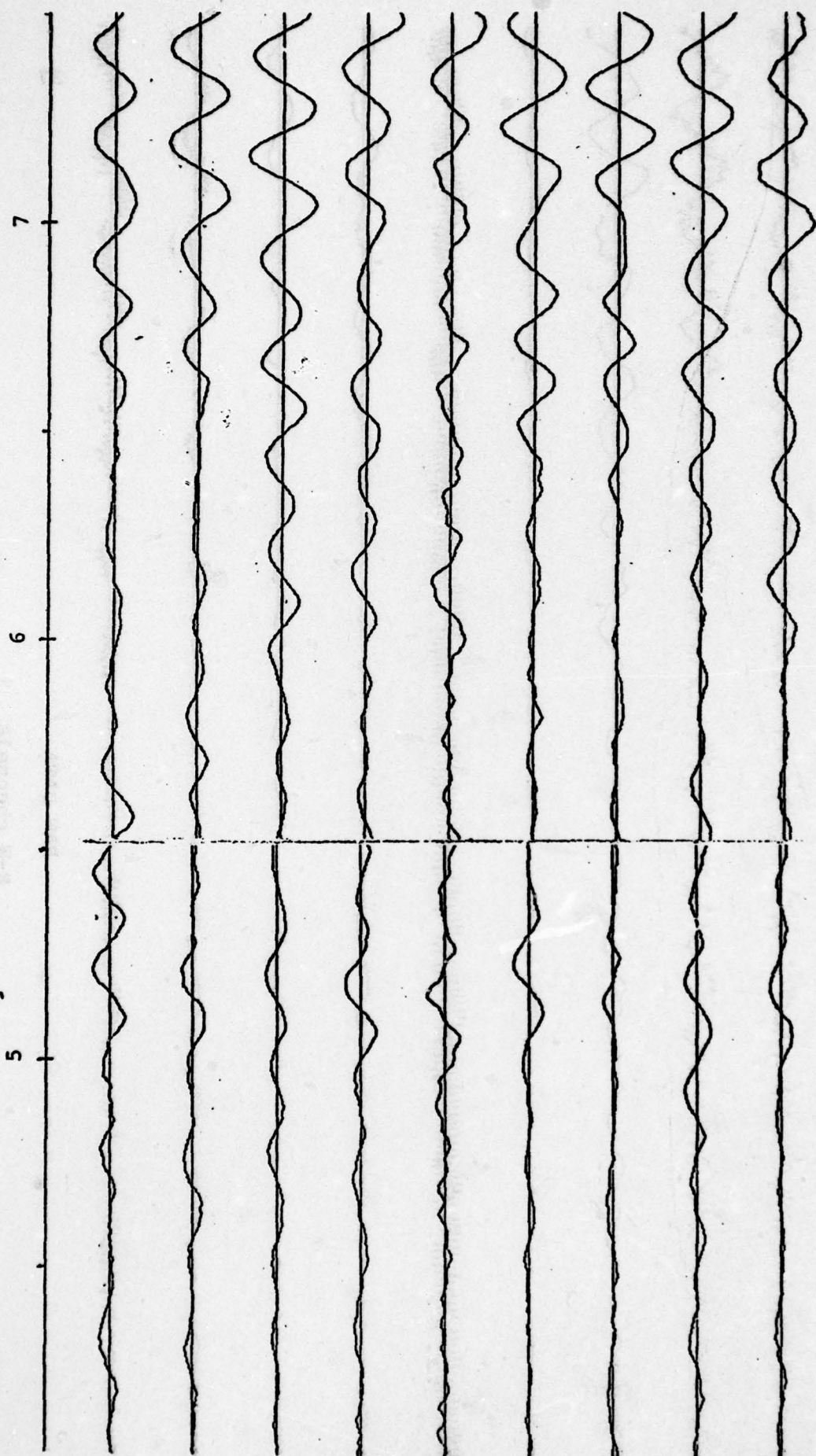
E-W channels

Event 9

Fig. 4.5(b)

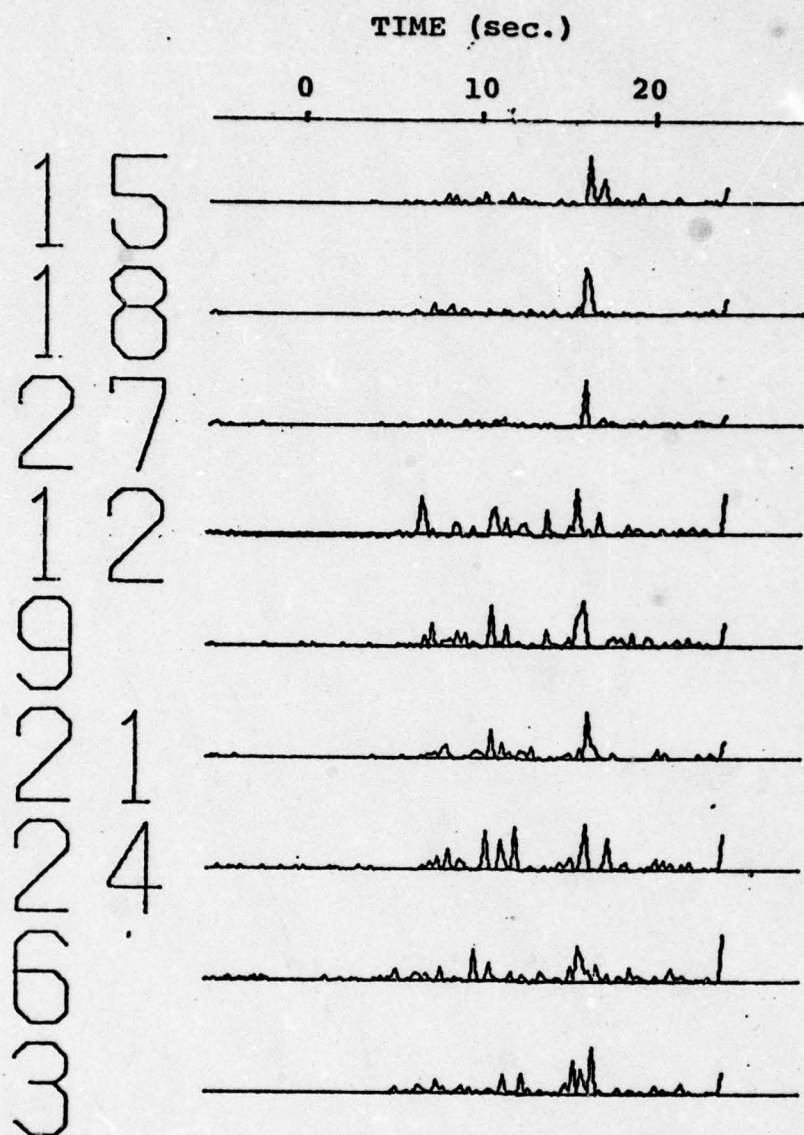


Time (sec.) elapsed after shot



HAAR FILTERED SERIES  $m=5$   
E-W channels

Event 9  
Fig. 4.5(c)

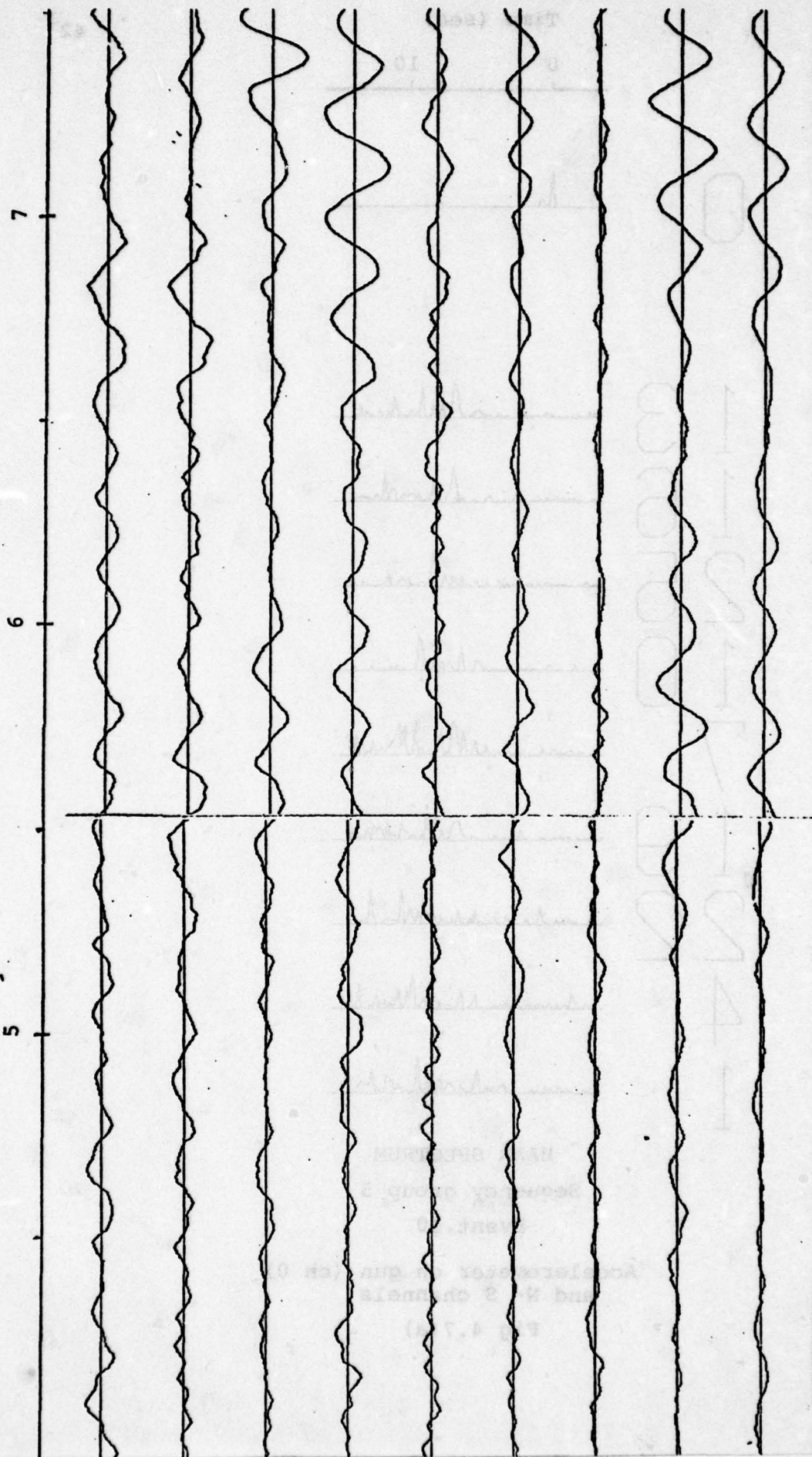


HAAR SPECTRUM  
Sequency group 5

Event 9  
Fig. 4.6(a)



Time (sec.) elapsed after shot



HAAR FILTERED SERIES  $m=5$

Vertical channels

Event 9

Fig 4.6(c)

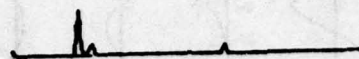
Time (sec)

42

0

10

0



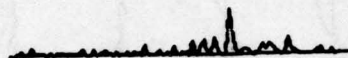
13



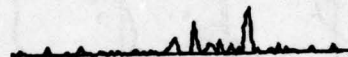
16



25



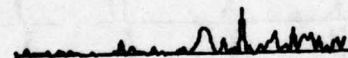
10



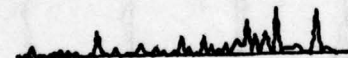
7



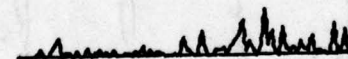
19



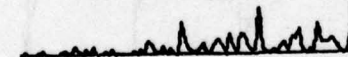
22



4



1



HAAR SPECTRUM

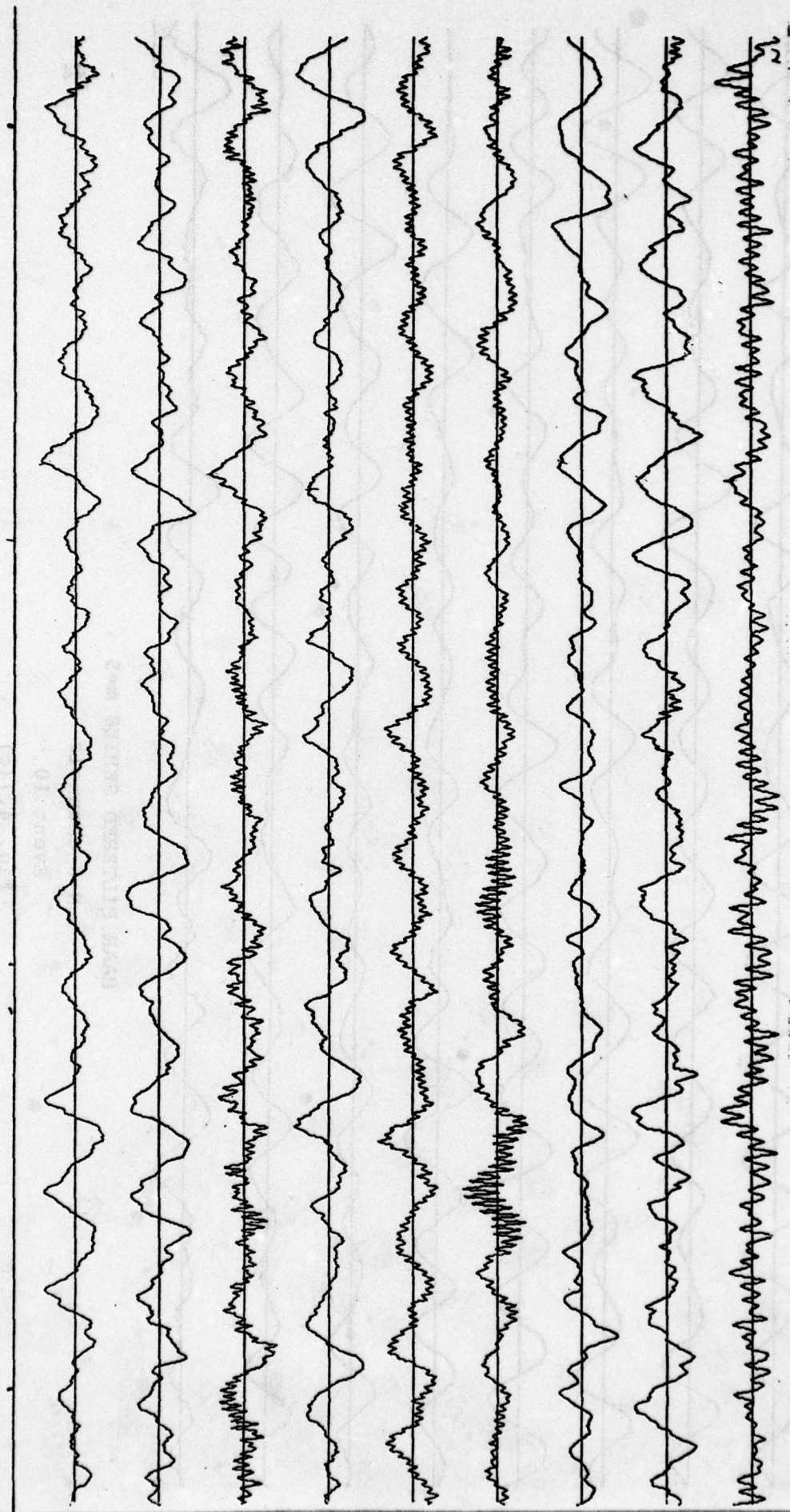
Sequency group 5

Event 10

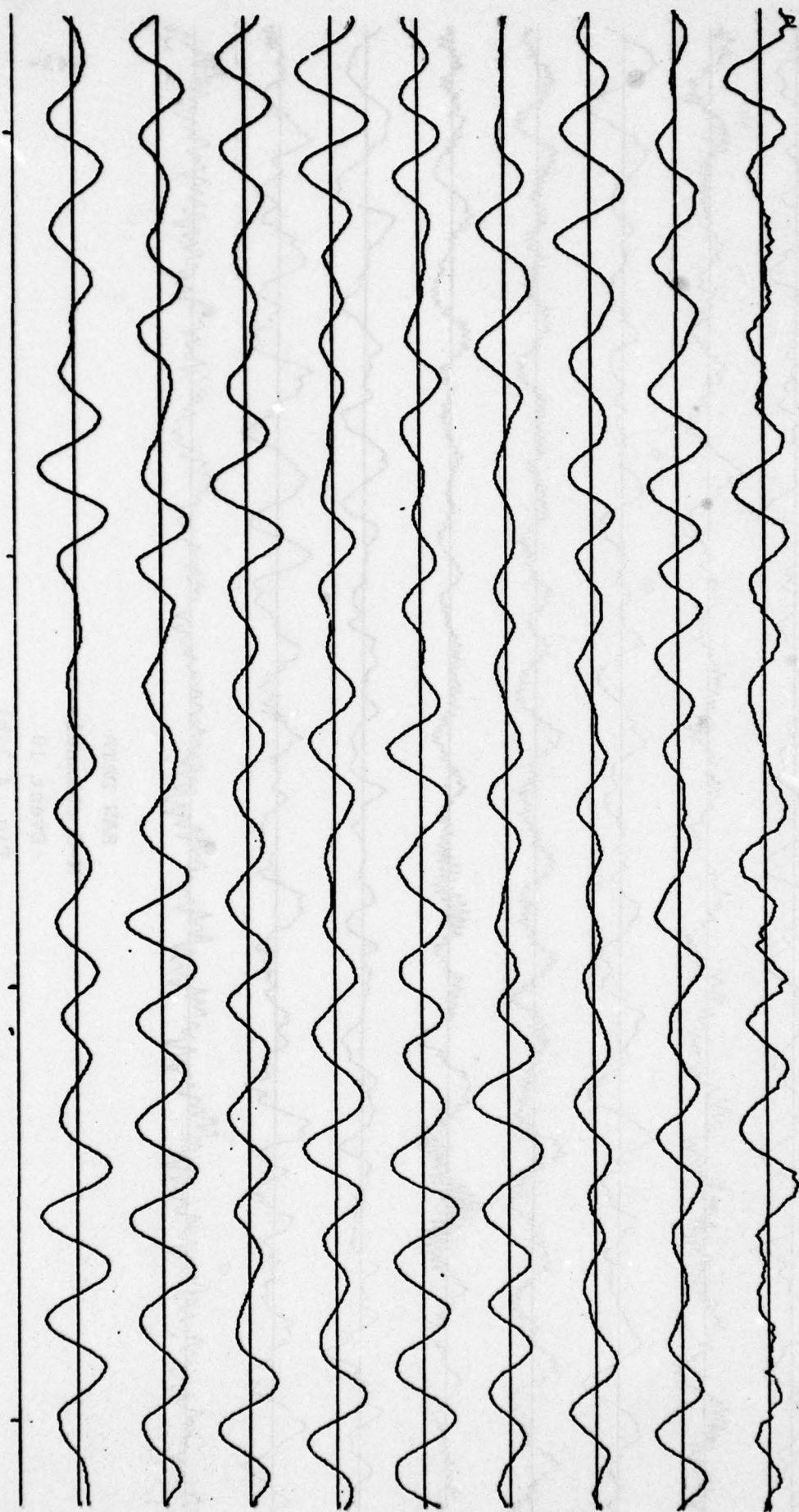
Accelerometer on gun (ch 0)  
and N- S channels

Fig 4.7(a)





RAW DATA  
N-S channels  
Event 10  
Fig. 4.7(b)



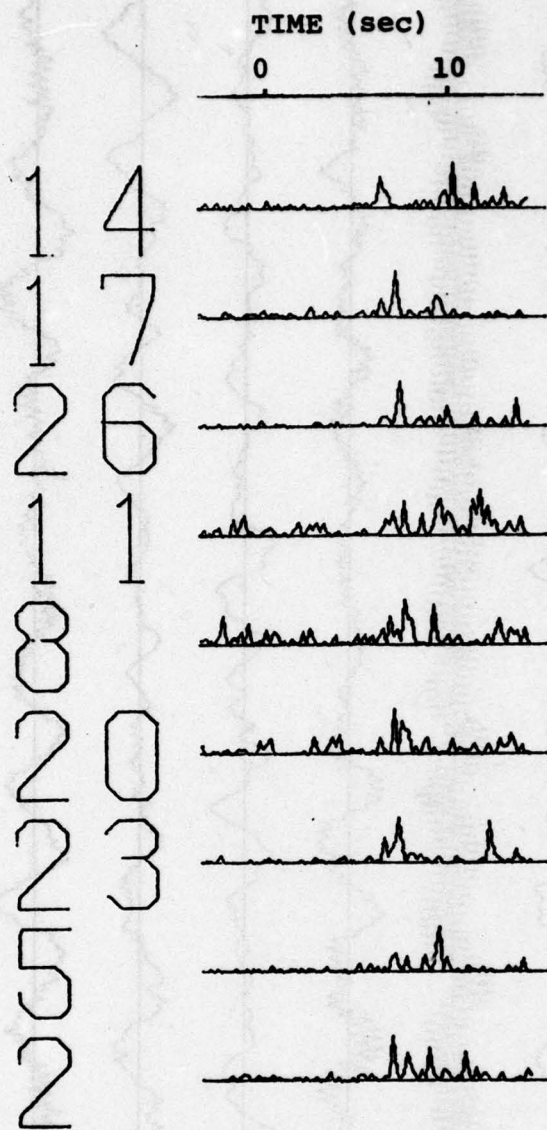
HAAR FILTERED SERIES  $m=5$

N-S channels

Event 10

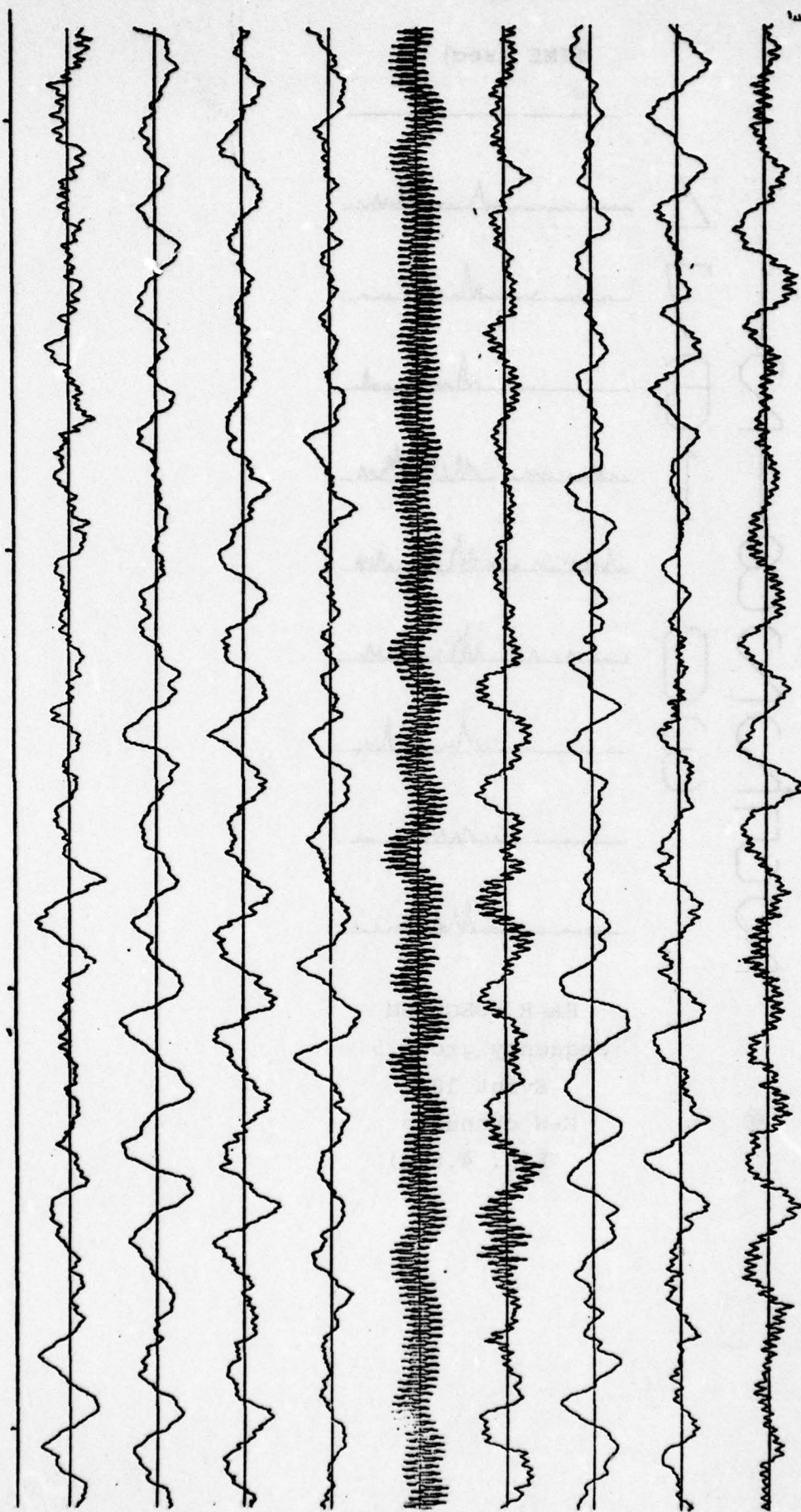
Fig. 4.7(c)





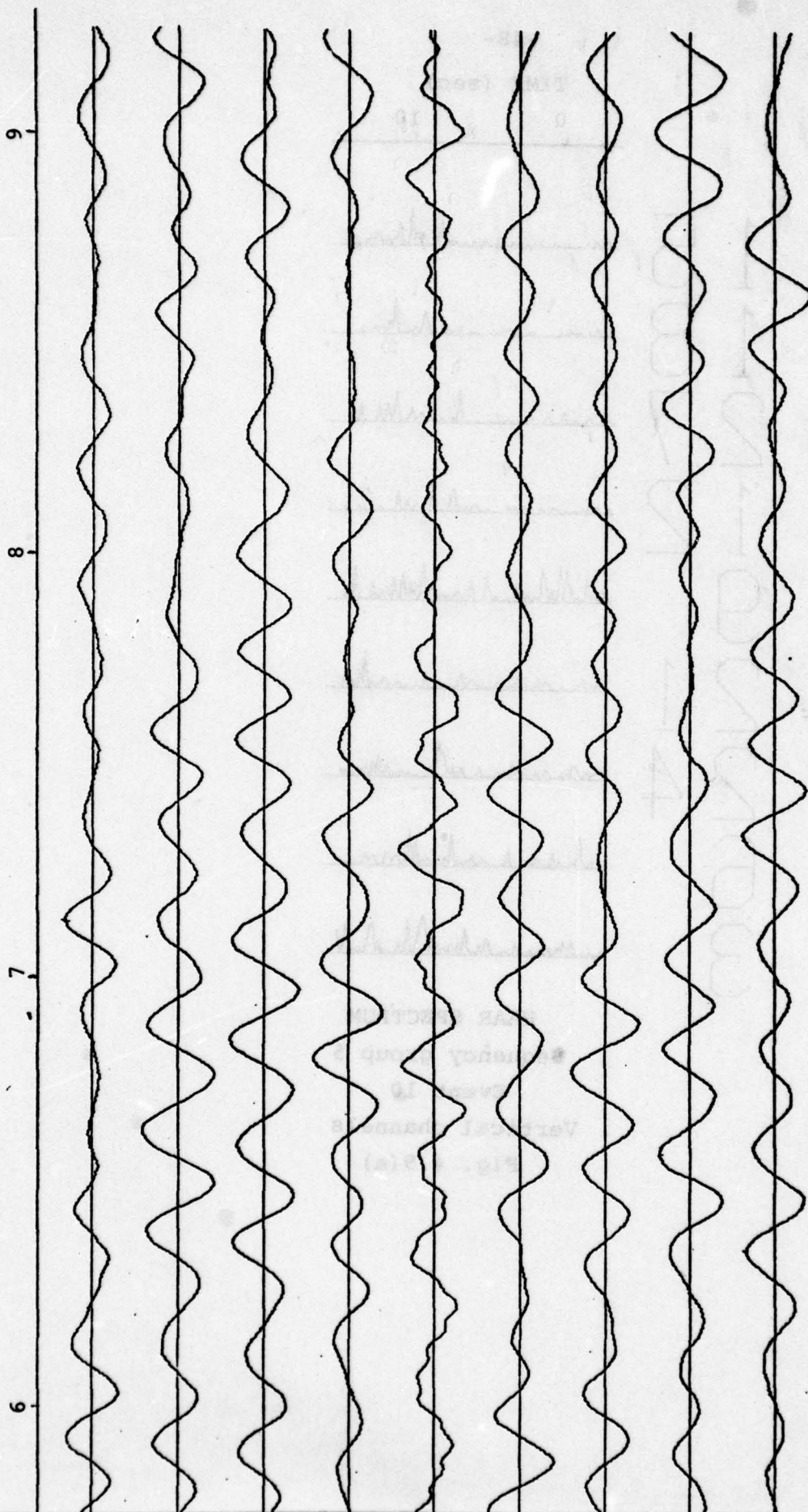
HAAR SPECTRUM  
Sequency group 5  
Event 10  
E-W channels  
Fig. 4.8(a)





RAW DATA  
E-W channels  
Event 10  
Fig. 4.8(b)

Time (sec.) elapsed after shot



HAAR FILTERED SERIES  $m=5$

E-W channels

Event 10

Fig 4.8(c)

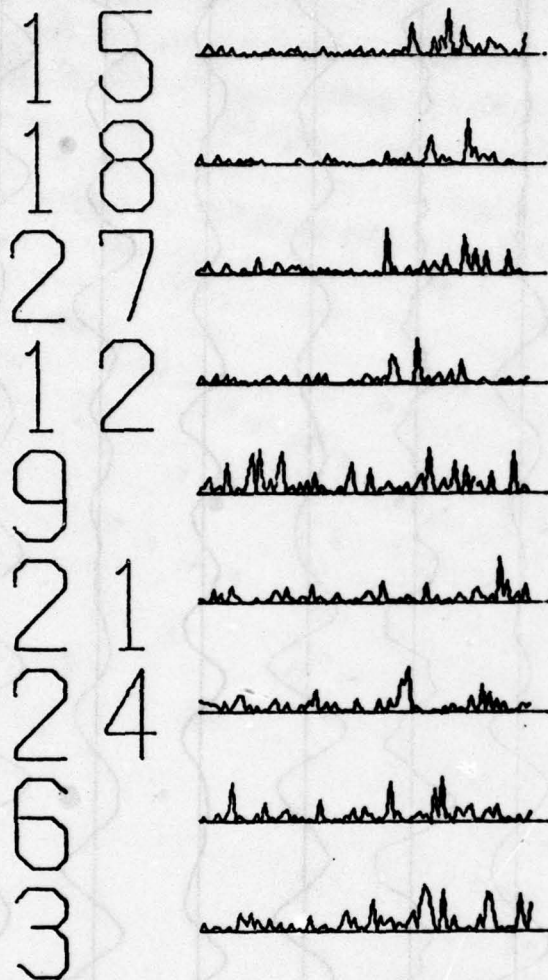


-48-

TIME (sec)

0

10



HAAR SPECTRUM

Sequency group 5

Event 10

Vertical channels

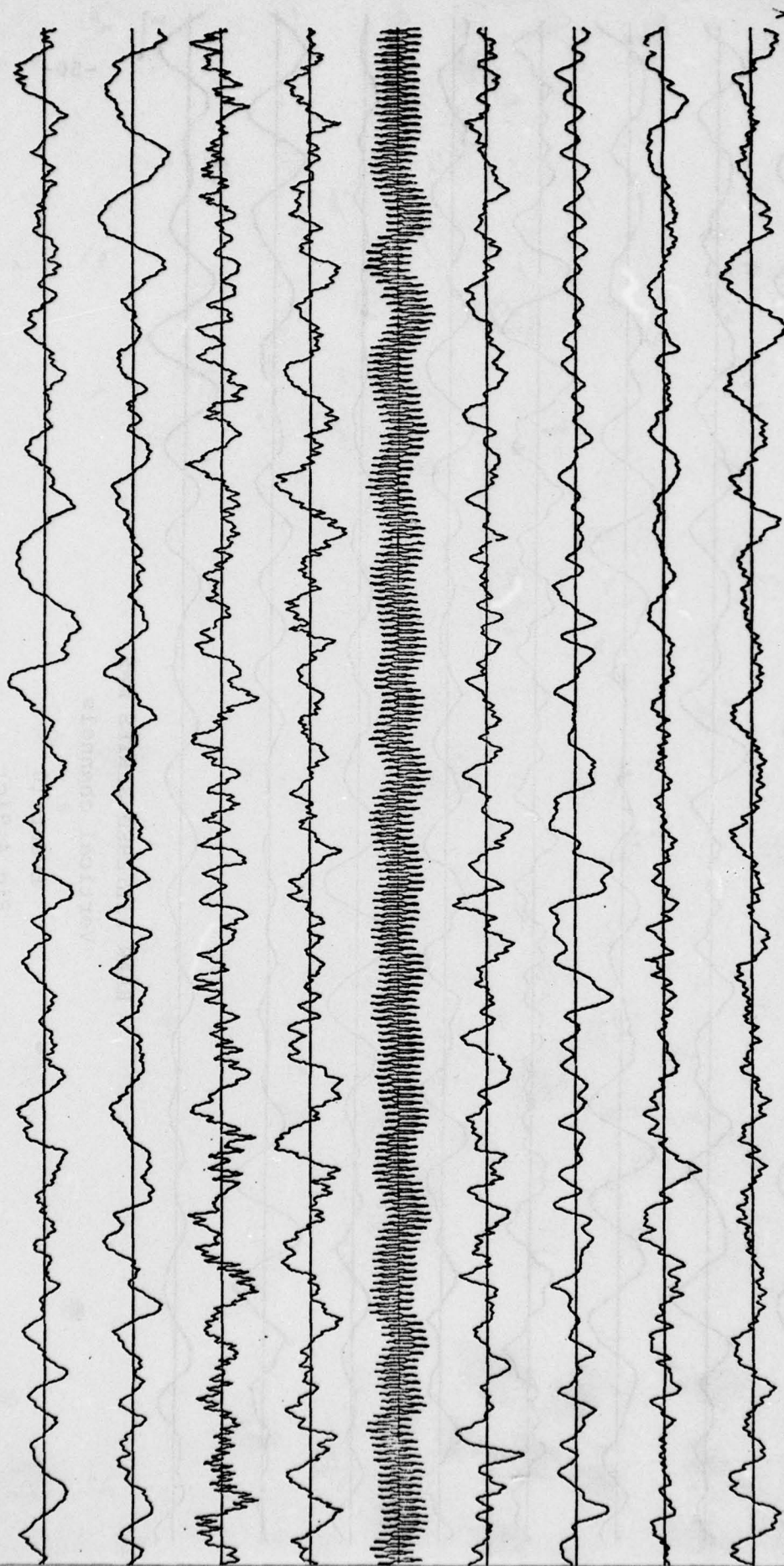
Fig. 4.9(a)

Time (sec.) elapsed after shot

7

8

9



RAW DATA

Vertical channels

Event 10

Fig 4.9(b)



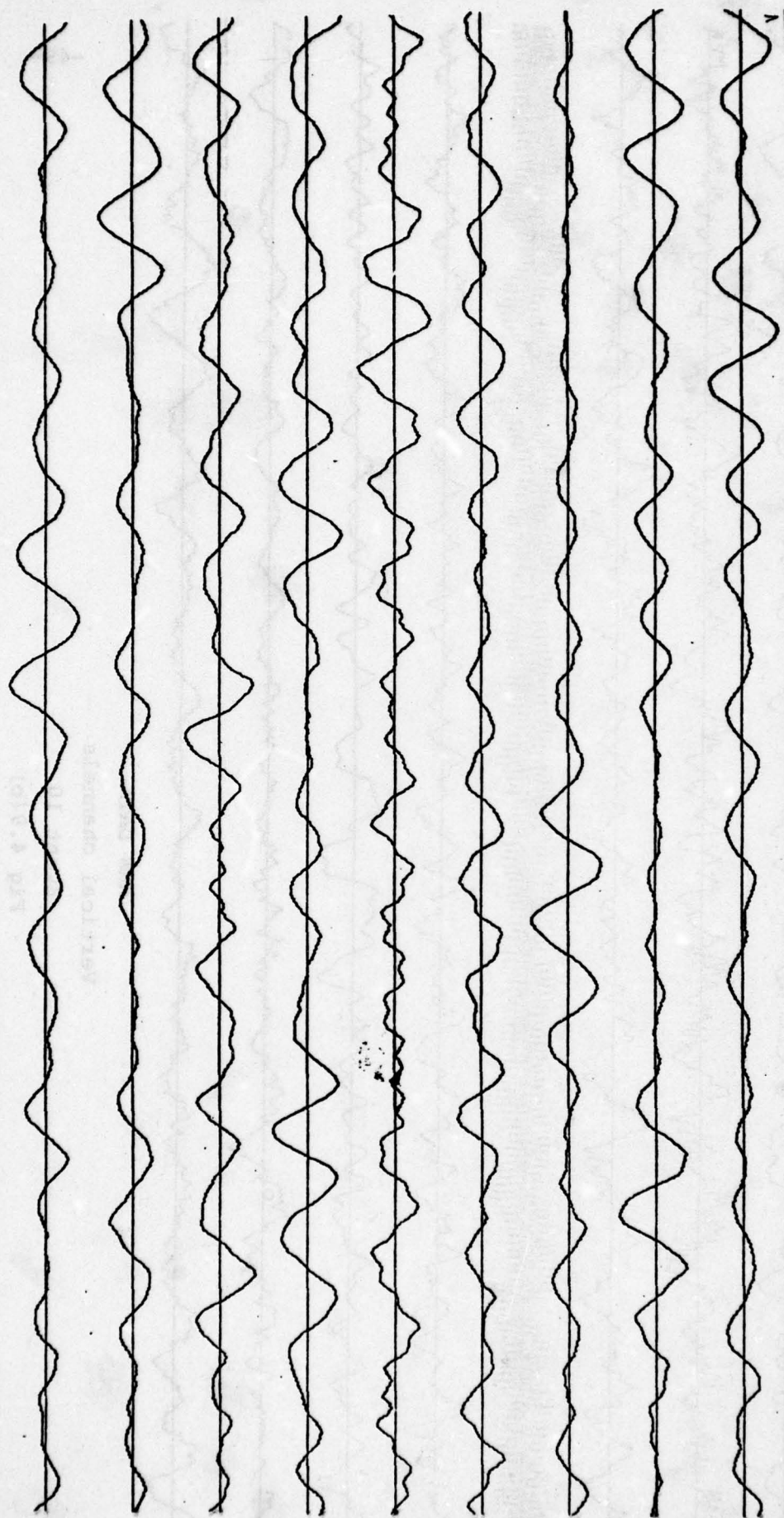
Time (sec.) elapsed after shot

6

7

8

9



HAAR FILTERED SERIES  $m=5$

Vertical channels

Event 10

Fig 4.9(c)

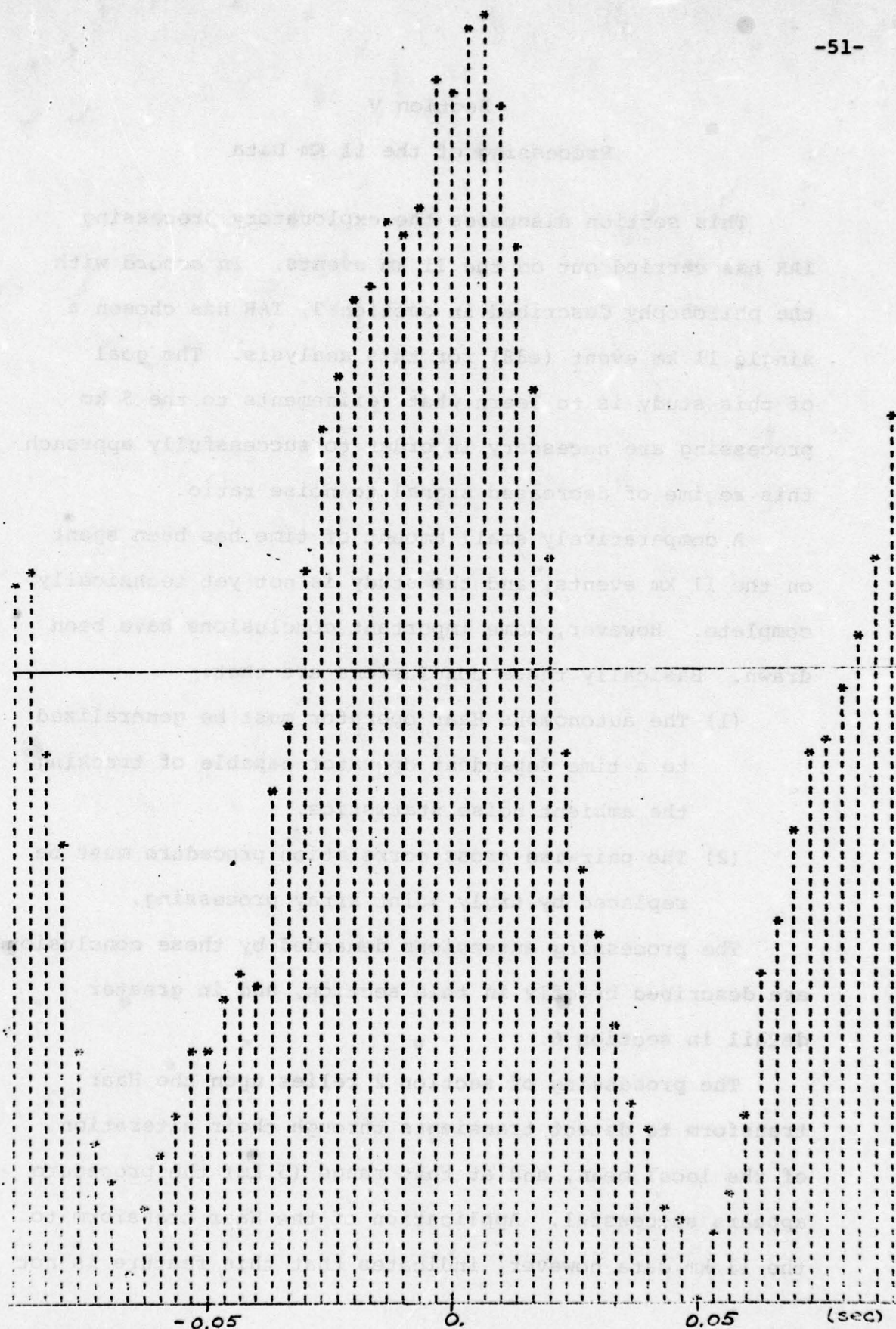


Fig. 4.10 X-Correlation (Chs. 19,25) Event 9



## Section V

### Processing of the 11 Km Data

This section discusses the exploratory processing IAR has carried out on the 11 km events. In accord with the philosophy described in section 3, IAR has chosen a single 11 km event (#38) for this analysis. The goal of this study is to learn what refinements to the 5 km processing are necessary in order to successfully approach this regime of decreased signal to noise ratio.

A comparatively small amount of time has been spent on the 11 km events, and the study is not yet technically complete. However, some important conclusions have been drawn. Basically these conclusions are that:

- (1) The autonomous Haar operator must be generalized to a time dependent operator capable of tracking the ambient noise statistics.
- (2) The pairwise cross correlation procedure must be replaced by truly joint array processing.

The processing extensions demanded by these conclusions are described briefly in this section, and in greater detail in section 6.

The processing of section 2 relies upon the Haar transform to detect transients through their alteration of the local mean, and at that range (5 km) the procedure appears successful. Application of the Haar transform to the 11 km data however, indicates that this feature is not

sensitive enough to serve as a reliable detector. Fig. 5.1 shows the application of the sequency 4 Haar transform to the raw data of event #38. It is clear that the number of false alarms is too great. (It should be noted however, that the 11 km air wave remains processable by the Haar method).

A signal, however, is seen to appear in the region bounded approximately by the vertical lines. This region occurs at about 13 secs after firing and corresponds to a group speed of about 850 m/sec. The zero crossing rate indicates an instantaneous frequency of about 4 Hz, and according to Appendix C this wave could therefore contain Love and Rayleigh components. The vertical channels exhibit significant correlation (esp. channels 6 and 27) which tends to strengthen the possibility of Rayleigh wave (denoted "R-wave) activity. The strongest signals at 5 km are thought to be Love waves (denoted "G-wave"), and this 11 km possible R wave therefore, indicates a further investigation of the 5 km vertical channels may sharpen the results there. The raw data corresponding to this Haar plot is presented in Fig. 5.2. The region within the vertical lines of Fig. 5.1 corresponds to about 18.5 sec on this Fig. 5.2. Again it is seen that packets are arriving in this interval (clearest in channels 13, 14, 15).

In the event these disturbances are howitzer induced R-waves the processing gain would be improved by rotation of the data to the approximate bearing followed by joint



processing of the longitudinal (with respect to the wave front) and vertical channels. The transverse channel would contain G-wave activity. IAR has not carried out this operation because final justification of the R-wave hypothesis would require that more 11 km events be surveyed, in order to eliminate the possibility of seismic noise generated locally to the array. It should be noted however, that the IAR propagation model is most accurate on Rayleigh waves. For this reason the issue deserves further exploration.

This observed R-wave possibility has led IAR to examine the possible existence of higher frequencies in the data. The rationale here is that, depending on the geology, R-waves may travel shorter paths than G-waves of the same frequency and consequently may be attenuated less. If this is so, the increased bandwidth (expected at higher frequencies) would allow more precise time estimates. In order to examine this issue, a series of power spectra were obtained using the Burg maximum entropy (auto regressive) method. Spectra were computed by this method on successive 512 point blocks of the raw data. The auto regressive model employed 64 coefficients which is sufficient to give good spectral resolution for frequencies above 2 Hz.

The results of this processing are illustrated in Figs. 5.3 through 5.29. These are graphic reproductions of computer generated printer plots which are too bulky

to include here. The originals are on file at IAR. The dashed curves denote ambient noise spectra before the howitzer firing. (In each case the block chosen is #3). The solid curves denote spectra after the howitzer firing corresponding to a portion of the signal region in Fig. 5.1. (In each case the block chosen is #13 beginning about 18 secs. after firing). Figures 5.3-5.11 are vertical channels; 5.12 - 5.20 are E-W channels; and 5.21 - 5.29 are N-S channels.

A number of observations can be made from these spectra:

- (1) Signal is appearing on all phones and all channels in the frequency regions 3-5 Hz and 20-25 Hz.
- (2) The ambient is also strong in the region 3-5 Hz.
- (3) The ambient is weak in the region 20-25 Hz. therefore the SNR ratio is good in this region.
- (4) The vertical channels appear especially strong in the high frequency region although the peak fluctuates in frequency somewhat more.

These observations lead to the following conclusions:

- (1) Rayleigh waves are probably being received at approximately 20-25 Hz.
- (2) Simple processing methods may be effective on these waves due to the good SNR.
- (3) The region 3-5 Hz shows promise but will require sophisticated processing to extract the signal from the noise. These methods may be required to utilize jointly (rather than pairwise) all array data; may require adaptive whitening; and possibly joint processing with the Rayleigh wave at 20-25 Hz.



The processing visualized as appropriate for the low frequency band is given in section 6. IAR has begun to implement this processing.

Before closing this section, it should be remarked that the spectra of Figs. 5.3 through 5.29 are almost certainly not as sharp as could be obtained. The spectra are computed from certain arbitrary choices of block size and bin width. The processing of section 6 is largely independent of such choices. Moreover at high frequencies then remains the possibly of poor ground-geophone coupling.

Finally we present a Fig. 5.30 which is pertinent to section 6. Classical theory of detection in colored noise entails whitening the background spectrum before performing any correlation analysis. Since the ambient spectrum is not known a priori, and in any event varies somewhat, the most-appropriate prewhitening technique is the adaptive autoregressive technique. (This technique also provides the foundation of the above mentioned spectral line tracking to be presented in section 6). For future reference, Figs. 5.30a and 5.30b illustrate the effect of this adaptive whitening operator.

A nine coefficient operator is employed here and is not expected to be able to whiten the low frequency lines. However, it can be seen that the filter does render this data more nearly white. Theory indicates that any pure line will not readily be whitened by this filter. Also the adaptation time of the filter has been chose to correspond to the time scale on which the ambient spectrum

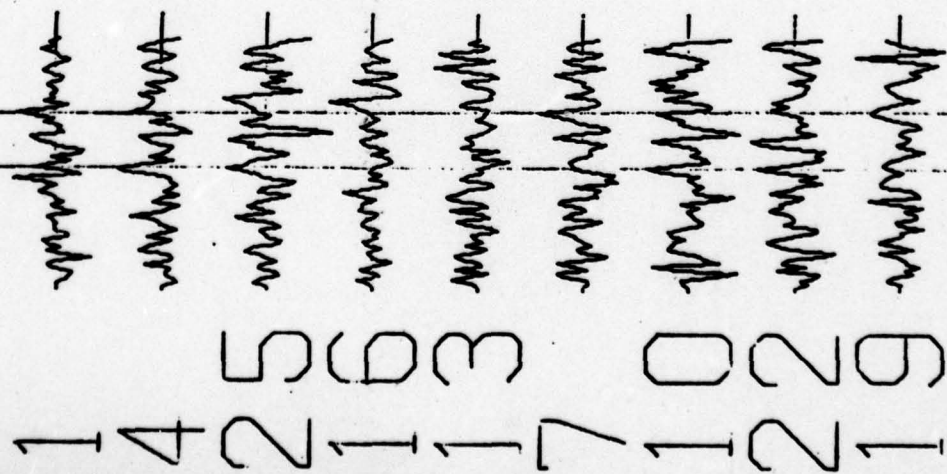
is changing, and not to that on which the signal transient makes its appearance. Therefore, it is to be expected that this filter will successfully sharpen the results of the correlation analysis on any data containing packets of small spectral width.



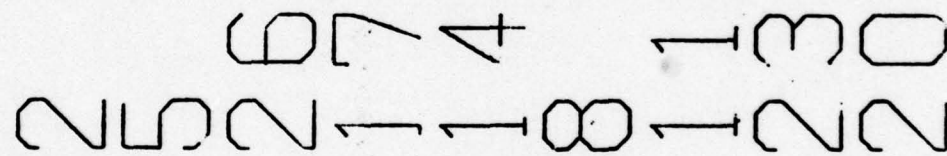
0



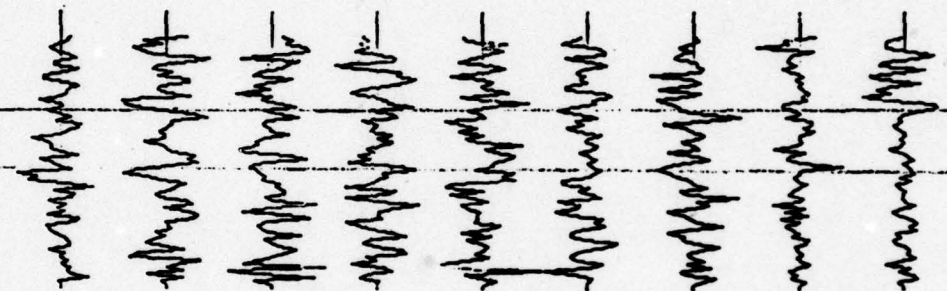
1 4 2 1 1 7 1 2 1



2 5 2 1 1 8 1 2 2



6 7 4 1 3 0



3 6 2 1 1 9 1 2 2



7 8 5 2 4 1

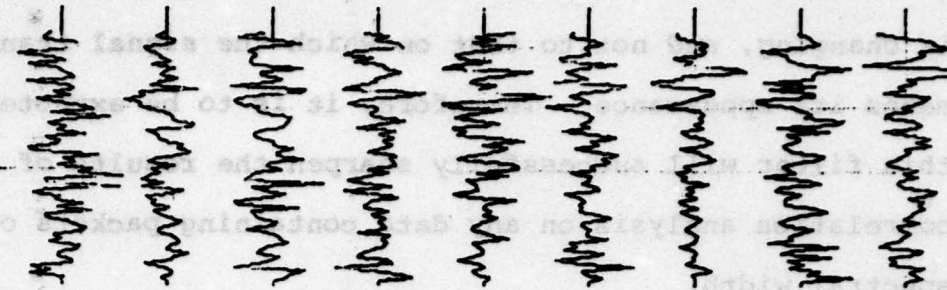


Fig. 5.1

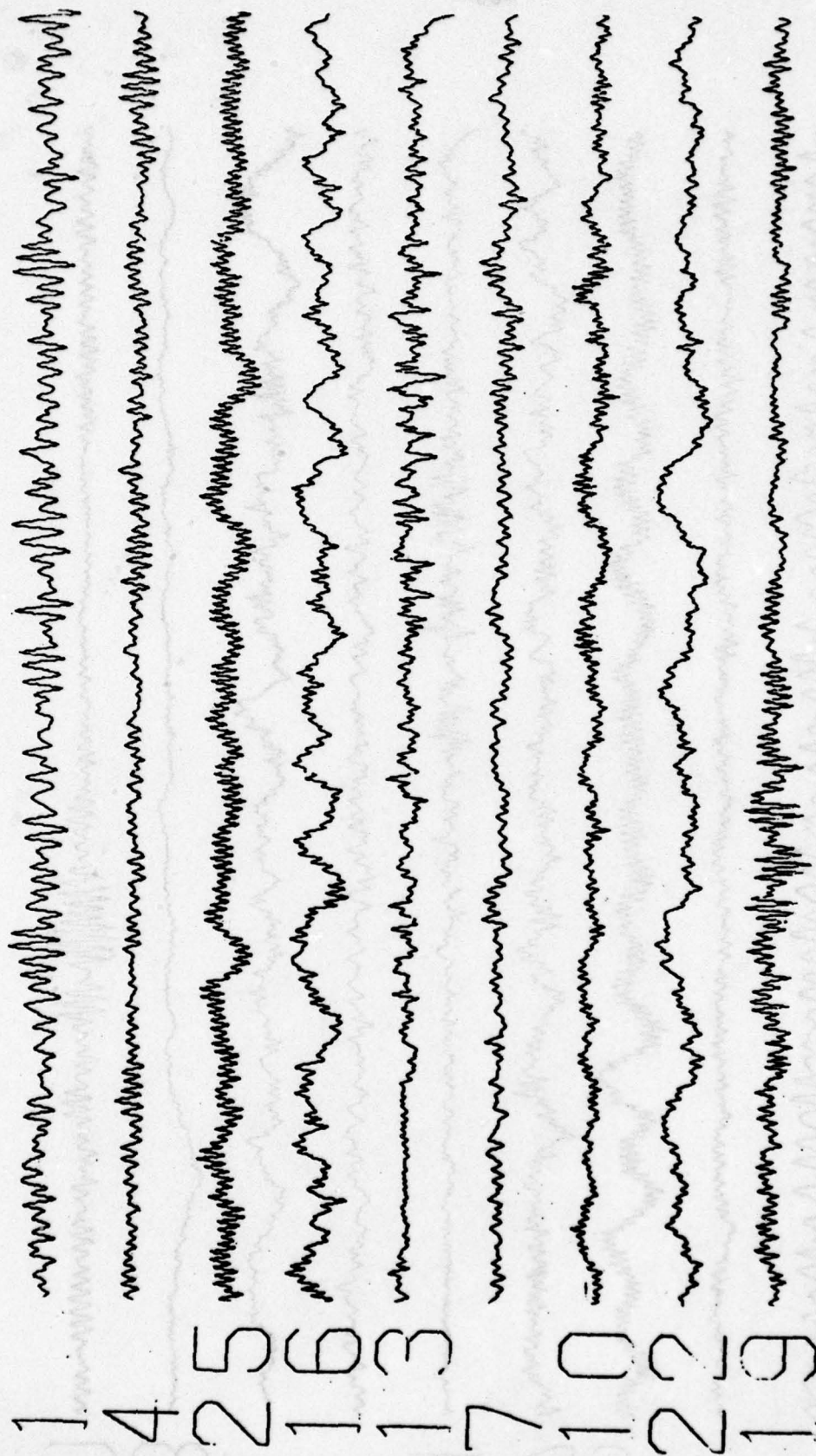


Fig. 5.2.1



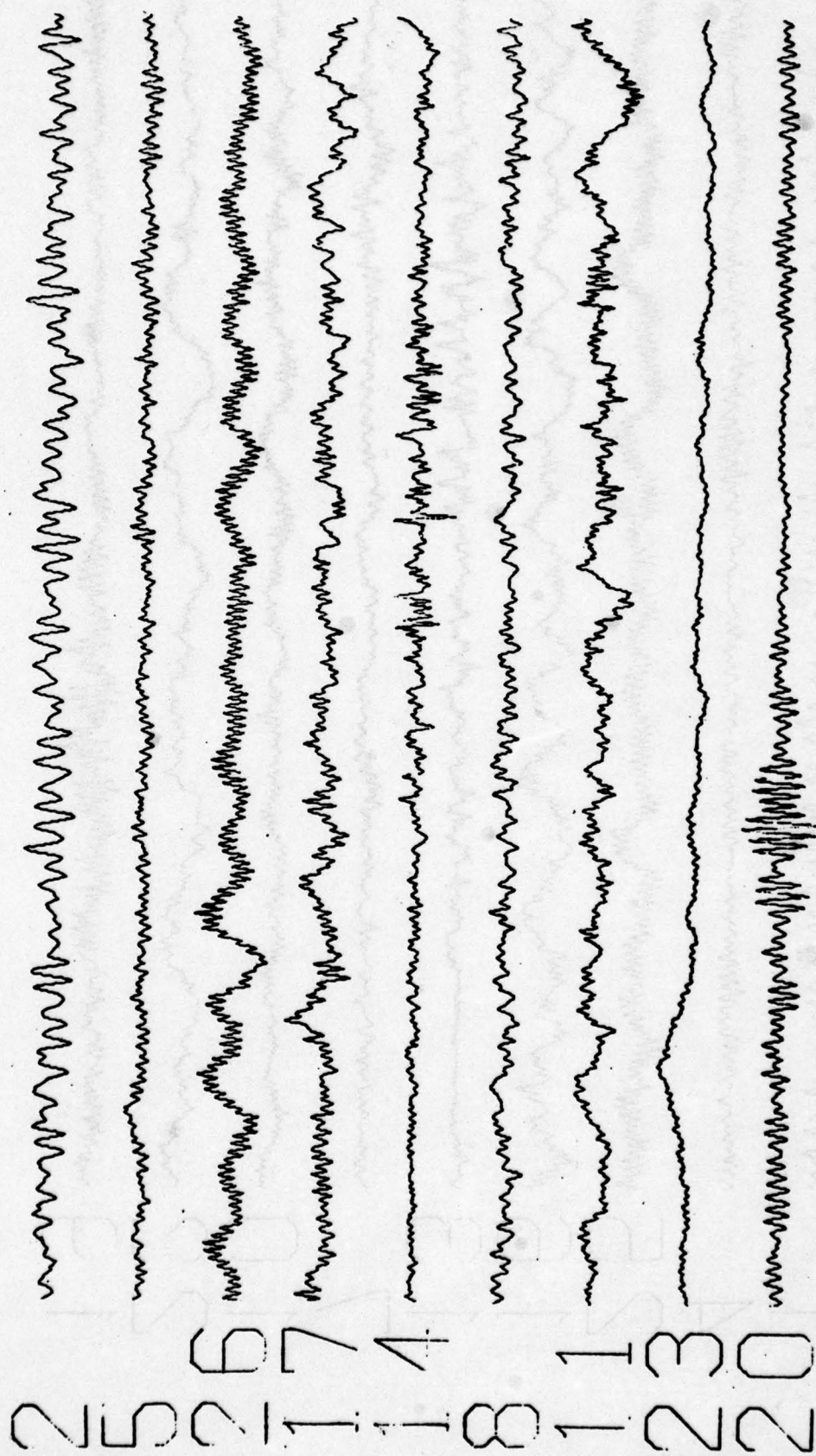


Fig. 5.2.2

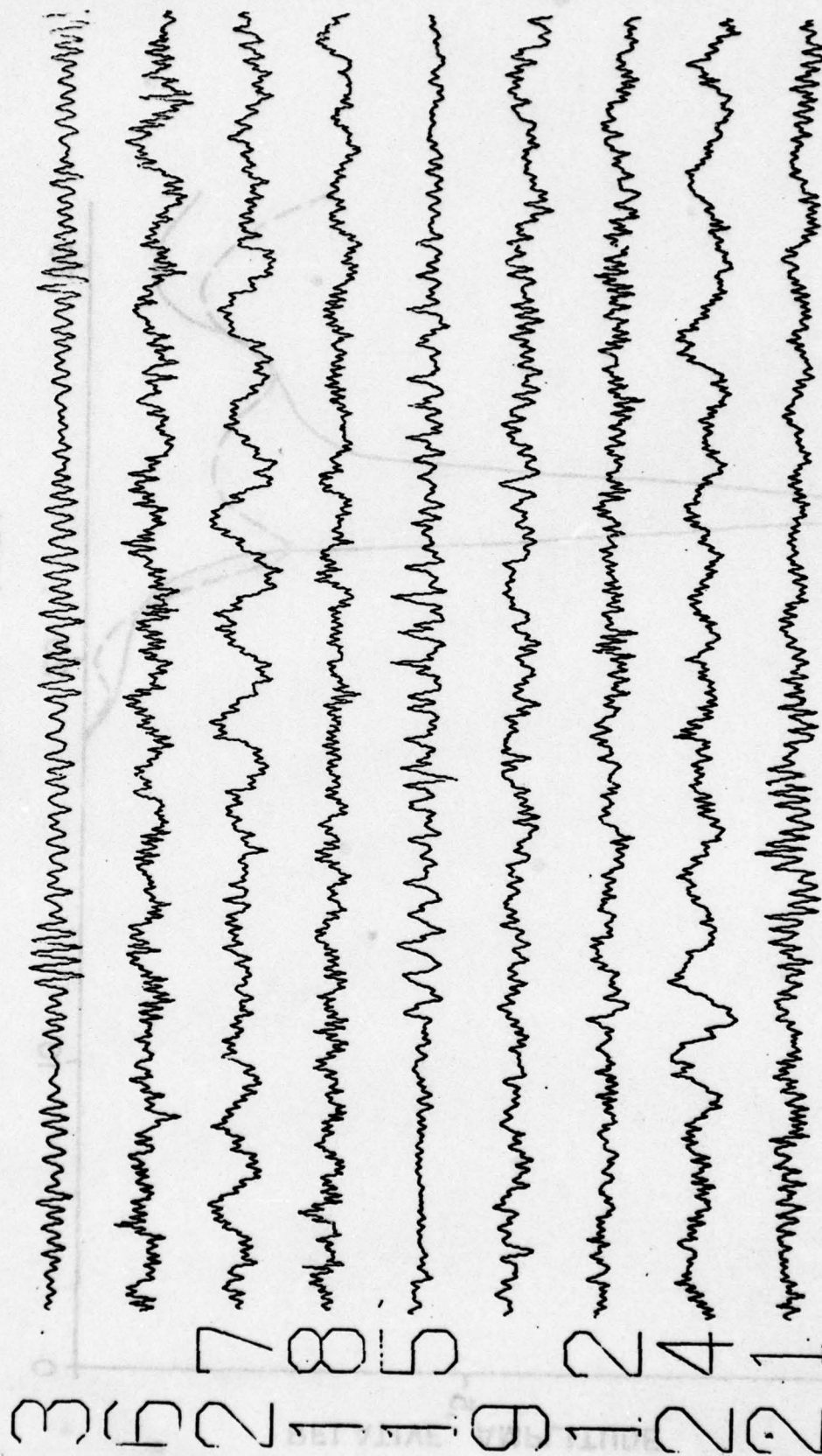


Fig. 5.2.3



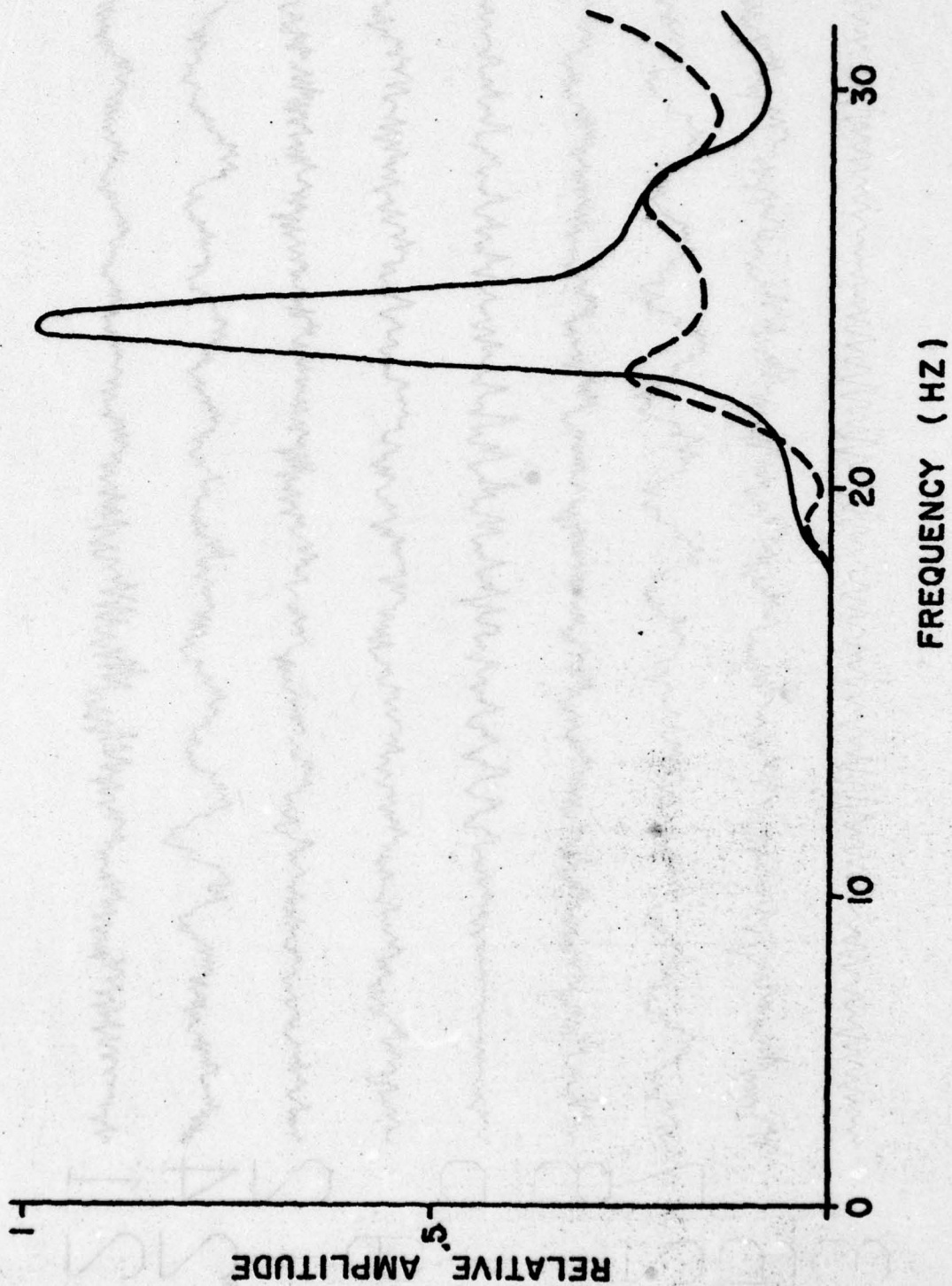


Fig. 5.3

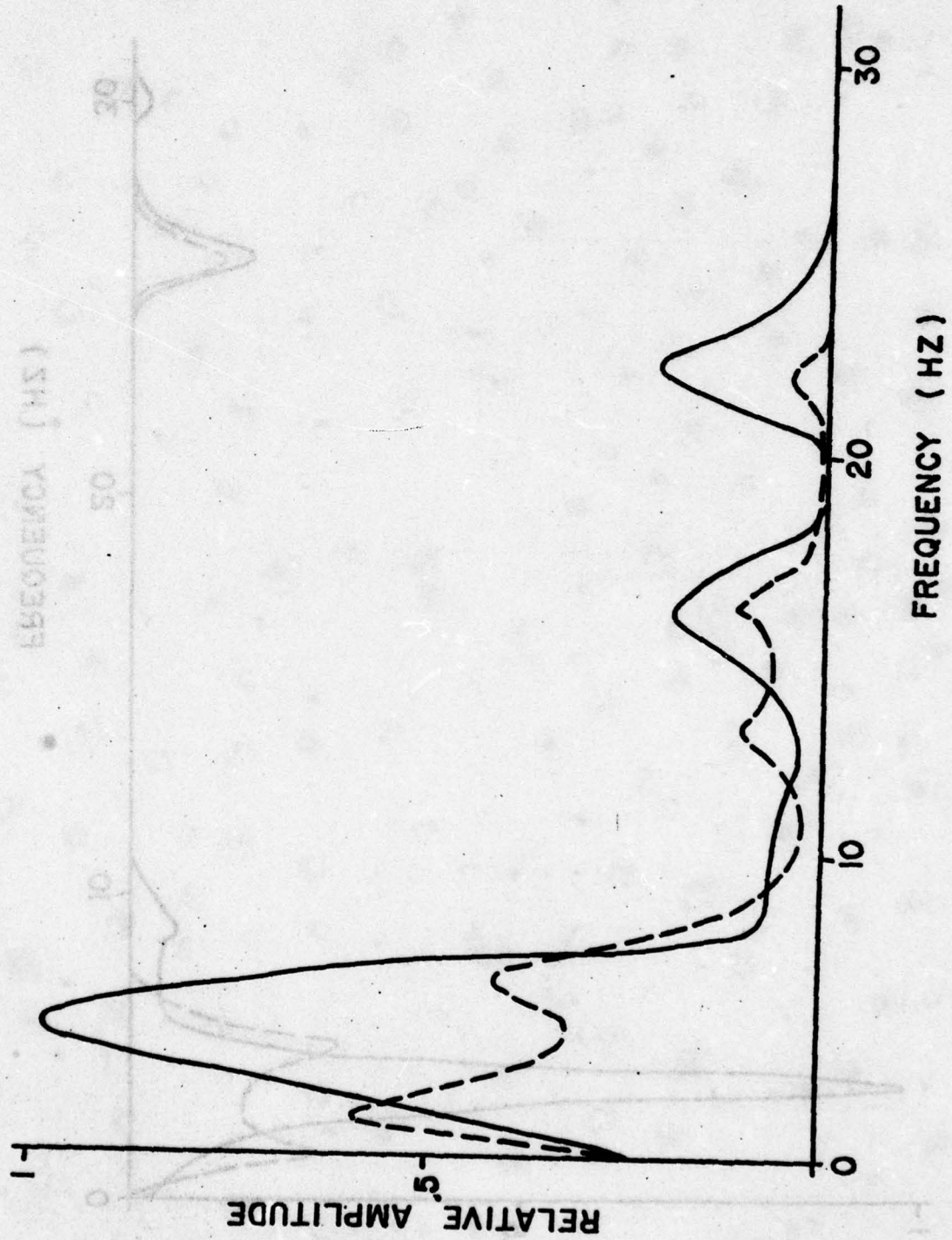


Fig. 5.4



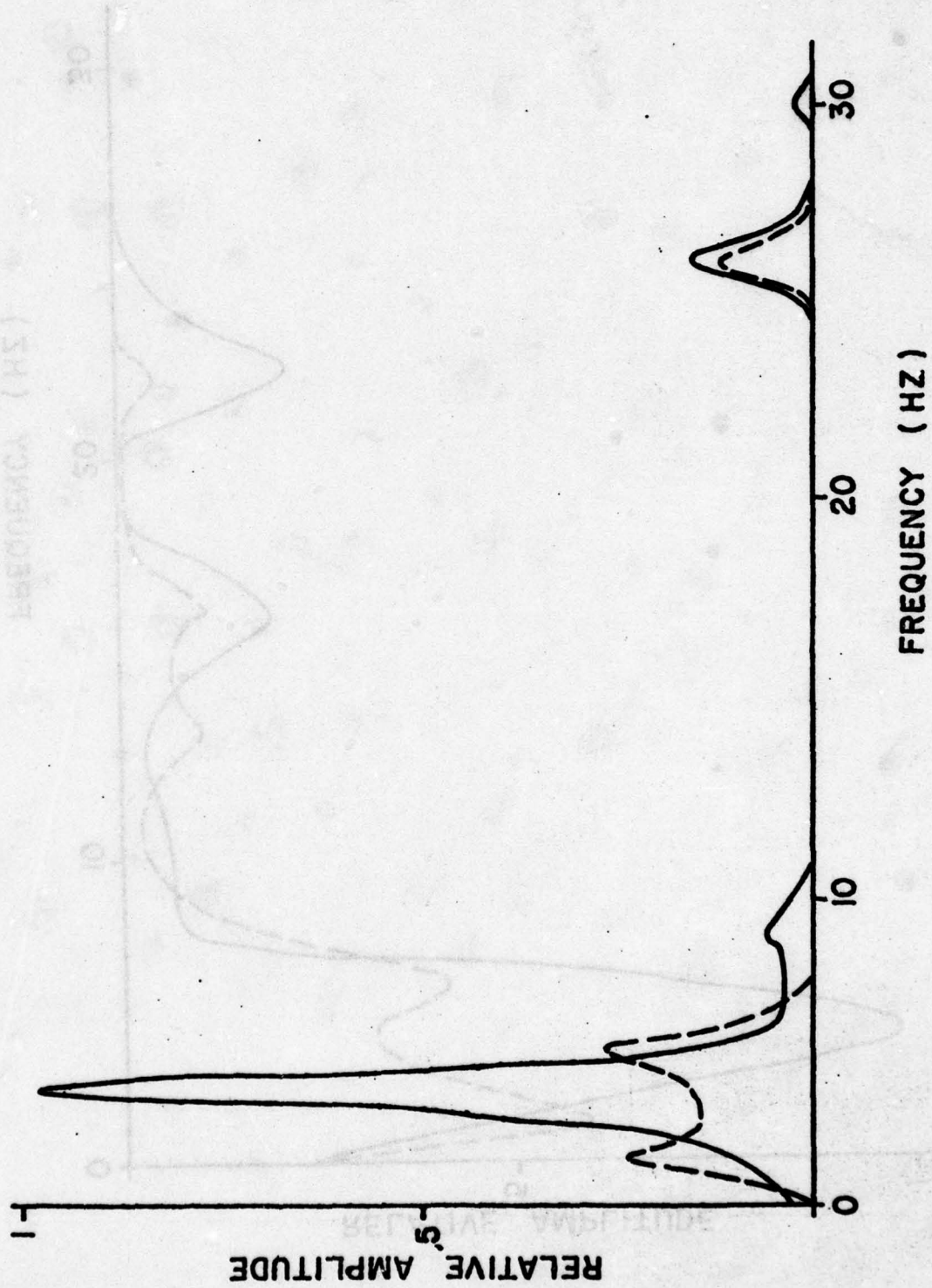


Fig. 5.5

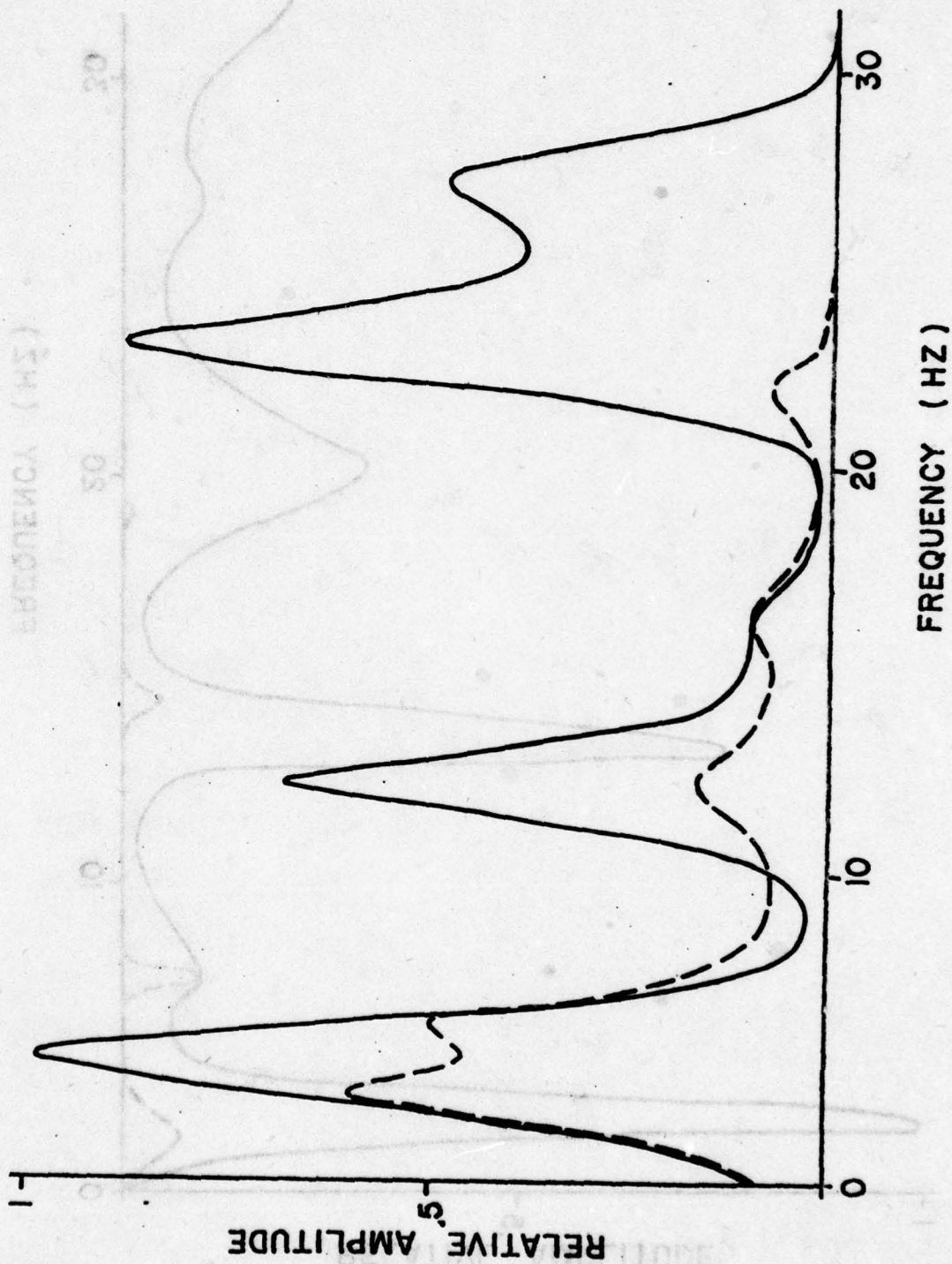


Fig. 5.6



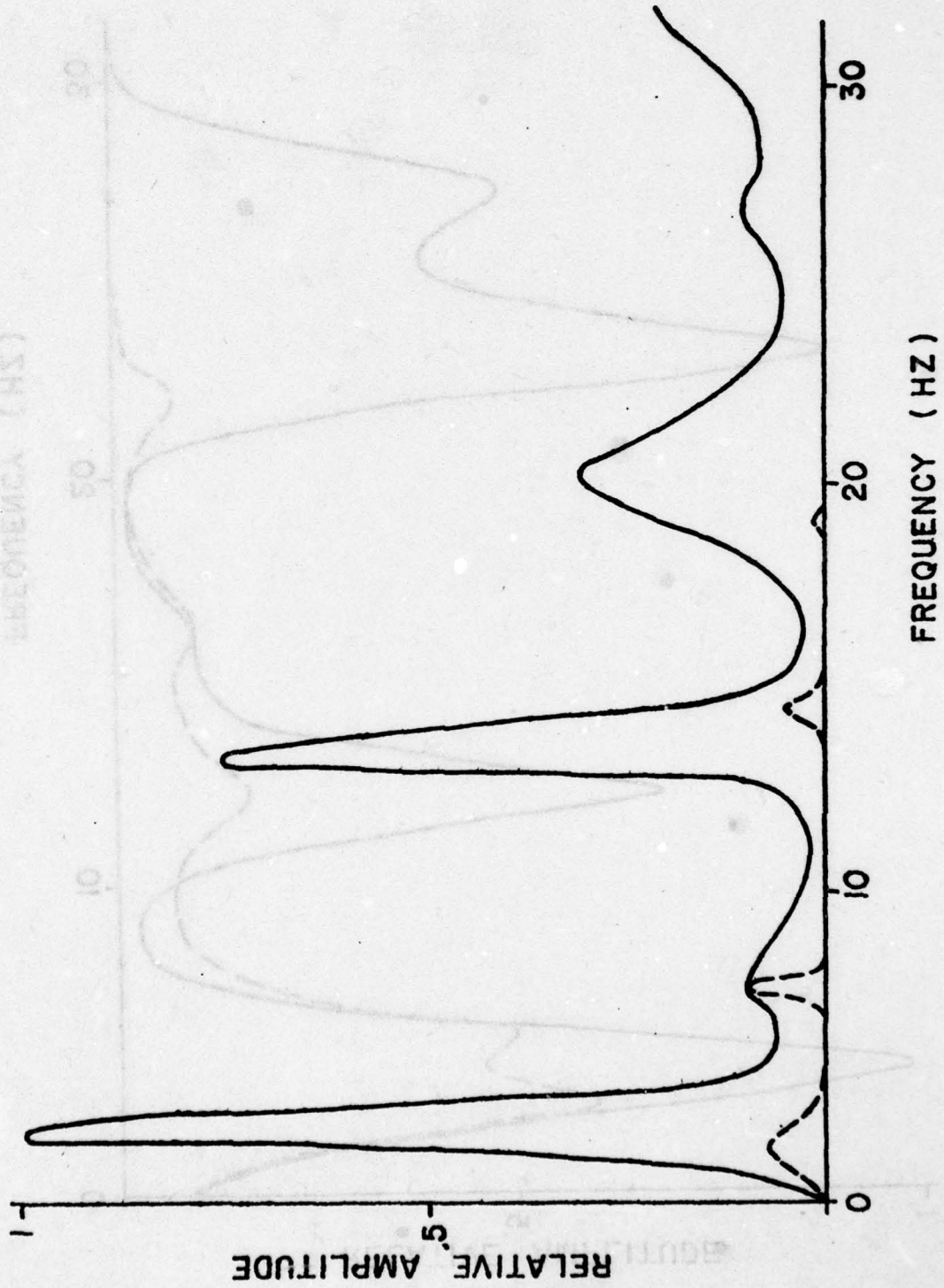


Fig. 5.7

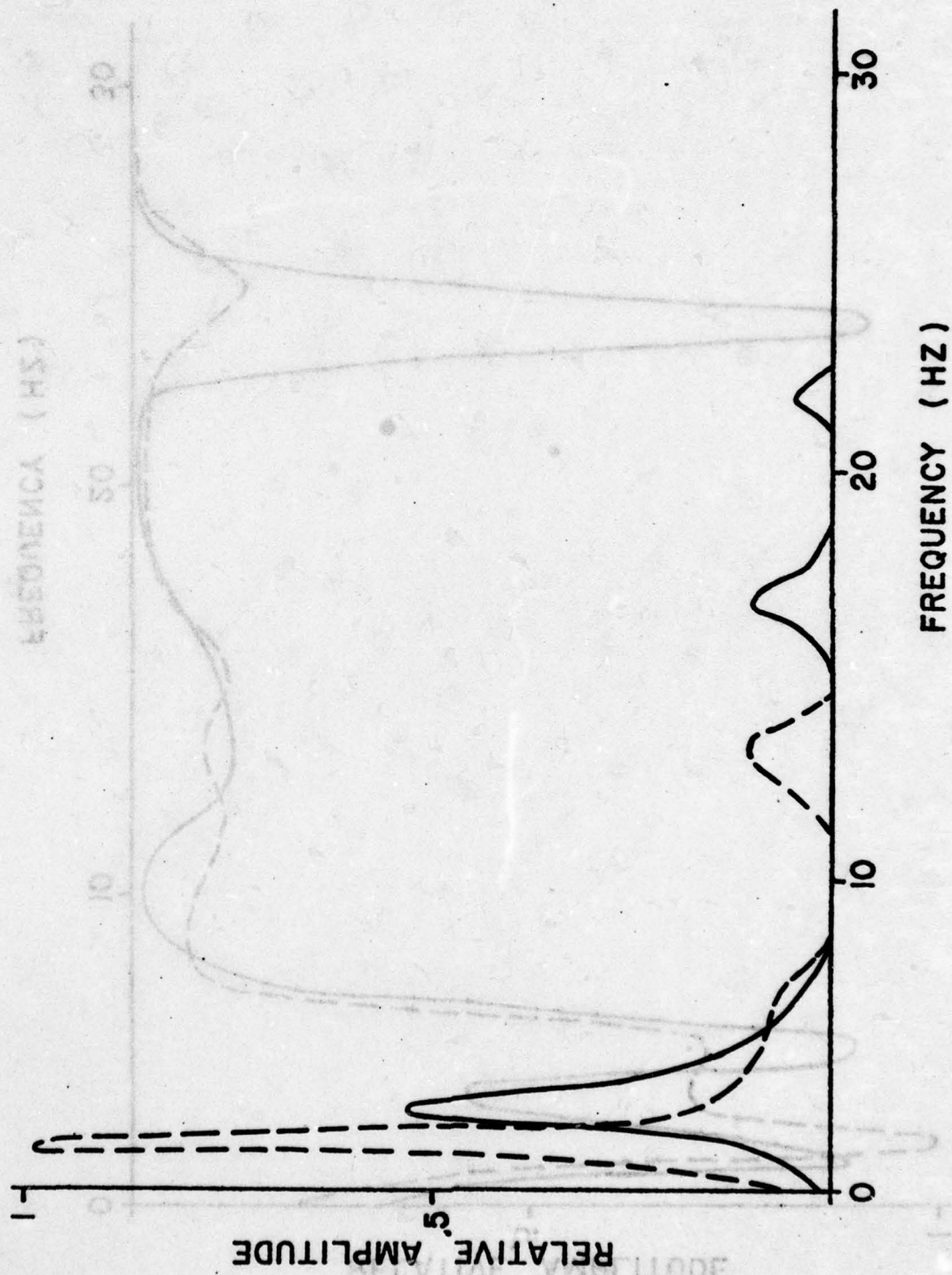


Fig. 5.8



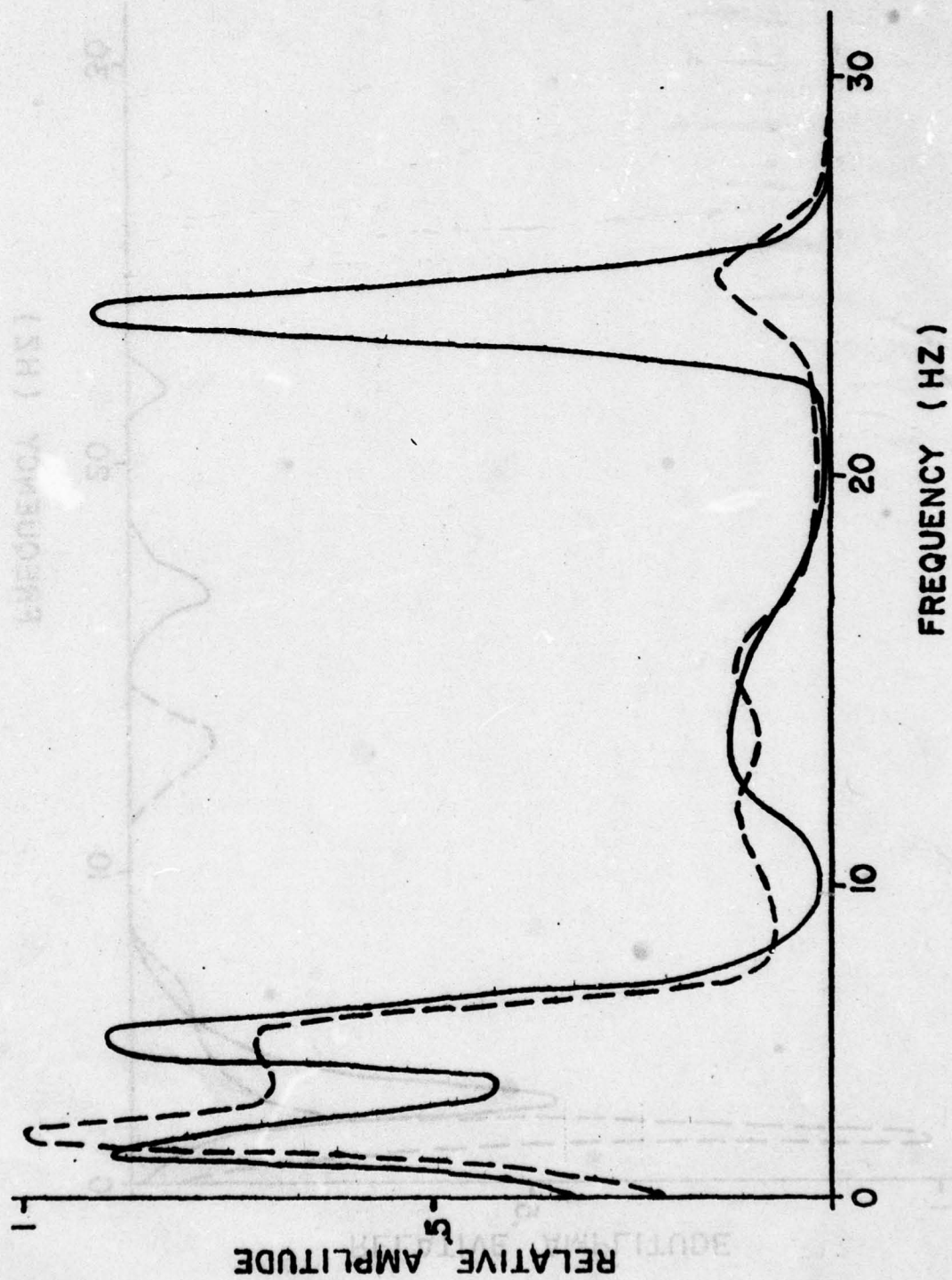


Fig. 5.9

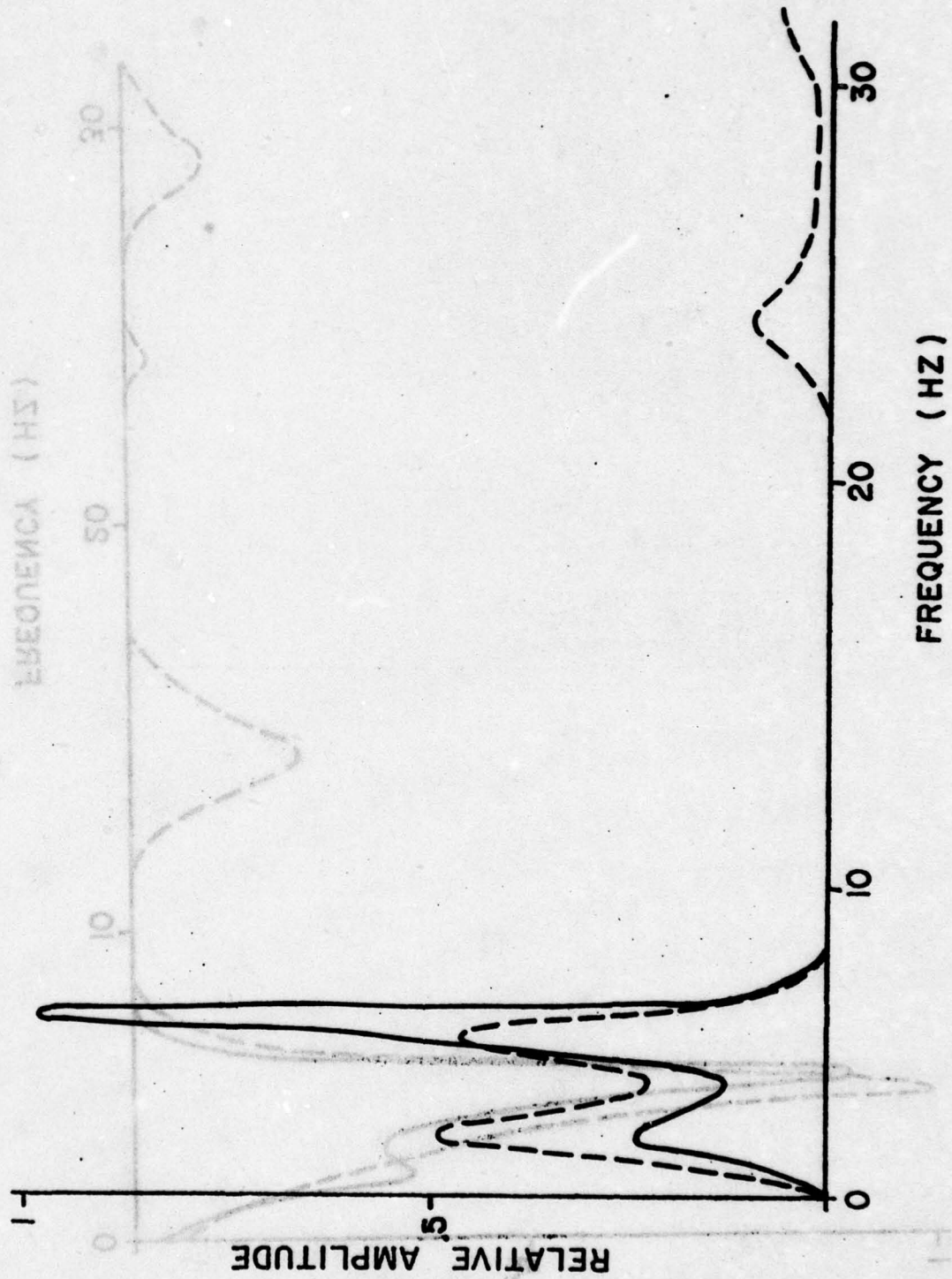


Fig. 5.10

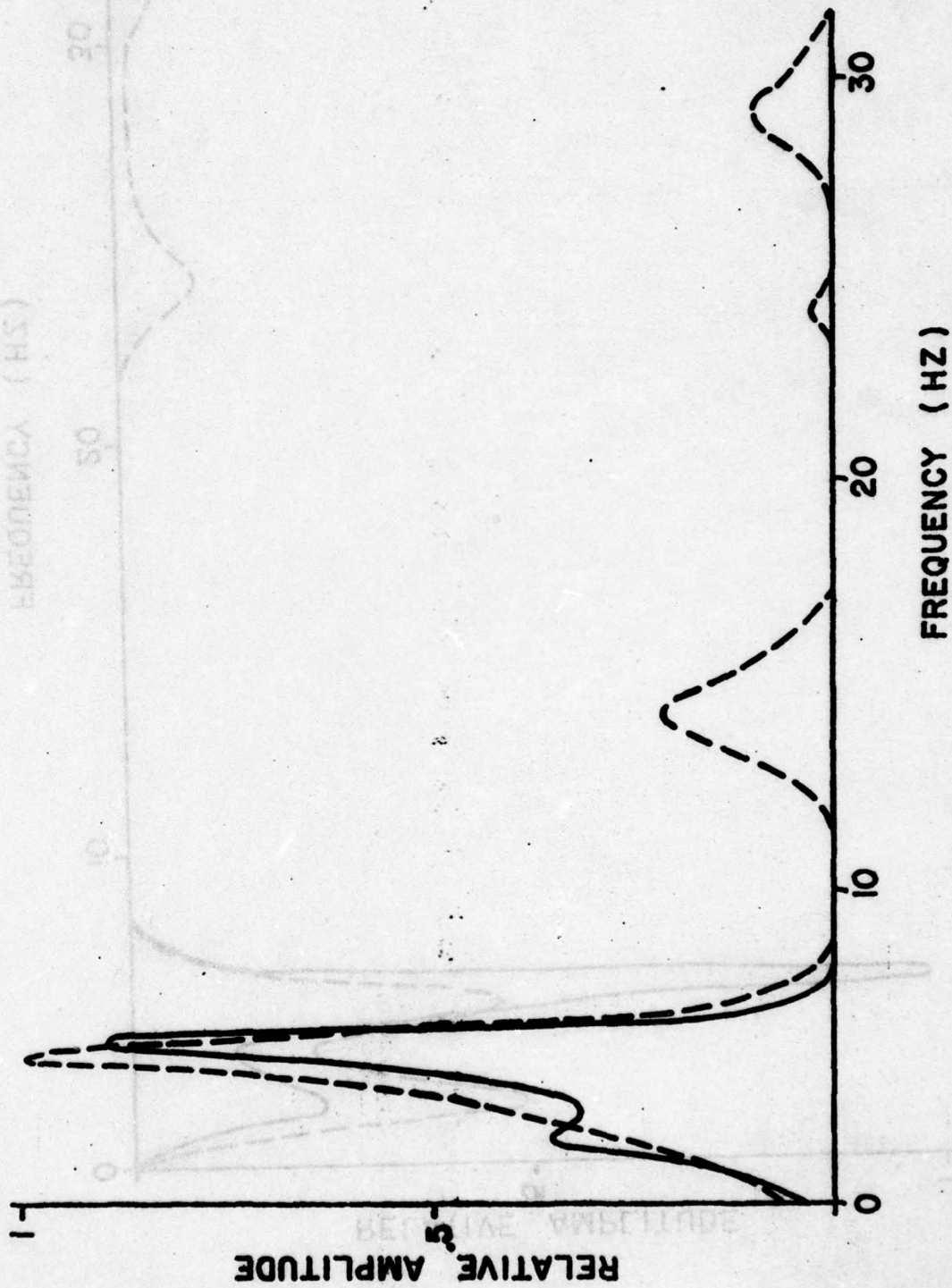


Fig. 5.11



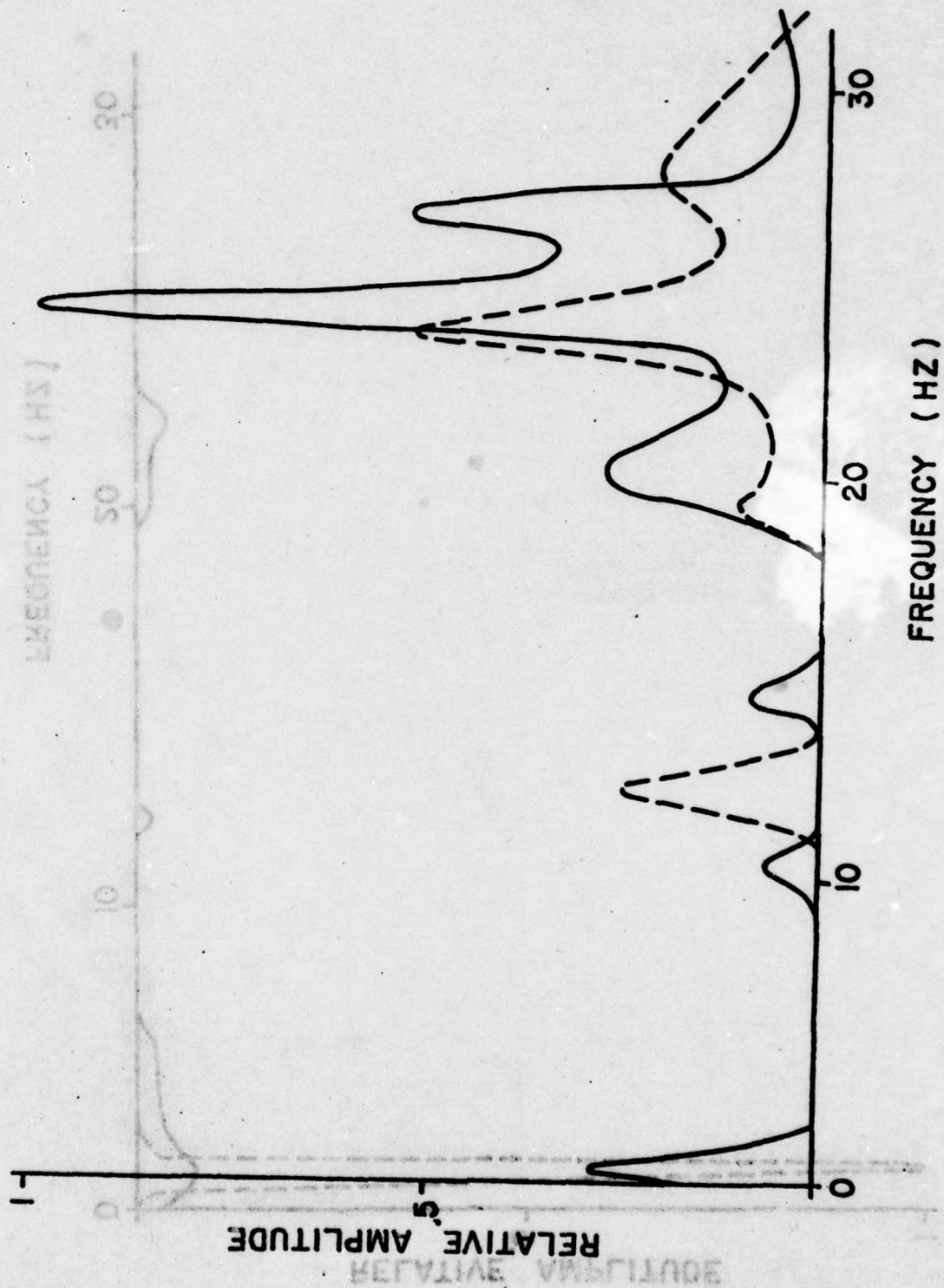
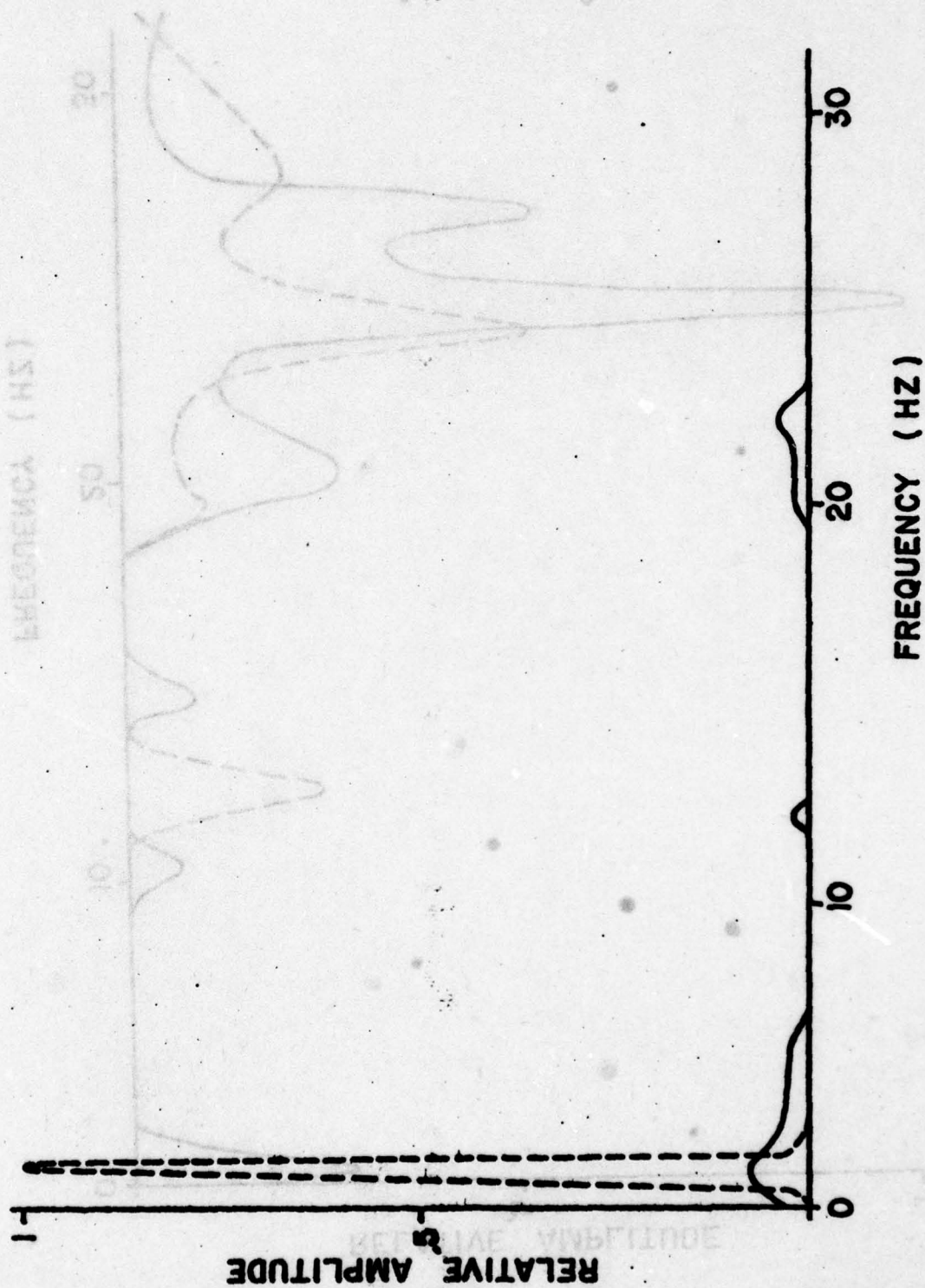


Fig. 5.12



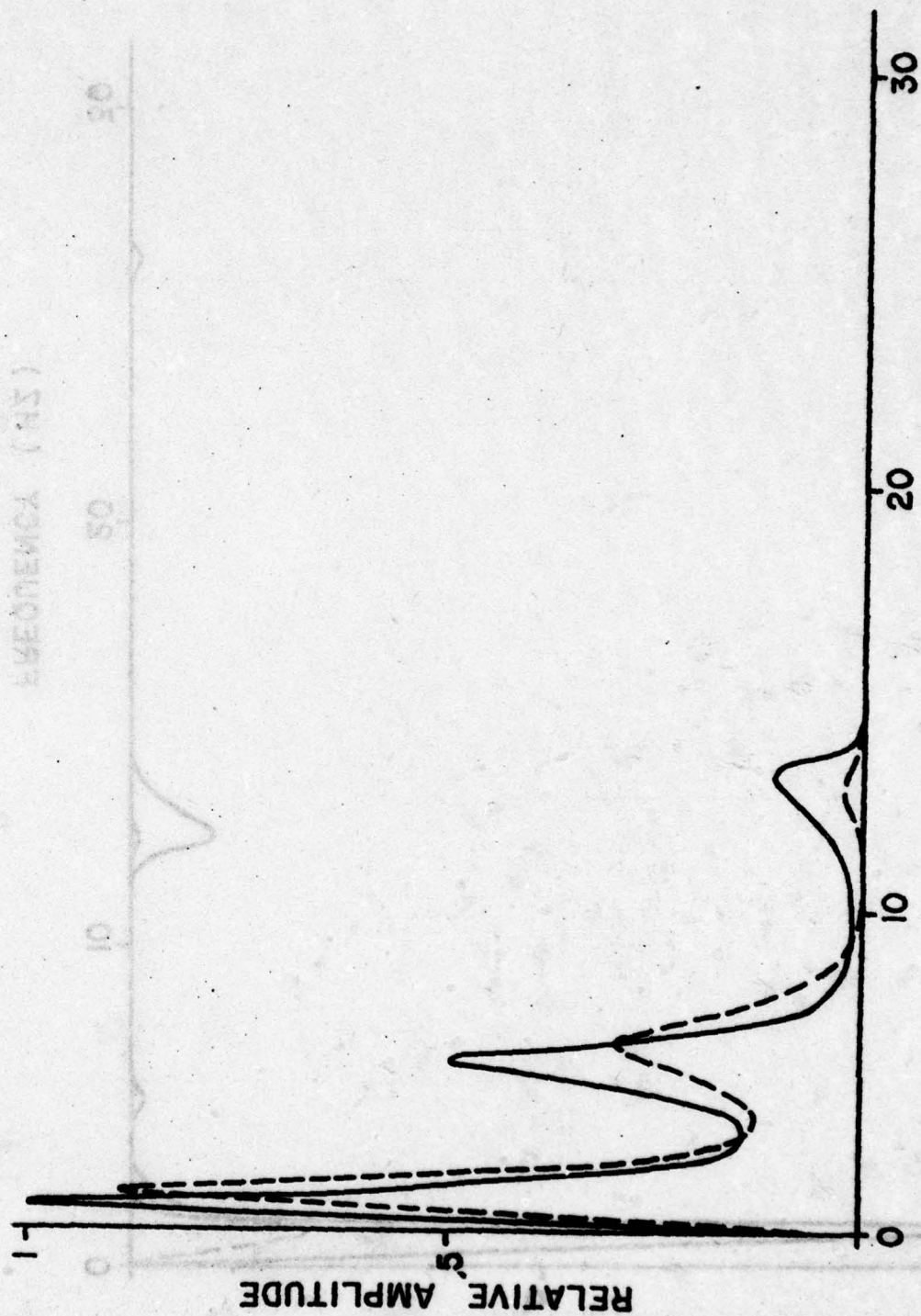


Fig. 5.14



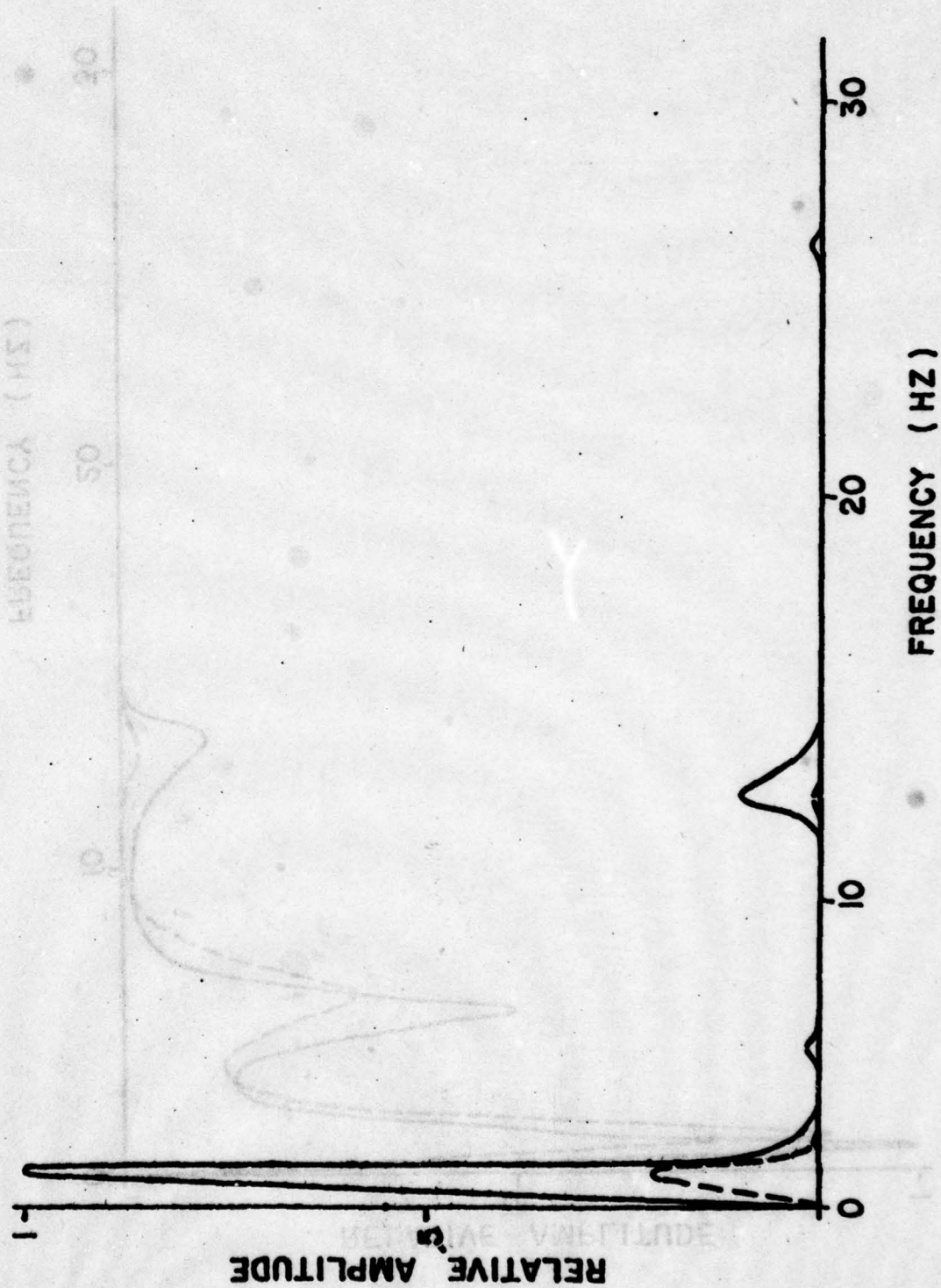


Fig. 5.15

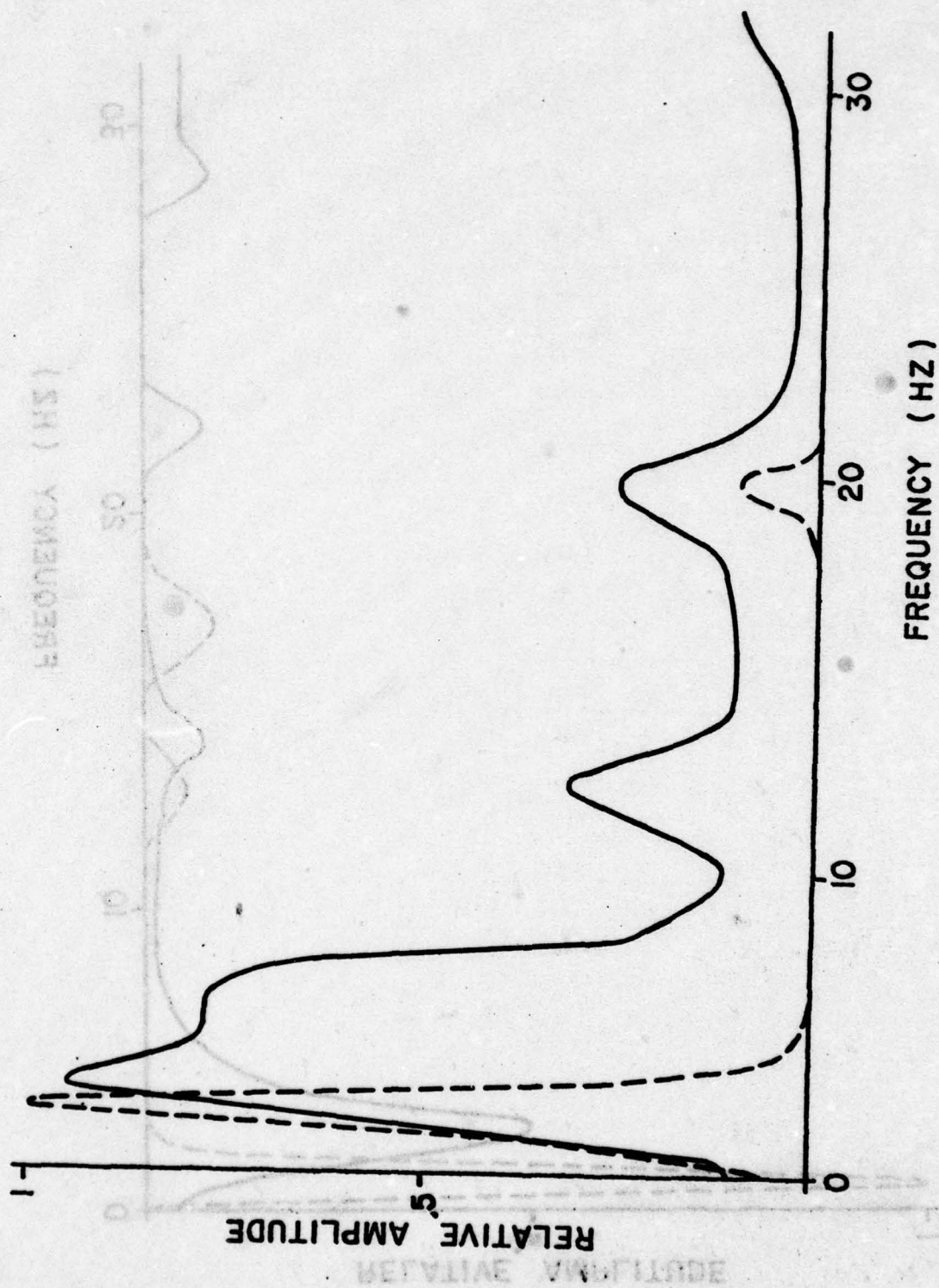


Fig. 5.16

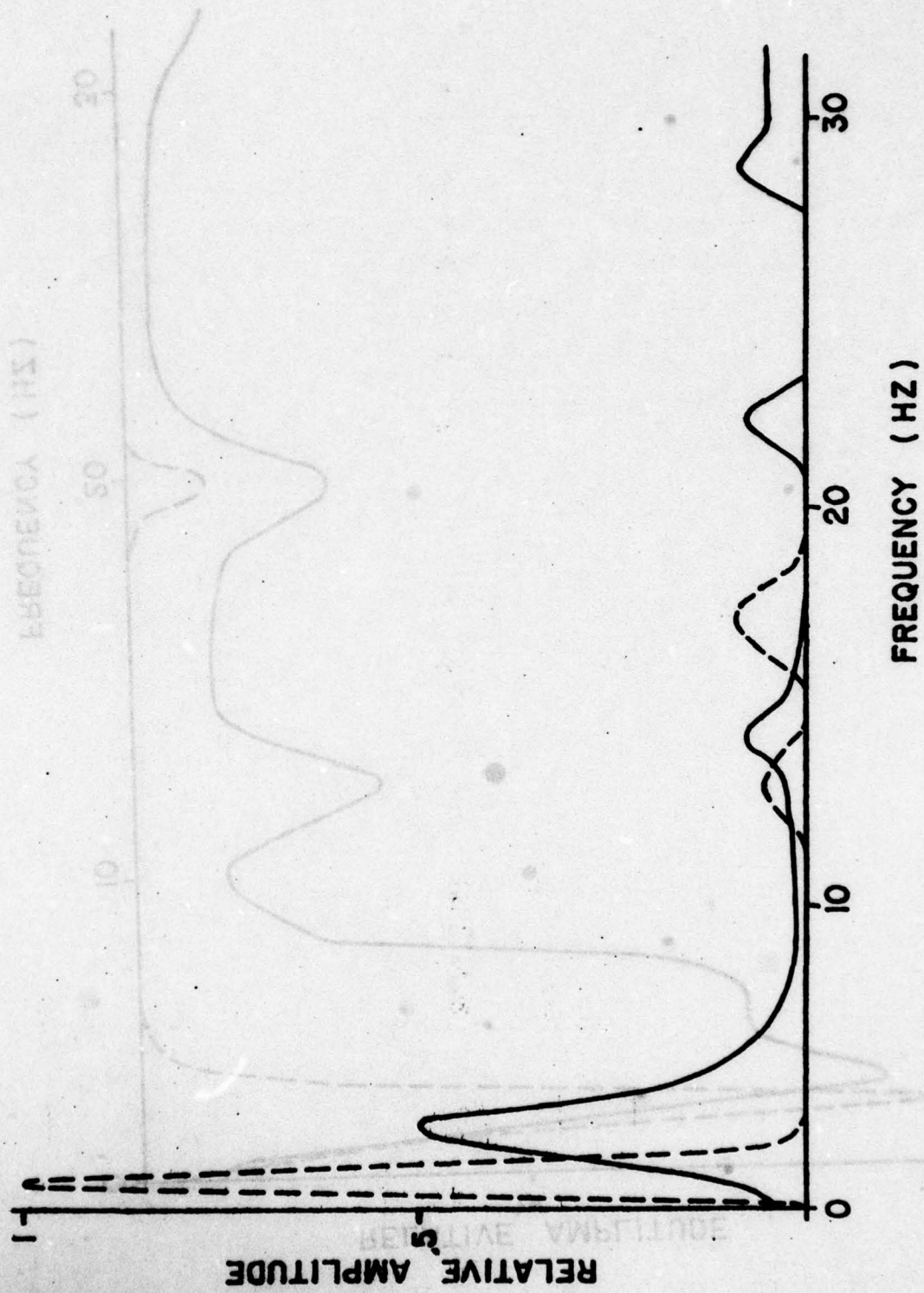


Fig. 5.17



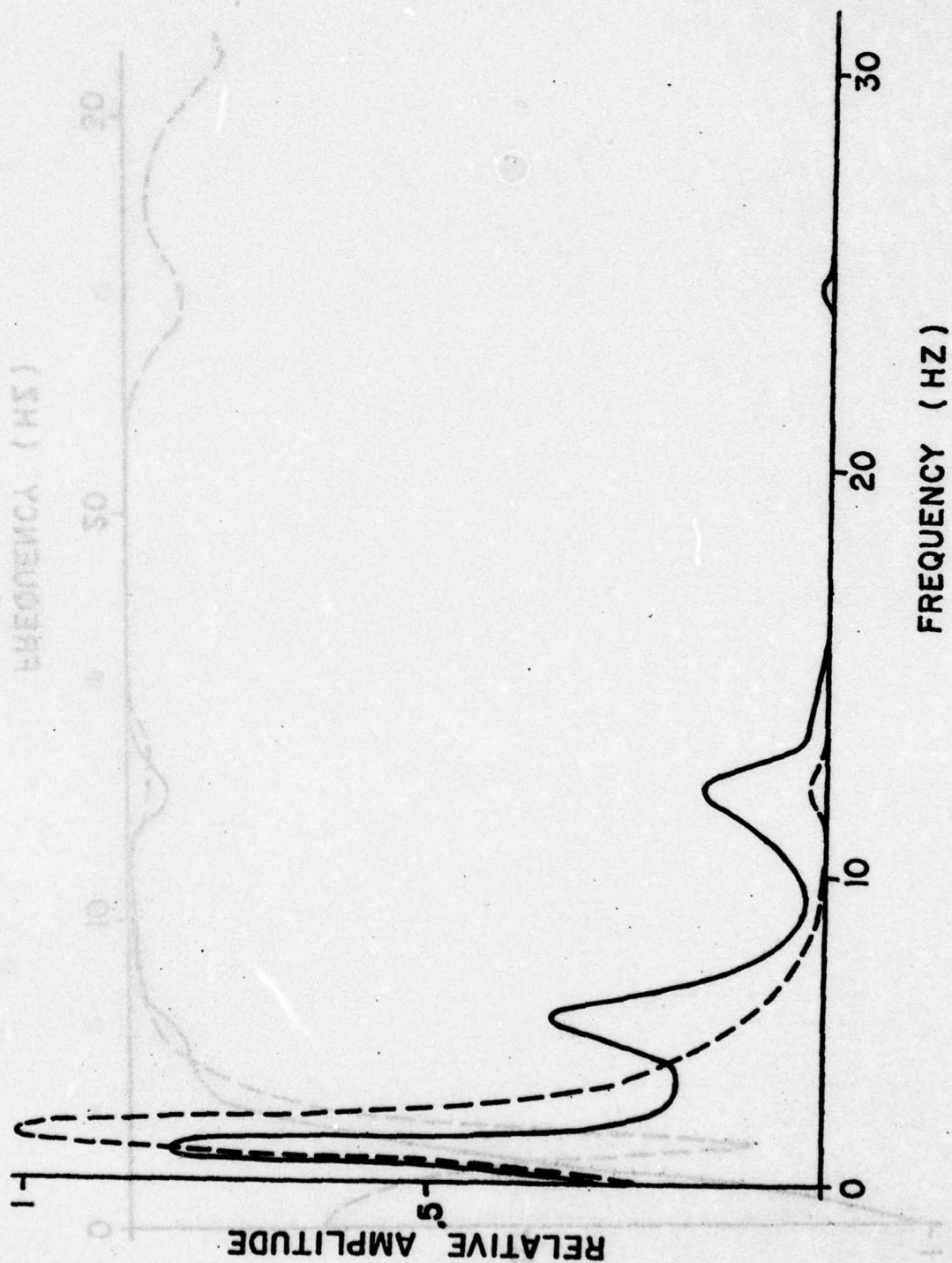


Fig. 5.18

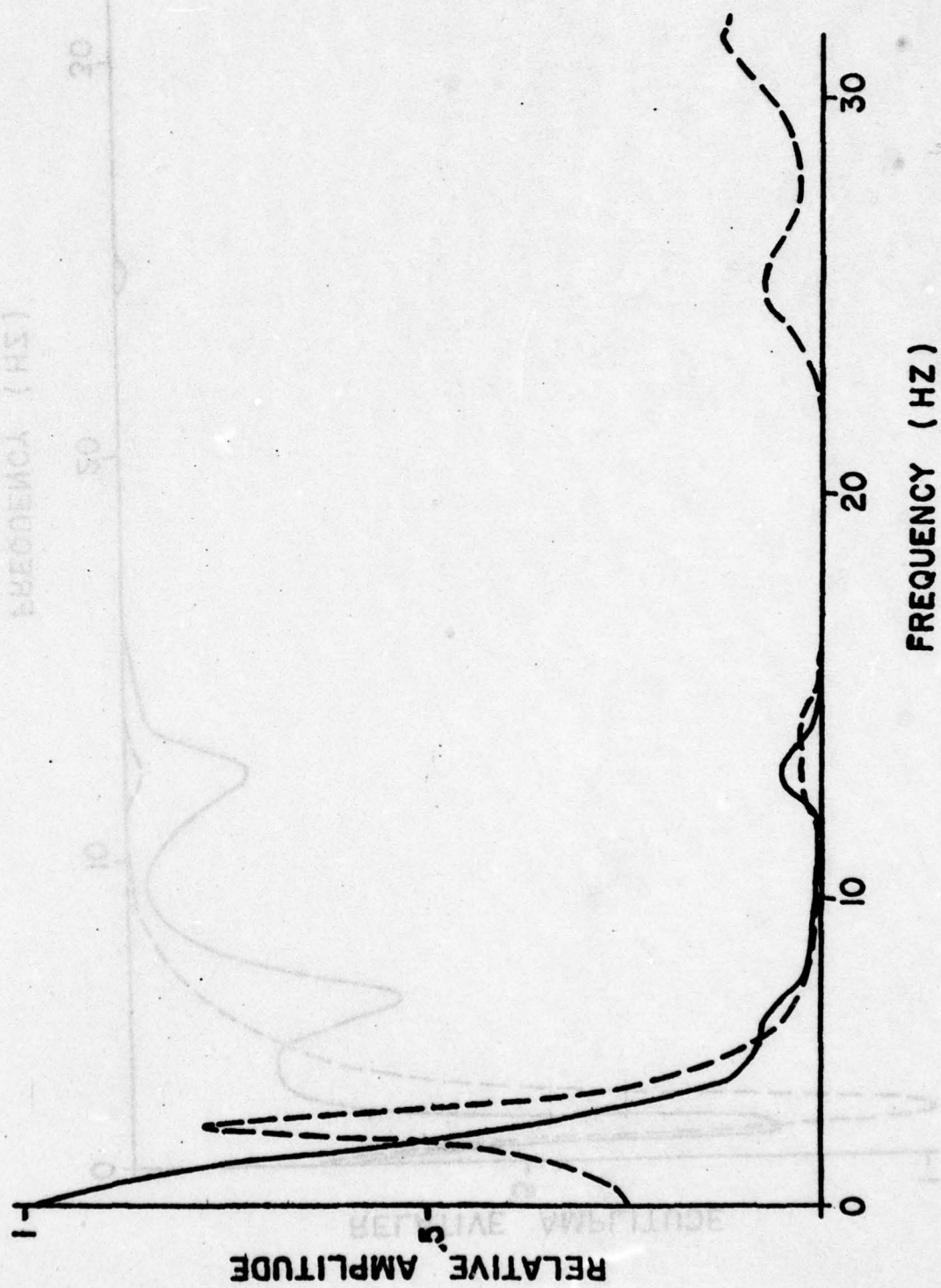


Fig. 5.19

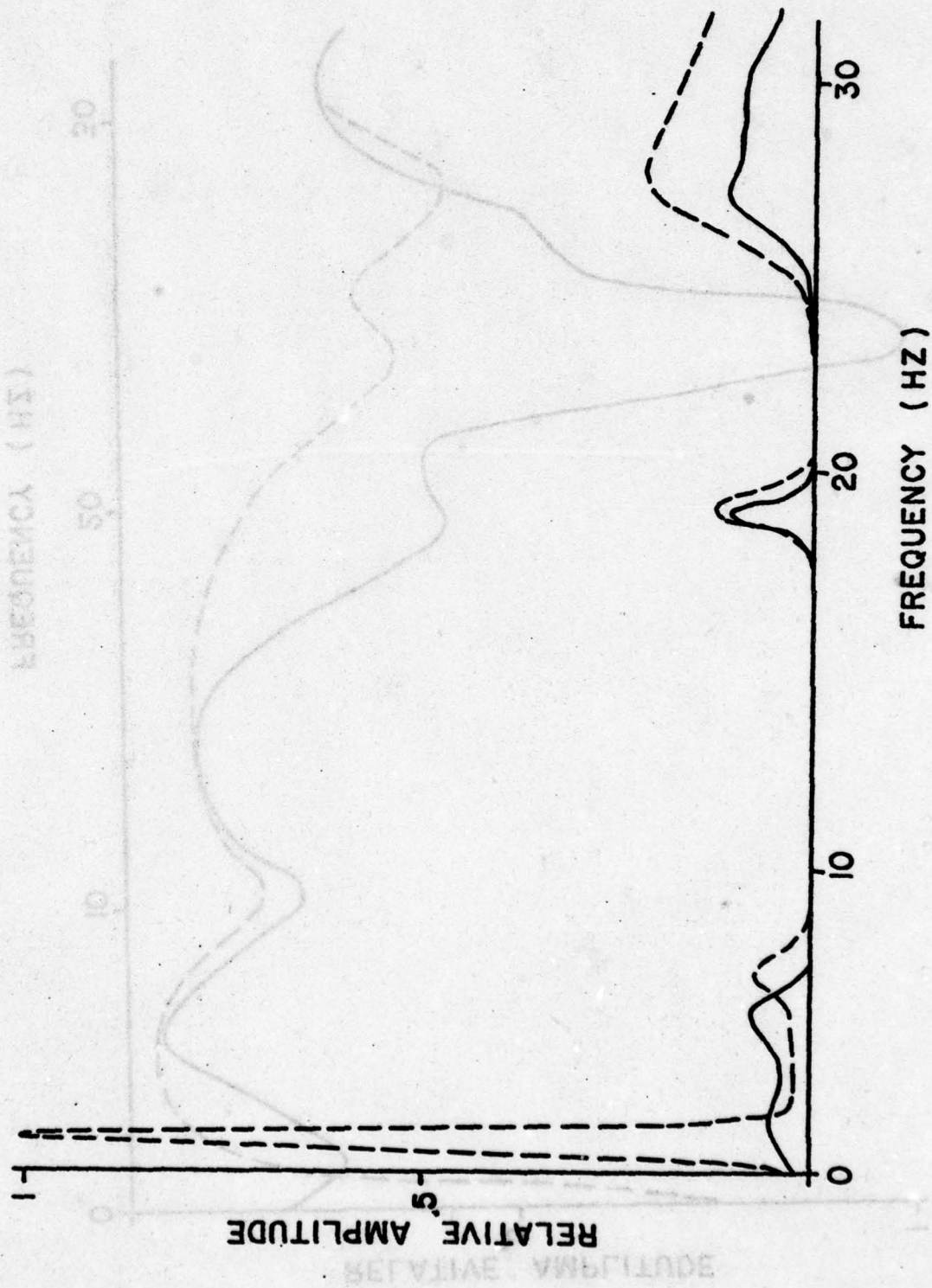


Fig. 5.20



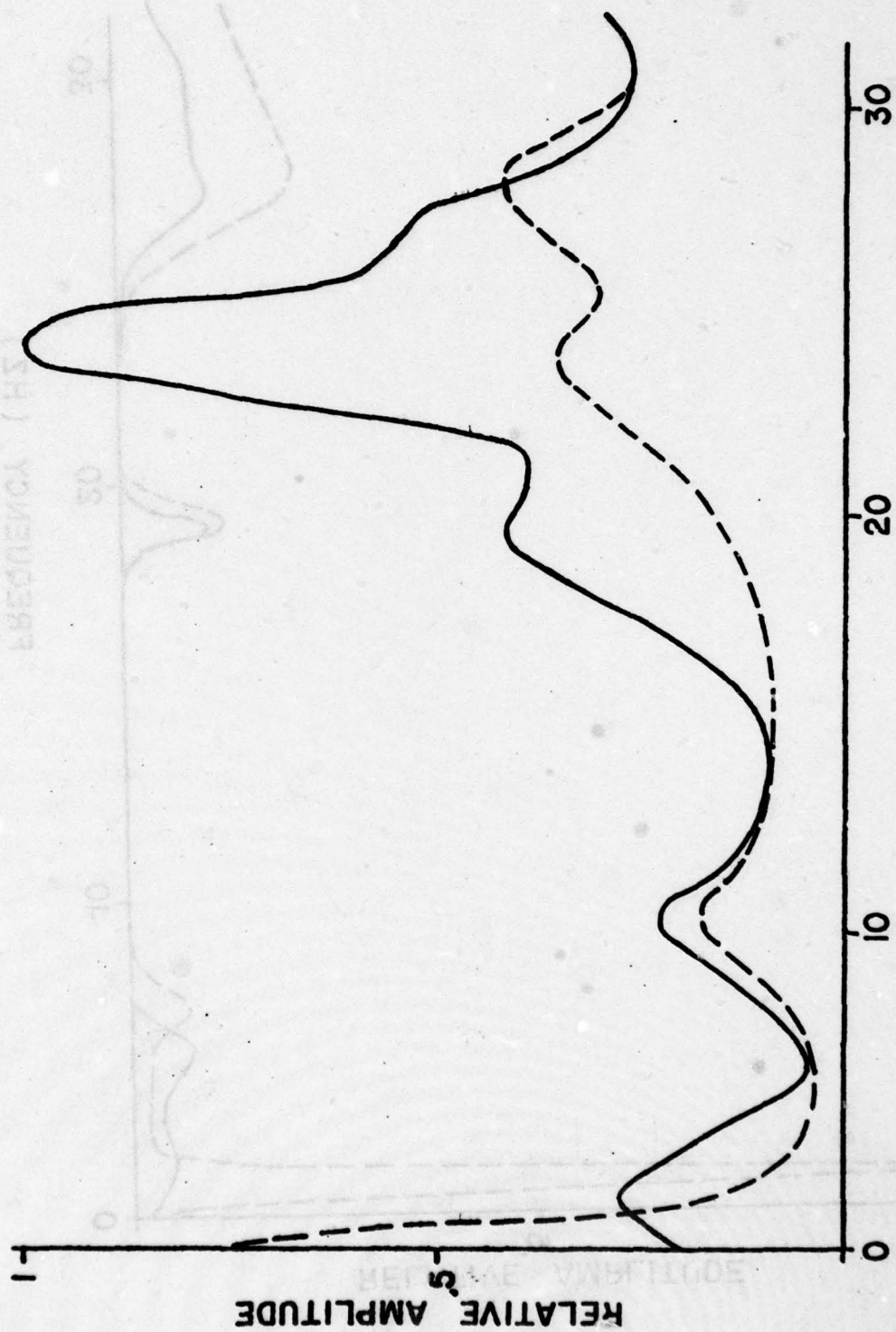


Fig. 5.21

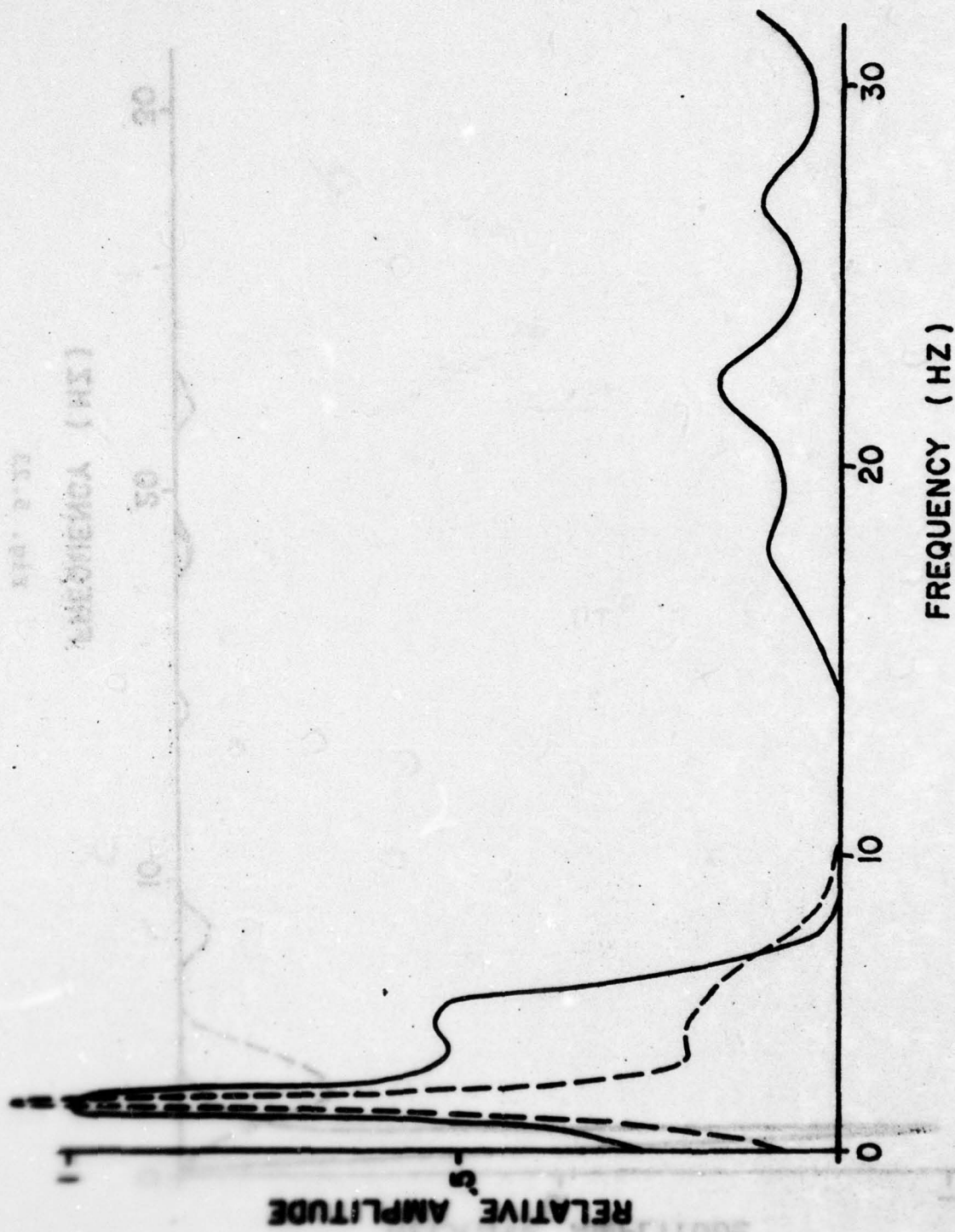


Fig. 5.22

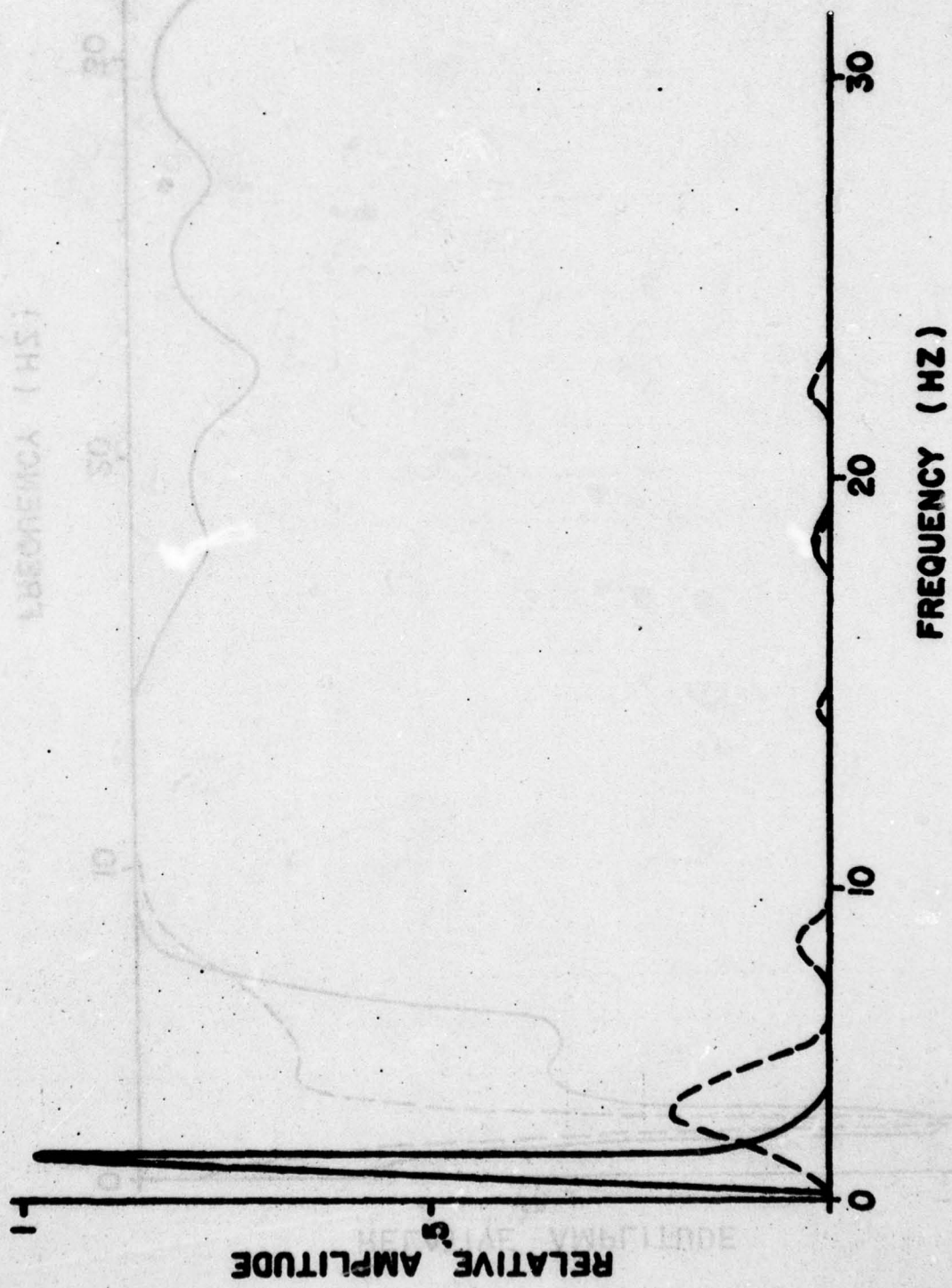


Fig. 5.23



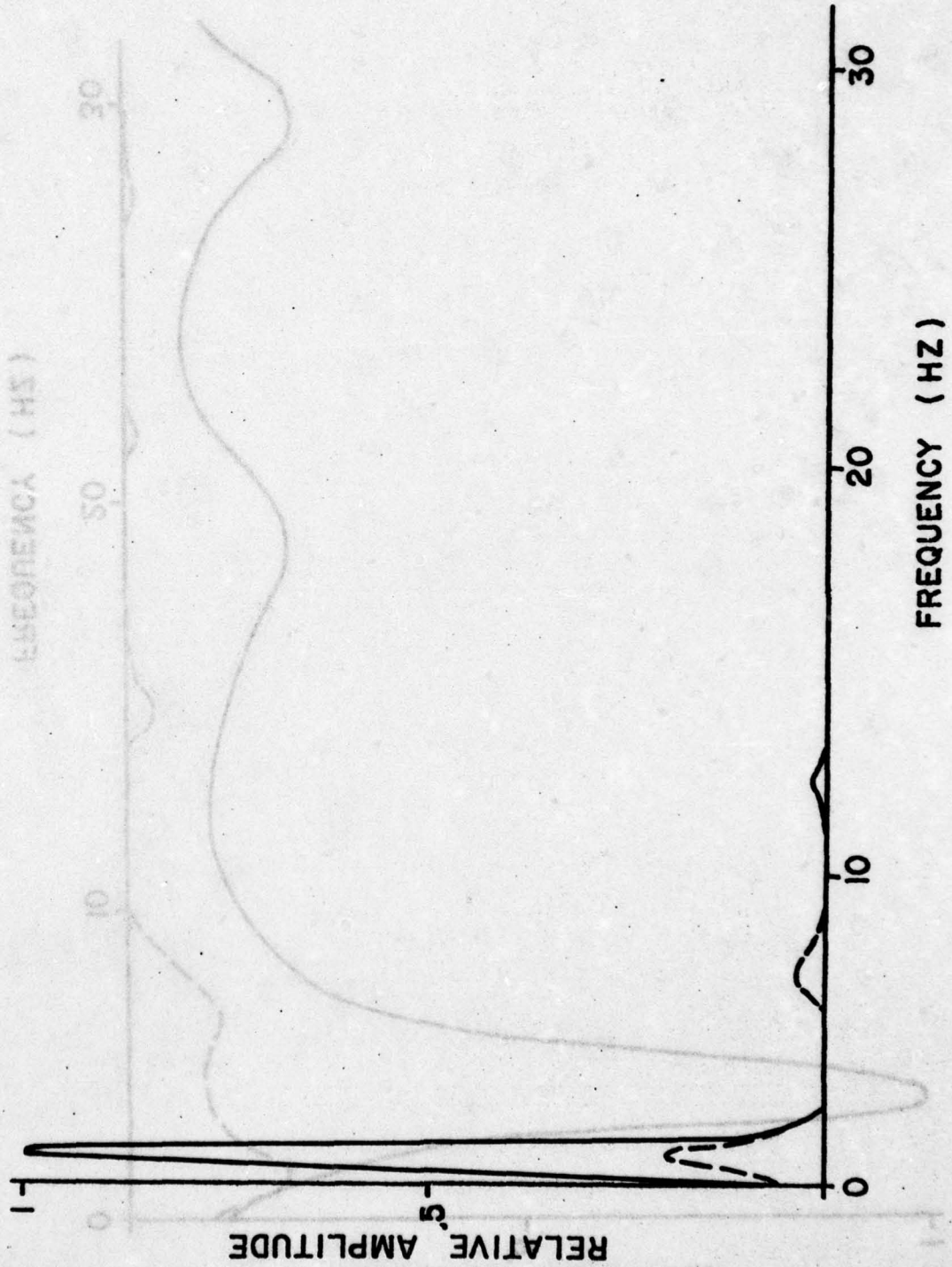


Fig. 5.24

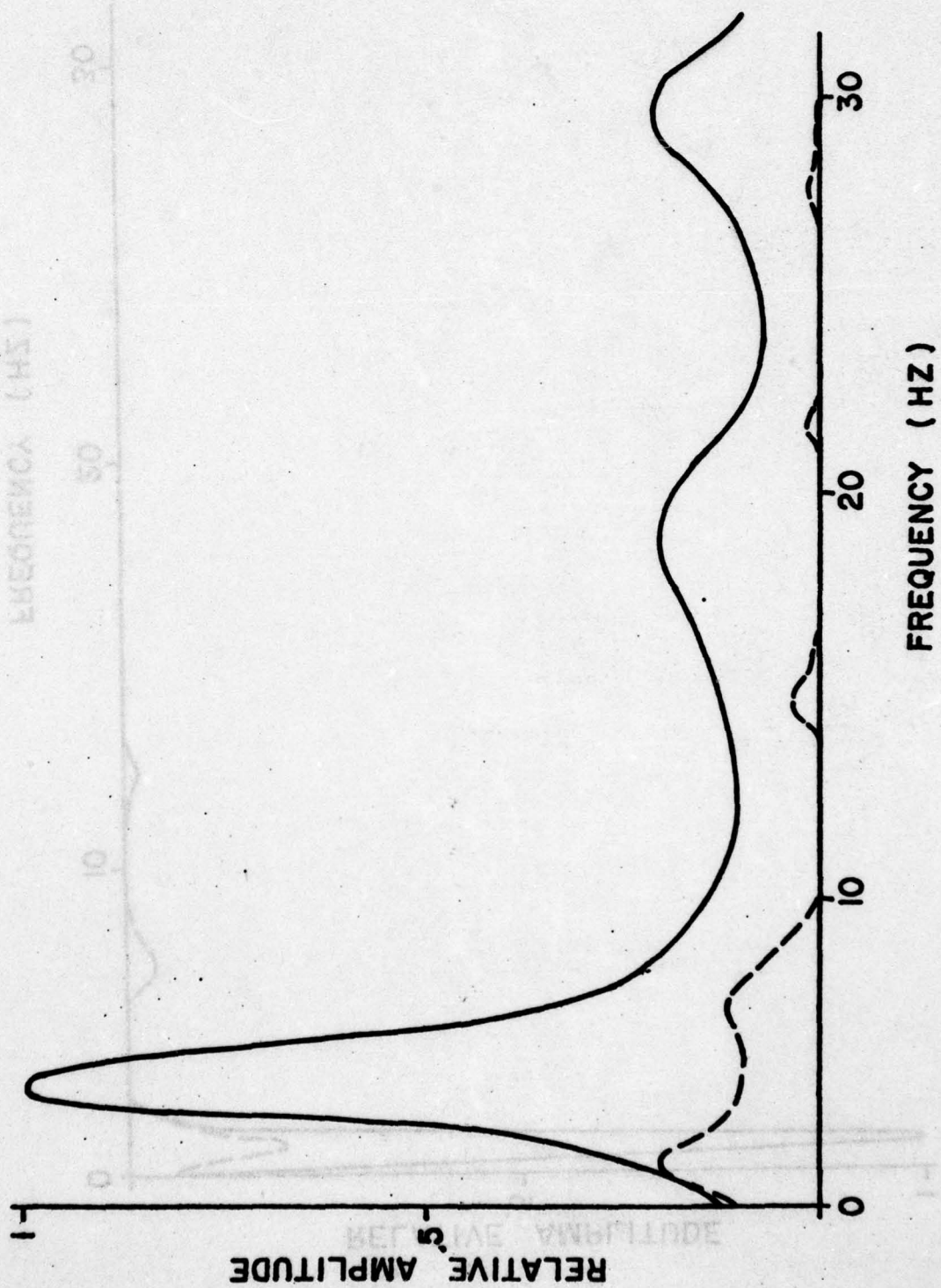


Fig. 5.25

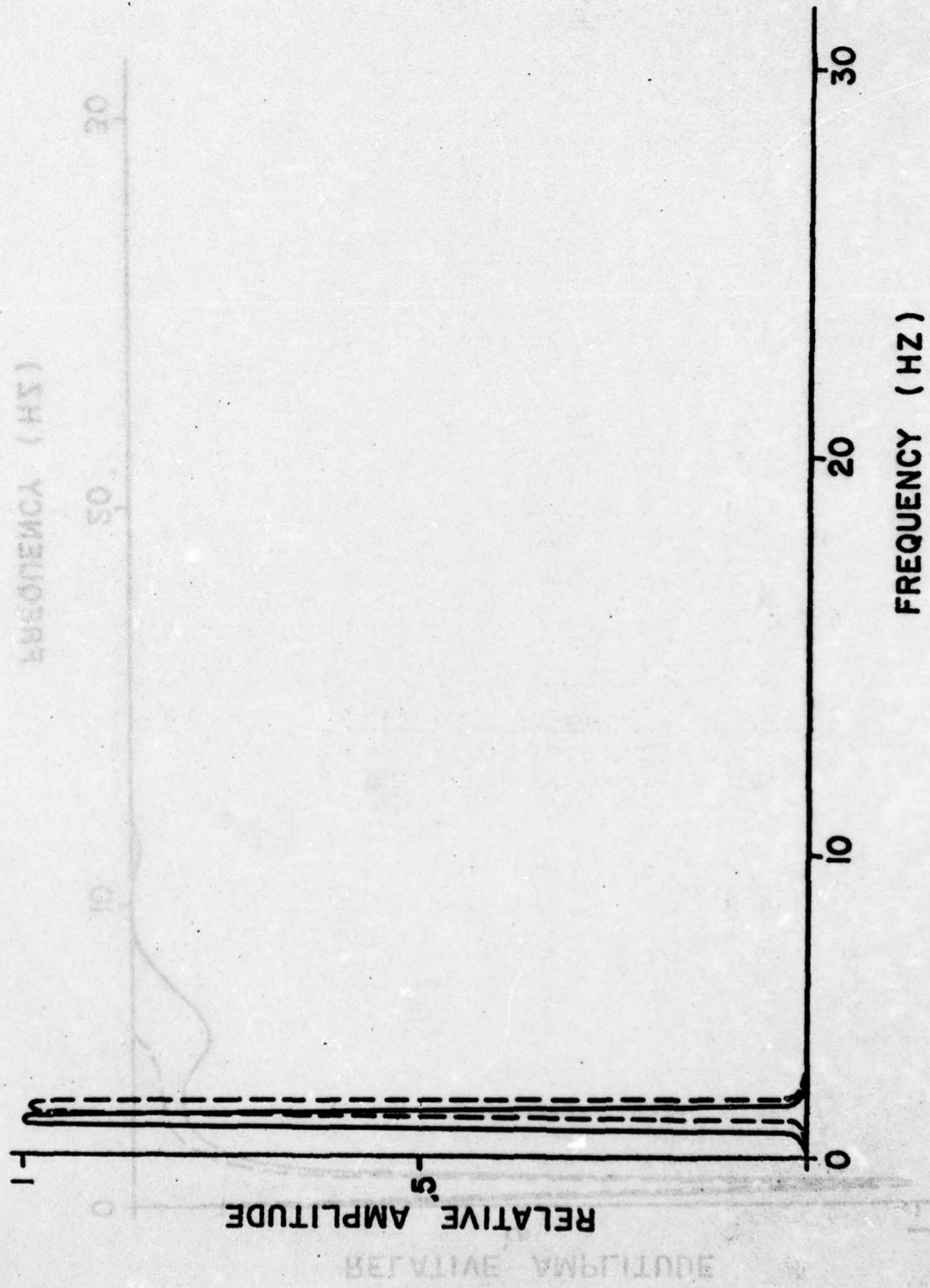


Fig. 5.26



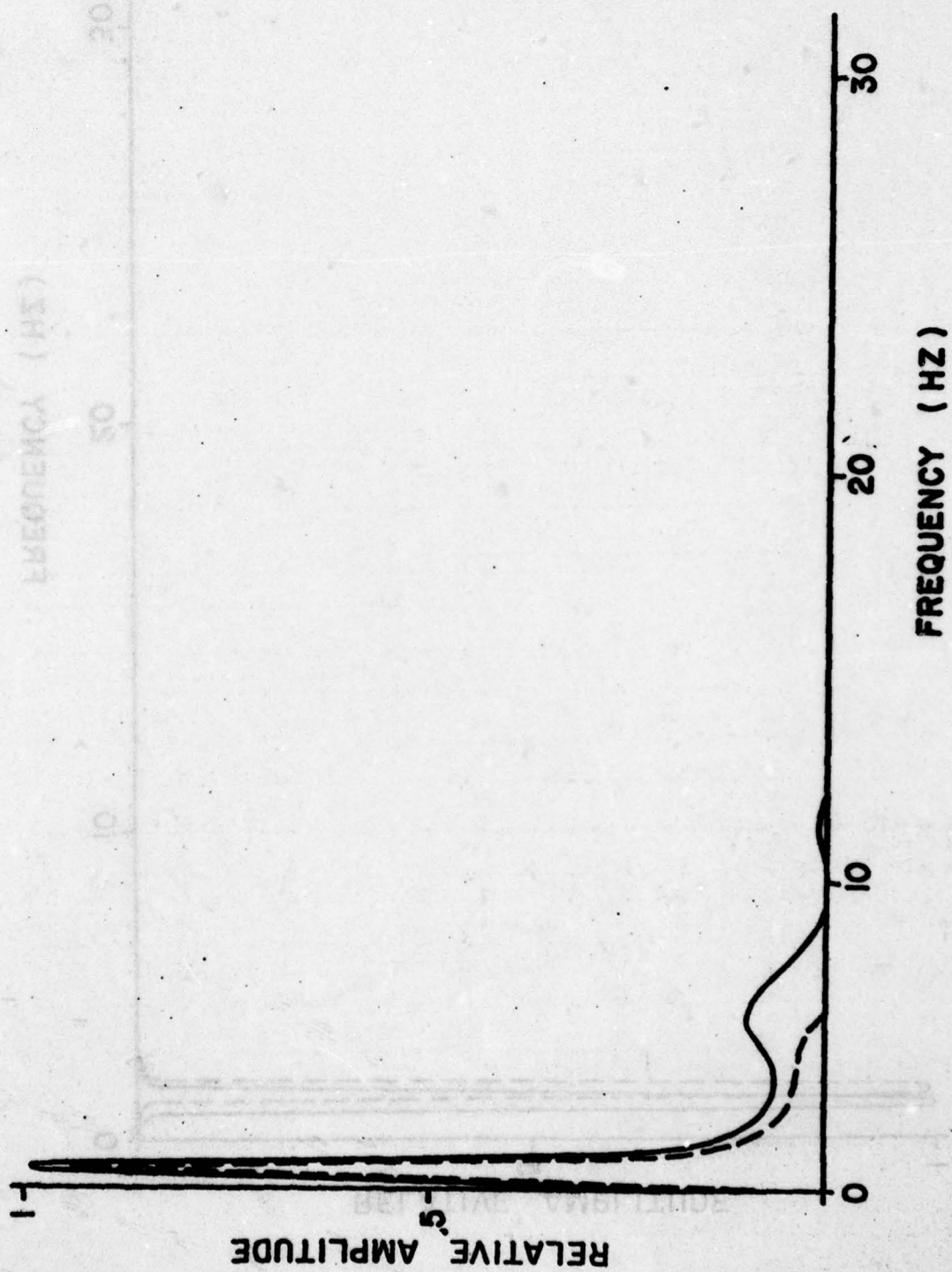


Fig. 5.27

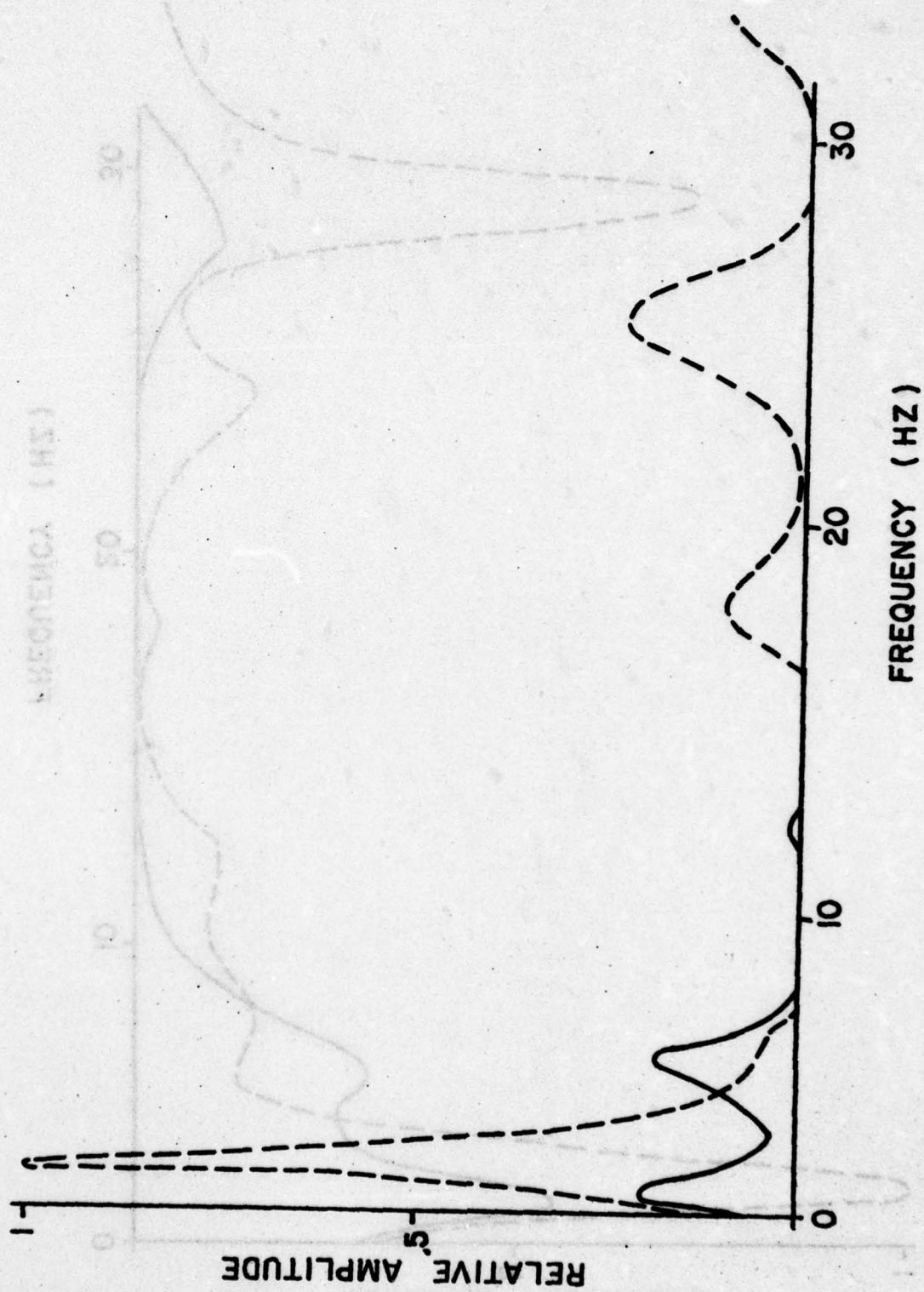


Fig. 5.28

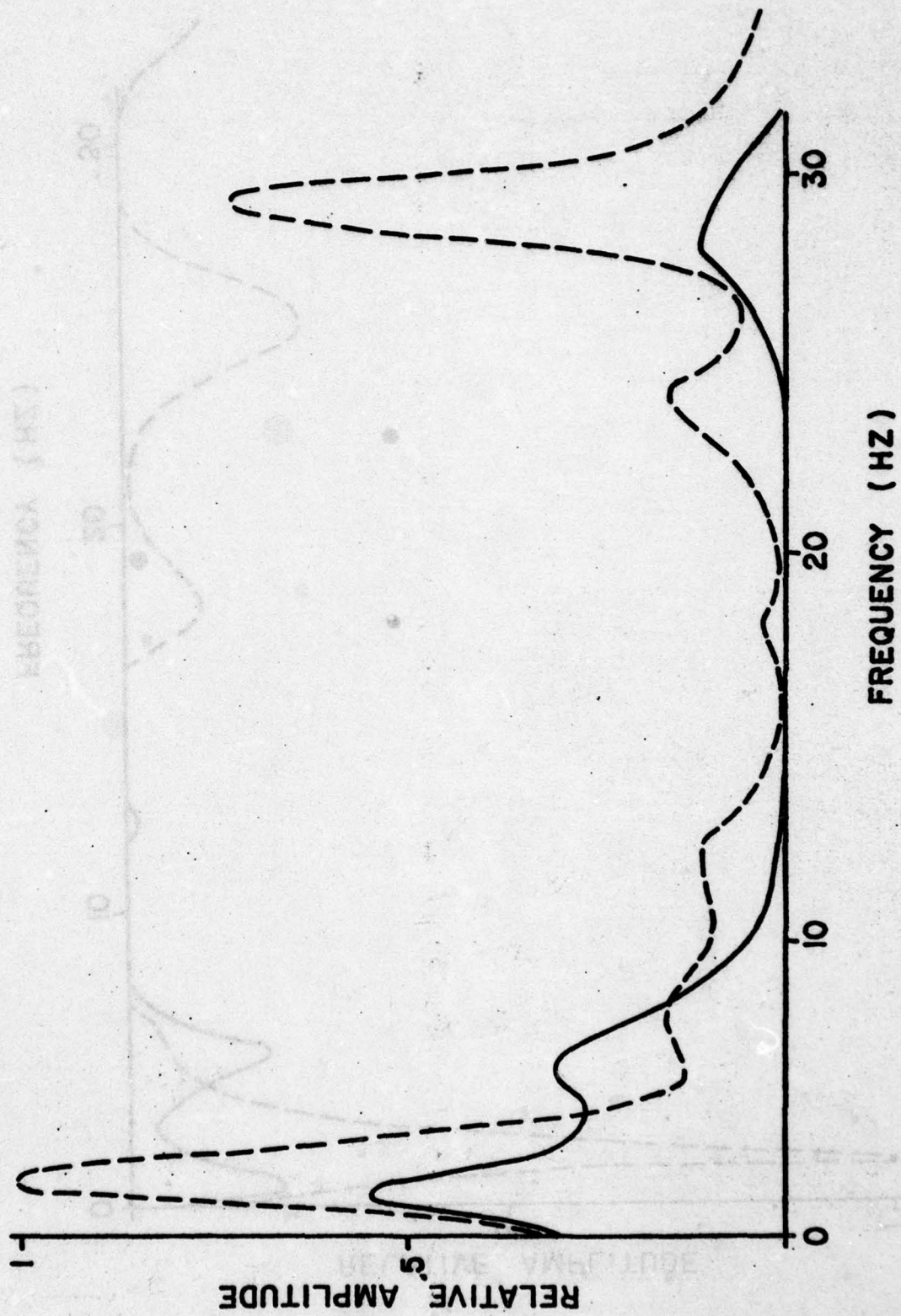


Fig. 5.29



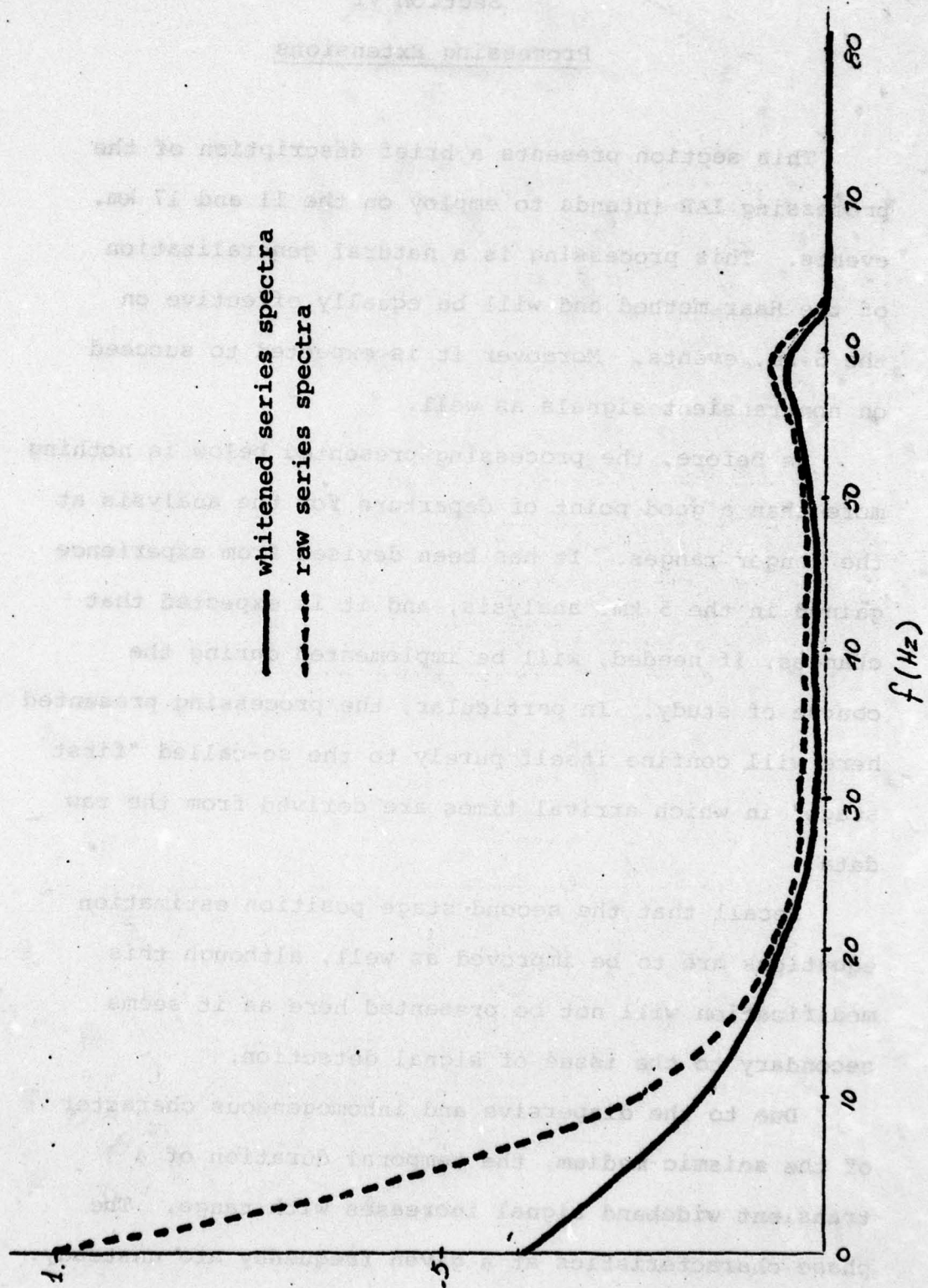


Fig. 5.30 A,B

## Section VI

### Processing Extensions

This section presents a brief description of the processing IAR intends to employ on the 11 and 17 km. events. This processing is a natural generalization of the Haar method and will be equally effective on the 5 km. events. Moreover it is expected to succeed on nontransient signals as well.

As before, the processing presented below is nothing more than a good point of departure for the analysis at the longer ranges. It has been devised from experience gained in the 5 km. analysis, and it is expected that changes, if needed, will be implemented during the course of study. In particular, the processing presented here will confine itself purely to the so-called "first stage" in which arrival times are derived from the raw data.

Recall that the second stage position estimation equations are to be improved as well, although this modification will not be presented here as it seems secondary to the issue of signal detection.

Due to the dispersive and inhomogeneous character of the seismic medium, the temporal duration of a transient wideband signal increases with range. The phase characteristics at a given frequency are unsteady.



There is, as well, geometric and absorptive attenuation (of which the later is markedly frequency dependent), and consequently the amplitude decreases with range.

It has been observed in the ERIM data that the local seismic noise characteristics vary significantly from geophone to geophone, and at the same phone there is considerable spectral variation between even the two horizontal channels. This ambient noise is not stationary, not white, and not known a priori. However, a given vertical geological layering will transmit certain frequency bands better than others and the energy both in the ambient and the received signal is concentrated in these bands though with significant fluctuation.

The time domain processing below has the following general structure:

- (1) The noise is independently (on each phone) whitened by an adaptive filter.
- (2) The whitened outputs are linearly combined under the assumption that a plane wave of unsteady frequency, phase, and amplitude is traversing the array.
- (3) The instantaneous line spectrum of the joint signal is examined.
- (4) If the "Q" of the line spectrum exceeds a threshold the local neighborhood is declared to be a "contender segment".



- (5) All joint cross-correlations  $\left(P \frac{(P-1)}{2}\right)$  of them where  $P$  is the # of array phones) are computed.
- (6) These cross correlations are passed to the second stage which combines the  $\frac{P}{2}$  estimates by the Gauss-Markov theorem.

Let  $x_p(n) = x_p(n\Delta t)$  denote the raw data recording on the  $p$ th geophone  $p = 1, \dots, P$  where  $P$  is the # of phones in the array, and let  $y_p(n)$  denote the adaptively whitened series. Then we have

$$y_p(n) = x_p(n) - \sum_{\ell=1}^L a_{p\ell}(n) x_p(n-\ell)$$

and

$$a_{p\ell}(n) = a_{p\ell}(n-1) + \mu x_p(n-\ell) y_p(n)$$

where  $L, \mu$  are chosen to model the seismic noise (confer Appendix G).

Now let

$$Z(n) = \sum_{p=1}^P y_p(n) \cos(k_1 x_p + k_2 y_p)$$

where  $(x_p, y_p)$  are the coordinates of the  $p$ th phone, and

$$k_1 = \frac{2\pi}{\lambda} \cos \theta$$

$$k_2 = \frac{2\pi}{\lambda} \sin \theta$$

where  $\lambda, \theta$  are wavelength and bearing of an (irregular) plane wave. In the data studies, we will fix  $\lambda$  and allow  $\theta$  to vary although, in fact,  $\theta$  is approximately known. The parameter  $\lambda$  can be determined in the second stage, however, this is considered a secondary issue.

We now model the joint series as an autoregressive series: Let  $\hat{z}(n)$  denote the predicted value of  $z(n)$ , then:

$$\hat{z}(n) = \sum_{m=1}^{M} \alpha_m(n) z(n-m)$$

where

$$\alpha_m(n+1) = \alpha_m(n) + \eta z(n-m) [z(n) - \hat{z}(n)]$$

The parameters  $M, \eta$  are chosen to model the signal process.

The instantaneous autoregressive power spectrum at time  $t_n = n\Delta t$  and frequency  $f$  is given by

$$G(f; n) = \frac{2\Delta t \sigma^2}{|H(f; n)|^2}$$

where  $\sigma^2$  is the noise power in the joint output (estimable by recursive average).

$H(f; n)$  denotes the complex function:

$$H(f; n) = 1 - \sum_{m=1}^M \alpha_m(n) \exp[-2\pi i f m \Delta t]$$

(confer appendix G).

Rather than compute the spectrum, it is faster and for our purposes more precise to examine the roots of

$$P(z, n) = 1 - \sum_{m=1}^M \alpha_m(n) z^m$$

The relation between P and H is clearly:

$$H(f; n) = \mathcal{P}(\exp(-2\pi i f \Delta t), n)$$

However, it seems sufficient to define the "Q" (not precisely the Q of RLC circuitry) as follows:

Let  $f_1, f_2$  be chosen such that for all  $f \in [f_1, f_2]$  the condition  $|P(f, n)| < \varepsilon$ . The parameter  $\varepsilon$  is to be chosen according to a statistical criterion described below. And let  $|P(f, n)|$  be minimized (within this interval) at  $f_0$ . Then define

$$Q(f_0, n) = \frac{f_0}{(f_2 - f_1) |P(f_0, n)|^2}$$

(This corresponds to a power weighted Q).

If  $Q(f_0, n) > T$  for a number of time steps  $n\Delta t$  then the temporal region is declared to be a "contender segment". The threshold T is, like  $\varepsilon$ , to be chosen as a result of data studies. The two thresholds together govern the probabilities of detection and false alarm. Their proper choice is based upon the statistics of Q. If this technique is successful then these statistics will be explored and rational choice of  $\varepsilon, T$  will be decided. In an operational environment they will be adaptively selected based on these studies.

The remaining parameters above, namely,  $\mu, \tau; L, M$  are not critical (cf Appendix G), and are intuitively clear being respectively the adaptation times and filter lengths for the noise and signal processes.



AD-A070 633

INSTITUTE FOR ACOUSTICAL RESEARCH MIAMI FLA  
SEISMIC LOCALIZATION OF HOSTILE ARTILLERY.(U)  
JUL 78 D C FLETCHER, X ZABALGOGEAZCOA

F/G 17/10

UNCLASSIFIED

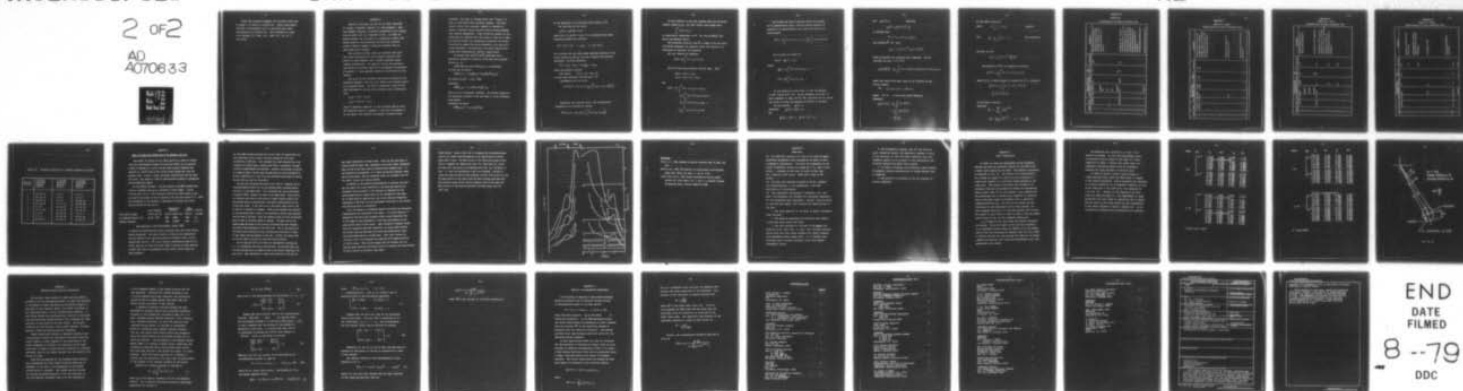
IAR-78002

N00014-77-C-0446

NL

2 of 2

AD  
A070633





MICROCOPY RESOLUTION TEST CHART  
NATIONAL BUREAU OF STANDARDS-1963-A

Given the contender segments the procedure described in steps 5 & 6 above is carried out. These steps depart from the 5 km procedure only in that many more cross correlations are carried out. This procedure is known to be optimal (rf. Hahn, W.R., JASA, Vol. 58, No. 1, July 1975).



## Appendix A

Section 2 discusses the use of the Haar transform to isolate "contender segments" on each geophone. Each such segment contains a transient suspected to be a signal from an event such as a howitzer firing. In order to decide whether the transient is a meaningful signal, the second stage of the processing utilizes the relative arrival times to compute a position estimate with an associated error ellipse.

The relative arrival times are obtained from pairwise cross correlation of the filtered, measured time series at each geophone with a common reference phone (chosen arbitrarily). An equation giving the precision with which the arrival times can be estimated is presented in section 2. This appendix presents a derivation of that formula.

Let  $y_0(t)$  be the filtered time series measured at the reference geophone, and let  $y_1(t)$  denote the filtered series on the second phone. All that is required is the arrival time difference so we can write without loss of generality that:

$$y_0(t) = S(t) + n_0(t)$$

$$y_1(t) = S(t-\tau) + n_1(t)$$

where  $\tau$  (possibly negative) is the relative time by which the received signal at geophone 1 lags that at geophone 0. In the above,  $S(t)$  denotes the unknown filtered signal

waveform. All that is assumed about this "signal" is that it lies within the contender segment. More precisely, within the contender segment is assumed to exist a transient whose filtered forms on each geophone have similar components. (Some dissimilar residue in the signal may be combined with the noise so long as it does not greatly affect our assumptions regarding the noise). Initially we assume the noise processes  $n_0(t)$  and  $n_1(t)$  to be stationary, uncorrelated, zero mean Gaussian processes with variances  $\sigma_{n_0}^2$  and  $\sigma_{n_1}^2$  respectively.

We choose that delay  $\tau$  which maximizes the a-posteriori probability density of  $\tau$  given the measured series  $y_0, y_1$ :

Choose  $\tau$  such that  $p(\tau/y_0, y_1)$  is maximized.

We have the following

$$p(\tau/y_0, y_1) = p(y_1|\tau, y_0) p(y_0, \tau) / p(y_0, y_1)$$

We assume  $p(y_0, \tau) = p(y_0) p(\tau)$

Therefore

$$p(\tau/y_0, y_1) = k_1 p(\tau) p(y_1|\tau, y_0)$$

where  $k_1$  is an irrelevant constant. We further assume we are maximally ignorant of  $\tau$ , and take it to be uniformly distributed.

Therefore we obtain

$$p(\tau/y_0, y_1) = k_2 p(y_1|\tau, y_0)$$



as the quantity to be maximized with respect to  $\tau$ .

We note that we can write

$$y_1(t) = y_0(t-\tau) + n(t)$$

where  $n(t) = n_0(t-\tau) + n_1(t)$  is a stationary zero mean Gaussian process with variance

$$\sigma_n^2 = \sigma_{n_0}^2 + \sigma_{n_1}^2 = 2\sigma_{n_0}^2 \quad (\text{if } \sigma_{n_1}^2 = \sigma_{n_0}^2).$$

Let  $N$  denote the one sided power spectral density of the noise process  $n_0$  and  $n_1$ , and let  $W$  denote the positive bandwidth. We have therefore

$$\sigma_n^2 = 2\sigma_{n_0}^2 = 2NW = 2N\left(\frac{1}{2\Delta t}\right) = N/\Delta t$$

using the Nyquist theorem.

The series  $Z(t) \equiv y_1(t) - y_0(t-\tau)$

is zero mean Gaussian with variance  $\sigma_n^2$ .

Consequently we can write

$$P(y_1|y_0, \tau) = K_3 \exp \left[ -\frac{1}{2N} \int_{\tau_1}^{\tau_2} [y_1(t) - y_0(t-\tau)]^2 dt \right]$$

Expanding the integral above, and accumulating constants of no interest we obtain

$$P(\tau | y_0, y_1) = K_4 \exp \left[ \frac{1}{N} \int_{\tau_1}^{\tau_2} y_1(t) y_0(t-\tau) dt \right]$$



In this formula it has been assumed that the contender segment length  $T_2 - T_1$ , has been chosen long enough that

$$\int_{T_1}^{T_2} \gamma_0^2(t - \tau) dt$$

is essentially independent of  $\tau$ . The IAR procedure computes the exponent above.

The estimated relative time  $\hat{\tau}$  is taken to be the value of  $\tau$  which maximizes the quantity above (for which it is sufficient to maximize the exponent).

Let  $q(\tau)$  denote the exponent

$$q(\tau) = \frac{1}{N} \int_{T_1}^{T_2} \gamma_1(t) \gamma_0(t - \tau) dt$$

Let  $\tau^*$  be the true relative arrival time. Then

$$\gamma_0(t) = S(t) + n_0(t)$$

$$\gamma_1(t) = S(t - \tau^*) + n_1(t)$$

and

$$\begin{aligned} q(\tau) = & \frac{1}{N} \int_{T_1}^{T_2} S(t - \tau^*) S(t - \tau) dt + \\ & + \frac{1}{N} \int_{T_1}^{T_2} S(t - \tau^*) n_0(t - \tau) dt + \\ & + \frac{1}{N} \int_{T_1}^{T_2} S(t - \tau) n_1(t) dt + \\ & + \frac{1}{N} \int_{T_1}^{T_2} n_0(t - \tau) n_1(t) dt \end{aligned}$$

The second and third integrals above are assumed to be approximately equal, and the fourth integral is assumed to be approximately zero since the series are uncorrelated :

$$q(\tau) = \frac{1}{N} \int_{\tau_1}^{\tau_2} s(t-\tau^*) s(t-\tau) dt + \frac{2}{N} \int_{\tau_1}^{\tau_2} s(t-\tau) n(t) dt$$

Let us write the above as:

$$q(\tau) = g(\tau) + h(\tau)$$

where

$$g(\tau) = \frac{1}{N} \int_{\tau_1}^{\tau_2} s(t-\tau^*) s(t-\tau) dt$$

$$h(\tau) = \frac{2}{N} \int_{\tau_1}^{\tau_2} s(t-\tau) n(t) dt$$

In the absence of noise  $h(\tau) = 0$  and the maximum of  $g(\tau)$  occurs at  $\tau = \tau^*$ . We are assuming that  $h(\tau)$  is small compared to  $g(\tau)$  near  $\tau = \tau^*$ , therefore we can assess the extent by which the maximum is shifted as follows:

At the maximum:  $q'(\hat{\tau}) = 0$

Therefore  $g'(\hat{\tau}) + h'(\hat{\tau}) = 0$

But

$$g'(\hat{\tau}) \approx g'(\tau^*) + g''(\tau^*)(\hat{\tau} - \tau^*)$$



and  $g'(\tau^*) = 0$

therefore

$$g'(\hat{\tau}) \approx g''(\tau^*)(\hat{\tau} - \tau^*)$$

It follows that

$$\hat{\tau} - \tau^* \approx -h'(\tau)/g''(\tau^*)$$

Let  $\Delta$  denote  $\hat{\tau} - \tau^*$ , then

$$\sigma_{\Delta}^2 = [g''(\tau^*)]^{-2} E_x[h'(\hat{\tau})^2]$$

where  $E_x$  denotes the expected value operator. We now consider the term  $E_x[h'(\hat{\tau})^2]$ .

$$E_x[h'(\hat{\tau})^2] = \frac{4}{N^2} \iint_{-\infty}^{\infty} s'(u - \hat{\tau}) s'(v - \hat{\tau}) E_x[n(u) n(v)] du dv$$

where the limits have been taken to be infinite by the earlier remark

$$\text{But } E_x[n(u) n(v)] = N \delta(u - v)$$

where  $\delta(u - v)$  is the Dirac delta function.

Therefore

$$\begin{aligned} E_x[h'(\hat{\tau})^2] &= \frac{4}{N} \int_{-\infty}^{\infty} [s'(u - \hat{\tau})]^2 du \\ &= \frac{4}{N} \int_{-\infty}^{\infty} [s'(u)]^2 du \\ &= \frac{4E}{N} \Delta_{\omega}^2 \end{aligned}$$



by the Gabor relations,

where

$$E = \int_{-\infty}^{\infty} c^2(u) du$$

(energy)

and

$$\Delta\omega^2 = \frac{1}{E} \int_{-\infty}^{\infty} c(t) c''(t) dt$$

(rms bandwidth)

We have, so far:

$$C_A^2 = [g''(\tau^*)]^{-2} \frac{4E}{N} \Delta\omega^2$$

The quantity  $g''(\tau^*)$  is computed as follows:

$$g''(\tau^*) = \frac{1}{N} \int_{T_1}^{T_2} s(t-\tau^*) s''(t-\tau^*) dt$$

Again  $T_2 - T_1$  is large enough to include all of  $S$ , therefore

$$g''(\tau^*) = \frac{1}{N} \int_{-\infty}^{\infty} s(t-\tau^*) s''(t-\tau^*) dt$$

$$g''(\tau^*) = \frac{E}{N} \Delta\omega^2$$

by the Gabor relations.

Therefore

$$\sigma_A = \frac{\sqrt{B}}{\Delta\omega} \left[ \frac{2E}{N} \right]^{-1/2}$$

$$\sigma_A = \frac{1}{2.2W} \left[ \frac{2E}{N} \right]^{-1/2} \quad \text{WITH } W \equiv \frac{\Delta\omega}{2\pi}$$

# Appendix B

## Table B-1

Transcription of data recording logs

EVENT	DATE	SITE	①,②,③ SOURCE	④,⑥ GAIN(dB)	⑤ TEMP (°F)	WIND (mph)	COMMENTS
1	12/2/75	5 km	15#TNT	54	-4	0-2	Snow cover at the recording site ranged from 18 inches in hollows to 2 inches on high spots. Shots were made from 10:00 a.m. to 3:30 p.m.
2							
3							
4			Ambient				
5			105				
6			155				
7							
8							Overnight low--12°. All shots made during 3:00 p.m. to 4:30 p.m. Snow depth similar to 5km site. The three channels of the northern most geophone were at 48 dB gain because of wind induced noise at that position (See Figure B-4, Appendix B)
9			109				
10							
11			Ambient		+10		
12	12/3/75	11 km	155	54(48)	+5	2-6	
13							
14							
15							Aircraft overhead during event 20
16							
17							
18							
19							
20							
21							
22			15#TNT				Events 22 and 23 were fired at the



## Appendix B

Table B-1 (cont)

Transcription of data recording logs

EVENT	DATE	SITE	①, ②, ③ SOURCE	④, ⑥ GAIN (dB)	⑤ TEMP (°F)	WIND (mph)	COMMENTS
23	12/3/75	11 km	15/TNT	54(48)	+5	2-6	Back stop--no zero time on record.
24	12/4/75	11 km	105	54(48)	+32	0-2	Overnight low 25°. Temperature inversion. Fog in a.m. Firing done from 11:00 a.m. to 1:30 p.m. See 12/3 comments on gain settings.
25							
26							
27							
28							
29							
30							
31							
32							
33							
34							
35							
36			109				Thirty seconds of ambient noise recorded after event 35.
37							
38							
39							
40							
41							Twenty seconds of ambient recorded after event 41.
42							
43							



## Appendix B

Table B-1 (cont)

Transcription of data recording logs

EVENT	DATE	SITE	①, ②, ③ SOURCE	④, ⑥ GAIN (dB)	⑤ TEMP (°F)	WIND (mph)	COMMENTS
44	12/4/75	11 km	109	54(48)	+32	0-2	Trapper walking from west to center of array during event 45.
45			35#TNT				
46			15#TNT				
47			Ambient				
48			155				
49							
50					+36		See sketch for array configuration.
51	12/5/75	17 km	155	54	+38	0-2	Overnight low--++36°. Heavy fog, clearing by 10:45 a.m. Firing from 11:15 a.m. to 3:30 p.m. Front passed recording site after event 55.
52							Twelve inch snow cover over recording area.
53							
54							
55							
56				48		4-8	
57							
58							
59							
60				42		8-16	
61							
62							
63							
64							
65							

## Appendix B

Table B-1 (cont)

Transcription of data recording logs

EVENT	DATE	SITE	①.②.③ SOURCE	④.⑤ GAIN(dB)	⑤ TEMP(°F)	WIND (mph)	COMMENTS
66	12/5/75	17 km	109	42	+38	8-16	Geophone 4 to 36 dB. Wind from north, 20 mph.  Wind rocking truck, very gusty. Geophone 5 to 36 dB. Estimated 40 mph gusts.  All channels to 36 dB.
67						20	
68							
69						20-40	
70							Forty seconds of ambient at end of event.
71							
72							
73							
74							Forty seconds of ambient at end of event.
75							
76							
77			105	36			
78							Forty seconds of ambient at end of event.
79							
80							
81							
82							Forty seconds of ambient at end of event.
83							
84							
85							
86							Forty seconds of ambient at end of event.
87							
88	12/5/75	17 km	15#TNT	36	+38	20-40	
89							
90			Ambient		+41	20-40	



Table B-2 Recording Channels for Standard Geophone Positions

Standard Position	5 km Site Recording Channel (N, E, V)	11 km Site Recording Channel (N, E, V)	17 km Site Recording Channel (N, E, V)
1	13, 14, 15	1, 2, 3	1, 2, 3
2	16, 17, 18	4, 5, 6	4, 5, 6
3	19, 20, 21	7, 8, 9	19, 20, 21
4	22, 23, 24	10, 11, 12	22, 23, 24
5	7, 8, 9	13, 14, 15	13, 14, 15
6	10, 11, 12	16, 17, 18	16, 17, 18
7	1, 2, 3	19, 20, 21	7, 8, 9
8	4, 5, 6	22, 23, 24	10, 11, 12
9	25, 26, 27	25, 26, 27	25, 26, 27



## Appendix C

### MODEL OF SEISMIC WAVE PROPAGATION AT THE HONEYWELL TEST SITE

From seismic ray theory and wave theory applied to a model of seismic layering at the Honeywell Ordnance Proving Ground (HOPG), we can construct a graph of frequency vs. arrival time and phase velocity (apparent wave velocity) vs. arrival time for the various seismic phases that cross the geophone array: P waves, S waves, Love waves, Rayleigh waves and the sound (air) wave. This graph is a guide to identification of phases on seismograms from the HOPG test program.

We first define the model. The test program at the HOPG included shots fired to a moveable array set up alternately at three ranges: 5.28 km, 11.04 km, and 17.12 km. Short refraction profiles at several points served to establish the nature of shallow layering in the area (see Larson et al., 1976). From information in that document, a representative geologic and seismic velocity section for the area is:

	Layer Thickness	Compressional Velocity	Shear Velocity	Density
Post-glacial outwash	9.144 m (30 ft)	762 m/s (2500 ft/s)	440 m/s	1.9 g/cm <sup>3</sup>
Ice-compacted glacial till	82.296 (270)	1829 (6000)	1056	2.3
Cambrian sandstone		3353 (11000)	1935	2.4

(See discussion in IAR Interim Report, January 1978).

In addition to simplifying the original refraction data, this table involves several assumptions: that shear velocity is related to the compressional velocity observed in the refraction profiles by Poisson's ratio = 0.25 or compressional velocity =  $\sqrt{3}$  x shear velocity; representative densities for similar materials are taken from Clark (1966) in absence of values measured at HOPG; that layers are homogeneous and have plane, parallel upper and lower boundaries.

For this model we have calculated the arrival times for compressional and shear body waves (P and S waves) refracted through the third layer (at 3353 m/s or 1935 m/s). This represents the least time path for P and S waves at all three ranges, assuming that there is no material of higher velocity at depth beneath the sandstone. Actually, the presence of granite at a depth of about 1 km may cause the body waves to arrive substantially earlier, especially at 11 and 17 km, than predicted by the model of shallow layering that was used for calculation.

We also have calculated the group arrival time vs. frequency and the associated phase velocity for Love and Rayleigh waves, assuming shallow layering as in the above table. This calculation was done by the method of Haskell (1953). Results are shown in the figure below. These results are affected very little by the granite or deeper layering because Love and Rayleigh waves are guided waves, with motion confined mainly to the surface wave guide. In the lower part of the figure, group arrival time is shown as a function of frequency. These curves represent the frequency of the wave motion that is seen on the recording at various times measured from the time of the shot. There are separate curves for Love and Rayleigh waves at each of the three ranges of interest. The upper part of the diagram shows the phase or wave velocity associated with each frequency and arrival time represented in the lower part. This is the velocity of individual waves crossing the array as measured by correlation of peaks or wave fronts from one geophone to the next. Finally, the figure shows the arrival time of a direct air wave travelling at 343 m/s.

The air wave and the P and S waves are represented as undispersed, i.e., all frequencies arriving at the same time. On the other hand, the Love and Rayleigh waves are dispersed due to the velocity layering of the wave guide: lower frequencies or longer waves generally arrive earlier



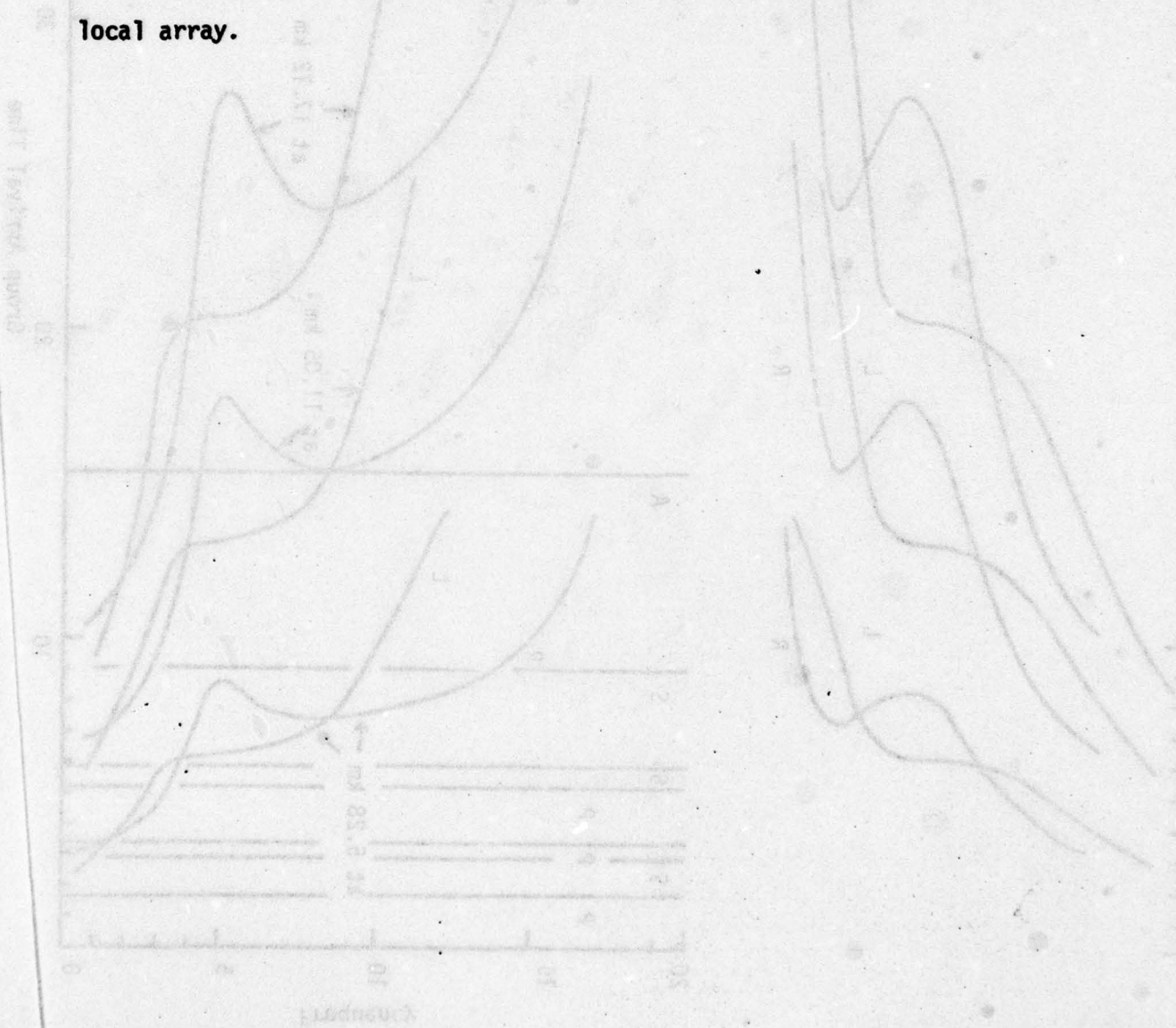
than higher frequencies or shorter waves. There are also some bands of inverse dispersion where lower frequencies arrive after higher frequencies. These are due to the sharp velocity discontinuities between layers. If the boundaries are gradational, or if there are velocity gradients rather than discontinuities, then the dispersion curves are straighter than for this model, and may lack inverse portions.

In addition to the simplified approximations of layering, the model may also depart from actual conditions in the sense that there may be substantial local variations in the thickness of compacted till and unconsolidated glacial outwash which are not represented in the model. Due to these possible complications, the arrival times and frequencies represented in the figure are only approximate indications of the relationships which may exist in seismograms.

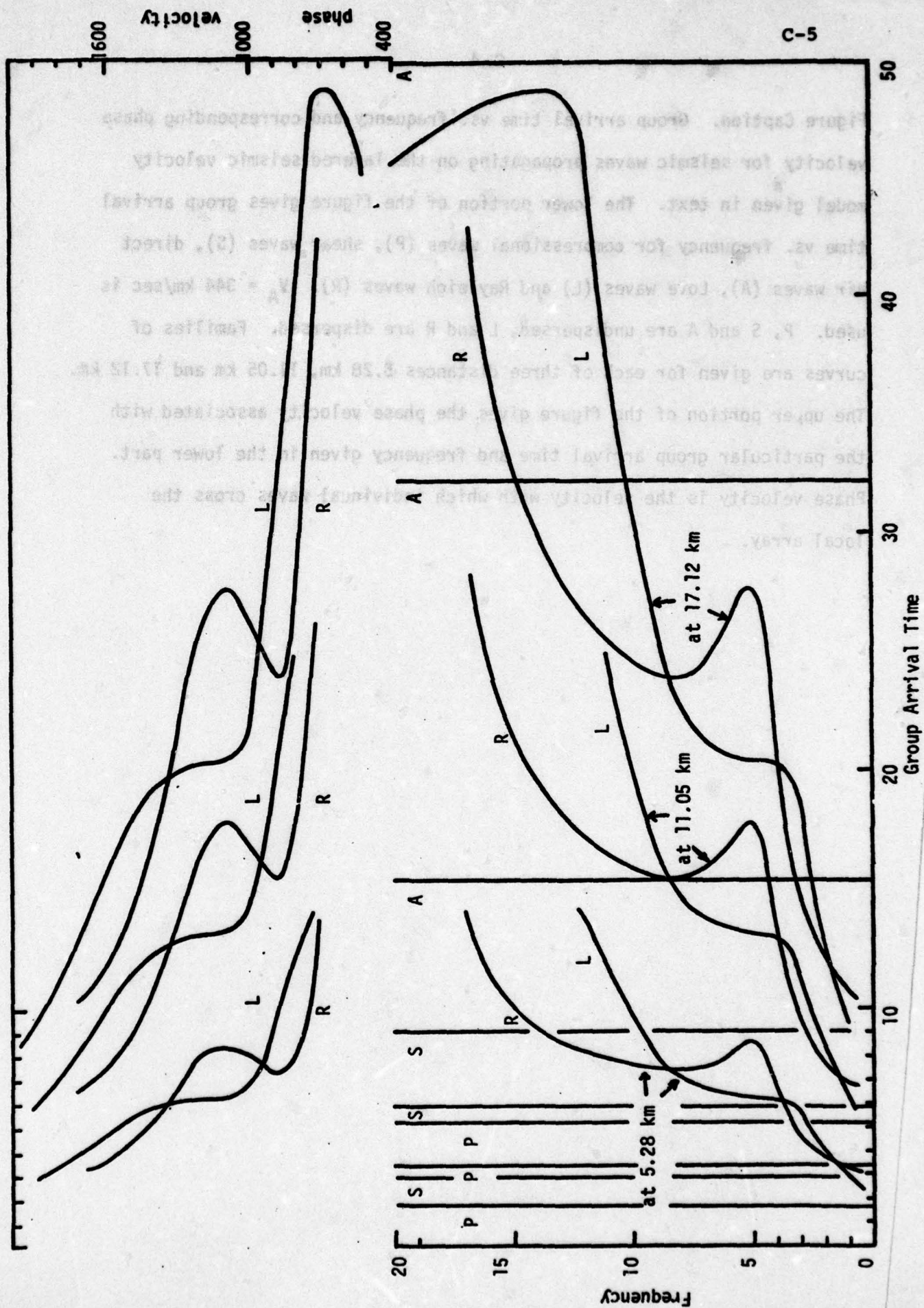
Also, the contents of seismograms depend on excitation and attenuation characteristics not represented in the figure. If a given frequency is generated at the source and propagates without strong attenuation then it will appear on the seismogram at a time shown approximately by the group arrival curves of the figures. Lower frequencies propagate farther with less attenuation than high frequencies in a given seismic medium; and surface (Love and Rayleigh) waves spread two-dimensionally rather than three-dimensionally as do body waves. Also, recoil sources are relatively rich in low frequencies by comparison with tamped explosions of similar energy. These factors suggest that low frequency Love and Rayleigh waves should be particularly useful for detection and identification of recoil sources at relatively large ranges.



**Figure Caption.** Group arrival time vs. frequency and corresponding phase velocity for seismic waves propagating on the layered seismic velocity model given in text. The lower portion of the figure gives group arrival time vs. frequency for compressional waves (P), shear waves (S), direct air waves (A), Love waves (L) and Rayleigh waves (R).  $V_A = 344$  km/sec is used. P, S and A are undispersed; L and R are dispersed. Families of curves are given for each of three distances 5.28 km, 11.05 km and 17.12 km. The upper portion of the figure gives the phase velocity associated with the particular group arrival time and frequency given in the lower part. Phase velocity is the velocity with which individual waves cross the local array.



$$V_a = 343.77 \text{ m/s.}$$





### References

- Clark, S. P., 1966, Handbook of physical constants, Mem. 97, Geol. Soc. Amer.
- Haskell, N.A., 1953, The dispersion of surface waves on multilayered media, Bull. Seism. Soc. Amer., v. 43, pp. 17-34.
- Larson, R.M., et al., 1976, Seismic techniques for hostile weapon location (U), Final Report, vol. 1, part 2. by Honeywell Systems and Research Center, Contract N00014-75-C-0928.



## Appendix D

### ERIM Data

(U) The ERIM data consists of a set of six digital tapes containing seismometer data recorded by an array of nine 3-component seismometers. The array was responding to the recoil of howitzer firings at ranges of 5, 11, and 17 kilometers. A diagram of the array is given in Fig. 3.2 for a typical (5 km) event. There are a total of 88 events.

(U) The data were low-pass filtered at 80 Hz., sampled (non-simultaneously) at 300 samples/sec., and then digitized at 14 bits/sample.

(U) This experiment was planned by Honeywell, Inc. and ERIM, and presumably the hardware was configured adequately for the processing they envisioned. However, from the point of view IAR must employ, the following are deficiencies in the data:

1. The array aperture is too small to obtain acceptable range accuracy.

2. The sampling technique was deficient with respect to rms time error across the array.

3. The gain settings at 5 km were 18 dB higher than those at 11 km. and 17 km. In fact, the 5 km gain settings are so high that they induce frequent non linear clipping with consequent power supply drain. It is thought that this must lead to severe transient cross talk between seismometer traces.

4. The seismometer channels (NS, EW, and vertical axes) themselves exhibit low separation (perhaps a result of the mounting) so that the large transverse Love wave component appears as an artefact in the longitudinal and vertical channels and masks those signals.

5. In order to evaluate our processing, some estimate of geophone location uncertainties is needed whereas none is supplied.

6. The polarity is reversed on the E-W channels of certain geophones.



## Appendix E

### Error Propagation

In order to study how measurement errors propagate through the position estimator system for the ERIM array a Monte Carlo simulation was made. The geometry considered is depicted in Fig. E1. The source of the perturbation was located at ranges of 5 and 11 km and a bearing of  $-1$  radian with respect to a cartesian system defined by the array axis. The seismic wave paths were assumed to be straight lines and the propagation medium was homogeneous. Exact travel times  $T_i^e$  to each sensor  $i$  were computed and were perturbed with a random noise component  $T_i$  obtained from a zero mean normal distribution with a specified standard deviation  $\sigma_N$ . For each of the ranges two distributions of the measurement errors were studied, one with standard deviation of 1 msec and another with 10 msec. The result of this study is given in Table 1 and the reader should refer to Fig. E1 for parameter definition.

It is observed that both range and bearing estimates are biased. Since the output of the position estimator is an unbiased estimate there are doubts as to the randomness of the time perturbation sequence used for this study. It must be pointed out that exactly the same set of random numbers was used for each range and measurement error case presented in the Tables.



The ERIM data was collected at a rate of 300 samples per second. In this case measurement errors are expected to be at least of the order of 3 msec. Inspection of Table I reveals that under these circumstances the bearing error might be acceptable although the range estimate is certainly poor.

In order to obtain a better range estimate a larger aperture array (than the ERIM array) is needed at the ranges considered. Signal reception was simulated to an array consisting of 18 geophones formed by two sub-arrays identical to the ERIM array, but separated by 1 km (Fig. E2). Results of the simulation for this array are given by Table II. The improvement in range estimation with this array is significant and to deploy such an array in the field should not add considerably to the labor involved in laying a smaller one. An investigation on optimal array configuration is planned.

RANGE	$\sigma_N$	$R_E$	$\Delta R$	$\theta_E$	$\Delta \theta$
5 Km	10 <sup>-2</sup>	-4.438	0.233	-6.066	1.176
		-4.075	0.840	-0.479	1.462
		*****NO CONVERGENCE*****			
		-4.635	0.267	-0.030	1.330
		-4.544	0.148	4.461	0.273
		-4.028	0.699	1.773	1.098
		-4.563	0.216	3.950	0.535
		-3.376	1.091	4.603	1.080
		-3.822	0.985	5.192	1.721
		-4.371	0.512	3.528	0.866
	10 <sup>-3</sup>	-2.291	0.155	-0.577	0.110
		-1.633	0.338	-0.063	0.173
		6.435	0.809	0.193	0.115
		-2.421	0.147	-0.099	0.214
		-2.143	0.055	0.402	0.021
		-1.137	0.206	0.150	0.088
		-2.638	0.103	0.397	0.059
		-0.564	0.176	0.473	0.055
		0.061	0.299	0.491	0.125
		-2.159	0.209	0.341	0.125
11 Km	10 <sup>-2</sup>	-10.432	0.268	-6.082	1.176
		-10.003	0.923	-0.512	1.474
		*****NO CONVERGENCE*****			
		-10.619	0.283	-0.085	1.377
		-10.519	0.157	4.409	0.276
		-9.869	0.812	1.737	1.098
		-10.545	0.224	3.949	0.547
		-8.737	1.502	4.593	1.057
		-9.576	1.192	5.115	1.705
		-10.330	0.543	3.528	0.873
	10 <sup>-3</sup>	-7.188	0.216	-0.578	0.110
		-5.745	0.528	-0.066	0.174
		*****NO CONVERGENCE*****			
		-7.376	0.204	-0.103	0.216
		-6.835	0.082	0.395	0.022
		-4.242	0.360	0.148	0.088
		-7.814	0.136	0.393	0.058
		-2.193	0.349	0.473	0.054
		0.424	0.681	0.487	0.124
		-6.903	0.299	0.338	0.125

9 Phone Array (ERIM)



RANGE	$\sigma_N$	$R_E$	$\Delta R$	$\theta_E$	$\Delta \theta$
5 Km	$10^{-2}$	20.620	0.602	-0.659	0.139
		-0.532	0.107	0.726	0.307
		-0.104	0.158	1.404	0.386
		-0.134	0.149	-1.797	0.393
		-1.478	0.107	-1.359	0.682
		-1.534	0.100	2.299	0.239
		-1.955	0.117	0.797	0.451
		-0.345	0.133	0.625	0.337
		-1.170	0.144	1.134	0.889
		-0.525	0.159	1.439	0.380
	$10^{-3}$	0.426	0.018	-0.027	0.019
		-0.057	0.012	0.107	0.007
		-0.011	0.015	0.180	0.068
		-0.018	0.012	-0.141	0.025
		-0.219	0.016	-0.084	0.075
		-0.190	0.012	0.245	0.017
		-0.300	0.019	0.112	0.043
		-0.044	0.015	0.103	0.020
		-0.155	0.018	0.146	0.084
		-0.058	0.017	0.180	0.014

11 Km	$10^{-2}$	*****NO CONVERGENCE*****			
		-1.581	0.211	0.671	0.298
		0.451	0.375	1.363	0.579
		-1.279	0.294	-1.788	0.391
		-3.590	0.163	-1.350	0.689
		-4.923	0.168	2.207	0.247
		-6.387	0.183	0.768	0.442
		-2.059	0.257	0.643	0.317
		-4.383	0.247	1.133	0.915
		-2.445	0.313	1.392	0.380
	$10^{-3}$	2.336	0.044	-0.023	0.017
		-0.159	0.024	0.102	0.006
		0.049	0.034	0.176	0.069
		-0.157	0.026	-0.140	0.023
		-1.174	0.033	-0.084	0.072
		-0.731	0.026	0.233	0.020
		-1.322	0.041	0.108	0.041
		-0.273	0.033	0.104	0.017
		-0.689	0.037	0.145	0.085
		-0.293	0.038	0.175	0.015

18 Phone ARRAY



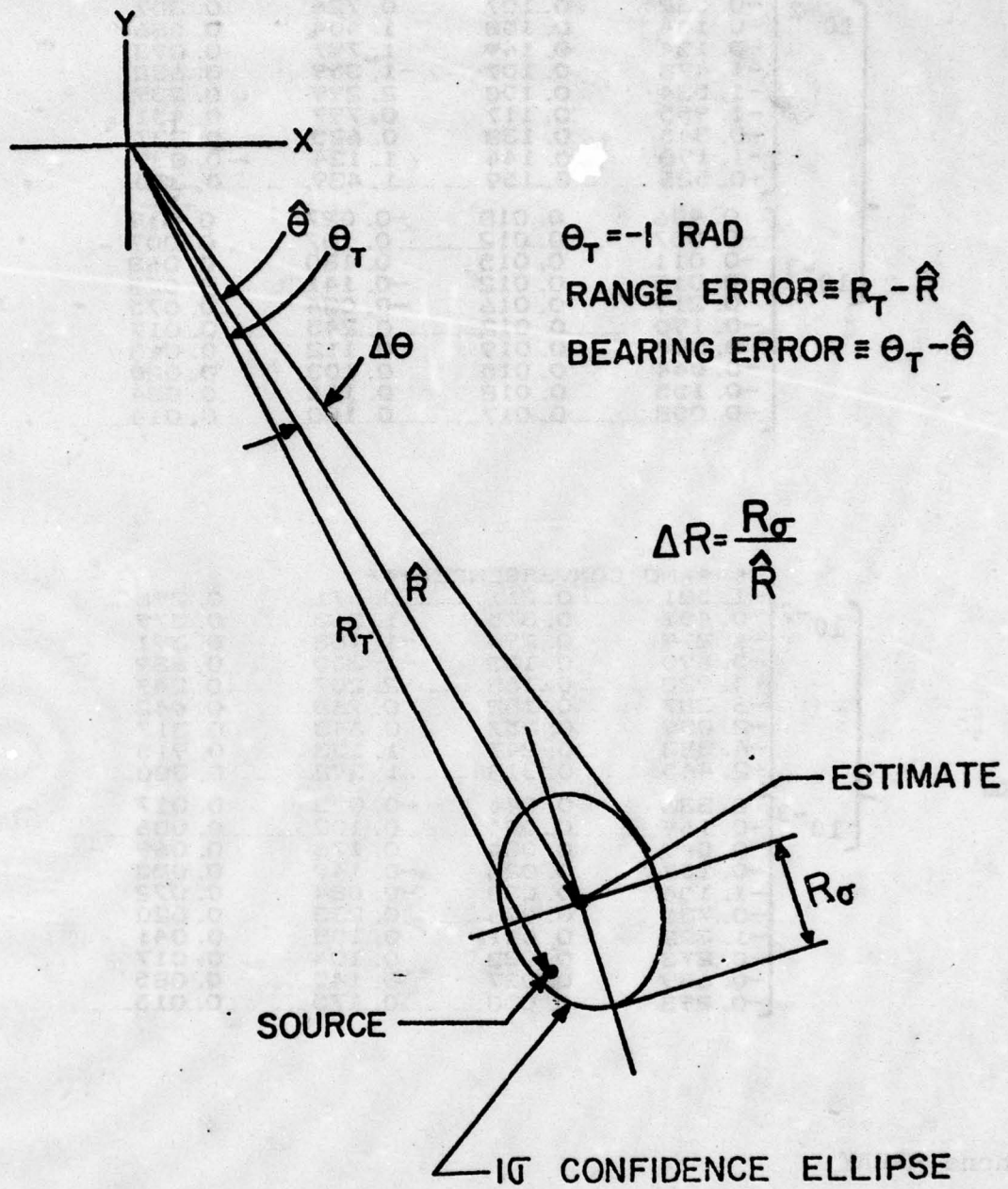


FIG. No. E1

## Appendix F

### Maximum Entropy Spectral Estimation

The two most common methods of power spectral density estimation are the periodogram method, in which the spectrum is estimated by either averaging over different samples or smoothing in the frequency domain the Fourier transform of the time-series data, and the Blackman-Tukey approach. In this latter method the autocorrelation function is estimated from the data using lagged products with a maximum lag taken typically as one tenth of the data record. The Fourier transform of this function, after proper tapering has been applied, yields the desired spectral estimates.

These conventional methods of spectrum estimation provide excellent results for stationary time series when the record length is large compared to the reciprocal of the lowest frequency of interest, but they have certain drawbacks when it comes to analyzing non stationary or transient phenomena, such as the signal coupled into the ground by the recoil of a gun.

Both the periodogram and the Blackman-Tukey spectrum have associated with them window functions which are independent of the data or the properties of the random process which is analyzed. The window function relates the average estimated spectrum to the true spectrum; in fact the spectral estimates tend to be the convolution



in the frequency domain of the window function and the true spectrum. Selection of a window function is not a trivial problem since good resolution and statistical stability must be traded against each other when the amount of data available is very limited.

A radically different nonlinear method has been developed to estimate spectra with increased resolution. Interest in this method was initiated by Burg (cf. J.P. Burg, "Maximum Entropy Spectral Analysis", Ph.D. dissertation, Stanford University, CA 1975) who used the term "maximum entropy method" to describe an algorithmic method of estimating power spectral density directly from the time series data without making any assumption about the characteristics of the series outside the observation interval. The philosophy of the maximum entropy method (MEM) is to design a unique filter, based upon the information contained within the available data record, such that when applied to the series the output is a white sequence. Since the output spectrum is a constant it follows that the spectrum of the input data is proportional to the inverse of the transfer function of the filter.

Entropy of a gaussian process is defined as

$$H = \frac{1}{4f_N} \int_{-f_N}^{f_N} \log S(f) df \quad (1)$$

where  $f_N$  is the Nyquist frequency and  $S(f)$  the spectral density. For a discrete stationary process an equivalent expression for entropy is

$$H = \frac{1}{2} \log (|C(N)|) \quad (2)$$

where  $C(N)$  is the autocovariance of the process  $X_i, i=1, \dots, N-1$

$$C(N) = \begin{pmatrix} \rho(0) & \rho(1) & \dots & \rho(N) \\ \rho(1) & \rho(0) & \dots & \rho(N-1) \\ \vdots & \vdots & \ddots & \vdots \\ \rho(N) & \rho(N-1) & \dots & \rho(0) \end{pmatrix} \quad (3)$$

Assume that the first  $M+1$  lags of the autocovariance function  $\rho(0), \rho(1), \dots, \rho(M)$  are exactly known. The idea behind the MEM is to determine  $\rho(M+1), \rho(M+2), \dots, \rho(N)$  in such a fashion that the entropy of the process is maximized at each step. It follows then that  $\rho(M+1)$  is determined by maximizing  $|C(M+1)|$  with respect to  $\rho(M+1)$  which is equivalent to setting

$$\begin{vmatrix} \rho(1) & \rho(0) & \dots & \rho(M-1) \\ \rho(2) & \rho(1) & & \rho(M-2) \\ \vdots & \vdots & \ddots & \vdots \\ \rho(M+1) & \rho(M) & \dots & \rho(1) \end{vmatrix} = 0 \quad (4)$$

Consider now that the process can be described as an autoregressive process of order  $M$ ;

$$X_n = \alpha_1 X_{n-1} + \alpha_2 X_{n-2} + \dots + \alpha_M X_{n-M} + e_n \quad (5)$$

where  $e_n$  is a white noise series. Multiplying by  $X_{n-k}$  and taking expected values:

$$\rho(k) = \alpha_1 \rho(k-1) + \alpha_2 \rho(k-2) + \dots + \alpha_M \rho(k-M) \quad (6)$$



since  $E(x_{n-k} e_n) = 0$  for  $k > 0$

Substituting  $k=1, \dots, M+1$  in (6) yields a set of equations known as the Yule-Walker equations

$$\begin{cases} \rho(1) - \alpha_1 \rho(0) - \dots - \alpha_M \rho(M-1) = 0 \\ \vdots \\ \rho(M+1) - \alpha_1 \rho(M) - \dots - \alpha_M \rho(1) = 0 \end{cases} \quad (7)$$

Suppose that the first  $M+1$  lags of the covariance function are known. From the first  $M$  equations of (7) the coefficients  $\alpha_1, \alpha_2, \dots, \alpha_M$  may be determined and the unknown  $\rho(M+1)$  may be obtained by solving

$$\begin{vmatrix} \rho(1) & \rho(0) & \dots & \rho(M-1) \\ \vdots & \vdots & & \vdots \\ \rho(M-1) & \rho(M) & \dots & \rho(1) \end{vmatrix} = 0 \quad (8)$$

Comparing (4) and (8) it can be seen that MEM spectral analysis is equivalent to fitting an autoregressive model to the process.

The impulse response of the autoregressive filter defined in (5) is

$$h(z) = 1 - \alpha_1 z^{-1} - \alpha_2 z^{-2} - \dots - \alpha_M z^{-M} \quad (9)$$

where  $z$  is the time step variable and the power spectrum of the linear process will then be:

$$S(f) = \frac{\sum \sigma_e^2}{\left| 1 - \sum_{j=1}^M \alpha_j e^{-i2\pi f j} \right|^2}$$

where  $\sigma_e^2$  is the variance of the white sequence  $e_n$ .



Appendix G  
Adaptive Autoregressive Techniques

It was proved in Appendix F that maximum entropy spectral estimation may be obtained through fitting an autoregressive model to the data series;

$$X_n = \alpha_1 X_{n-1} + \alpha_2 X_{n-2} + \dots + \alpha_M X_{n-M} + e_n$$

where the white sequence  $e_n = \{e(n\Delta t)\}$  is termed the innovation. In the MEM developed by Burg the filter coefficients are determined in such a fashion that the variance  $\sigma_e^2$  of the innovation process is minimized over the observation interval. This method provides block type estimates which are valid over the appropriate design segments.

In many applications where not only the existence but the evolution in frequency of signal lines is to be analyzed an adaptive autoregressive filter is in order. A time varying whitening filter may be constructed using a simple algorithm based on the method of steepest descents. The filter coefficients are updated as each data sample is processed in the following fashion

$$\alpha_j(n+1) = \alpha_j(n) + \mu e_n X_{n-j}$$

where

$$e_n = X_n - \sum_{m=1}^M \alpha_m(n) X_{n-m}$$

and  $\mu$  is a parameter which controls the adaptive time constant and other properties of the algorithm. Convergence of the algorithm is assured provided that

$$\mu = \frac{\beta}{M \sigma_x^2}$$

where  $\sigma_x^2$  is the input power level and  $0 < \beta < 2$

In processing the ERIM tapes IAR has found that the algorithm is not too sensitive to variations of  $\beta$  within this range. The adaptation time constant of the algorithm expressed in number of data points is

$$\tau = \frac{-1}{\ln(1 - \beta/M)}$$

Finally, the instantaneous frequency spectrum is given by

$$S(f; n) = \frac{2 \sigma_{en}^2}{\left| 1 - \sum_{m=1}^M \alpha_m(n) e^{-i2\pi f m} \right|}$$



DISTRIBUTION LIST

Copies

Prof. Melvin J. HINICH  
Building 276  
Economics Department  
VPI  
Blacksburg, Va. 24061

1

Prof. M. Ross LEADBETTER  
Dept. of Statistics  
University of North Carolina  
Chapel Hill, North Carolina 27514

1

Commanding General  
U.S. Army Electronics R&D Command  
Att: 1) J. SILVERSTEIN, CSTA Laboratory  
2) J. SCHOENING, CSTA Laboratory  
Fort Monmouth, New Jersey 07703

2

Commander  
Naval Sea Systems Command  
Code 034  
Washington, D.C. 20362

1

Environmental Research Institute of Michigan  
P.O. Box 618  
Att: Dr. Roger TURPENING  
Ann Arbor, Michigan

1

Dr. Forrest DOWLING  
RR-3 Box 123  
Westby, Wisconsin 54667

1

Office of Naval Research  
Att: 1) Code 432  
2) Code 100M  
3) Code 463  
800 North Quincy Street  
Arlington, Virginia 22217

3

Director  
USAE WES  
Att: WES-FE  
Box 631  
Vicksburg, Mississippi 39180

1

Institute for Acoustical Research  
615 S.W. 2nd Avenue  
Att: Mr. M. KRONENGOLD  
Miami, Florida 33130

1

DISTRIBUTION LIST (cont)

Director, Lincoln Laboratory 1  
Att: Mr. L. LYNN  
Lexington, Massachusetts 02173

Director 1  
Defense Advanced Research Projects Agency  
Att: Col FEDERHAN (DARPA-TT)  
Arlington, Virginia 22333

Commander 2  
Naval Ocean Systems Center  
Att: Code 8214  
Code 8105  
San Diego, California 92152

Commander 2  
Naval Coastal Systems Laboratory  
Att: Code 510  
Code 790  
Panama City, Florida 32407

Chief of Naval Material 1  
Code 08T2M  
CP #5, Rm 1028  
Washington, D.C. 20360

Commander 3  
Naval Electronics Systems Command  
Att: 1) Elex 5402  
2) Elex 03  
3) Elex 330  
Washington, D.C. 20360

Prof. Norman BLEISTEIN 1  
University of Denver  
Dept. of Mathematics  
Denver, Colorado 80210

Dr. Norbert BOJARSKI 1  
16 Pine Valley Lane  
Newport Beach, California 92660

Prof. Michael ATHANS 1  
Massachusetts Institute of Technology  
Electronic Systems Laboratory  
Cambridge, Massachusetts 02139

Dr. Raman K. MEHRA 1  
Scientific Systems, Inc. (S<sup>2</sup>I)  
1640 Massachusetts Avenue  
Cambridge, Massachusetts 02318



DISTRIBUTION LIST (cont.)

Dr. Robert KAHN  
DARPA  
1400 Wilson Blvd.  
Arlington, Virginia 22209

2

1) Dr. Richard LACOSS  
2) Dr. Thomas LANDERS  
MIT, Lincoln Labs  
Applied Seismology Group  
42 Carlton Street  
Cambridge, Massachusetts 02142

2

1) Dr. Carl ROMNEY  
2) Dr. Ralph ALEWINE  
DARPA  
1400 Wilson Blvd.  
Arlington, Va. 22209

2

Dr. Ker C. THOMSON  
Director, Terrestrial Sciences Div.  
Air Force Geophysics Laboratory  
Hanscom AFB, Ma. 01731

1

Commanding General  
U.S. Army Mobility Equipment R&D Command  
Att: DRDME-XS  
Fort Belvoir, Virginia 22060

1

Commander  
MERADCOM  
Att: Charles B. GREEN  
Sensors & Barriers Div.  
Fort Belvoir, Virginia 22060

1

The University of Texas  
Marine Science Institute  
Geophysics Laboratory  
Galveston, Texas 77550  
Att: Dr. J. Dorman

1

Analytical Services Inc.  
3613 Leesburg Pike  
Att: R.J. SCHNEIDER  
Falls Church, Virginia 22401

1

Commanding Officer  
U.S. Army Field Artillery Command  
Att: T. RICHTER (ATSF-CD-R)  
Ft. Sill, Oklahoma 73503

1

DISTRIBUTION LIST (cont)

U.S. Army Corps of Engineers  
Huntsville Division  
P.O. Box 1600, West Station  
Att: R.J. BRADSHAW, Jr.  
Huntsville, Alabama 35807

Commander  
ARRADCOM  
Att: Mr. Walter J. DZIWAK  
Dover, New Jersey 07801

Capt. Mike SHORE, USAF  
AFTAC/VSC  
312 Montgomery St.  
Alexandria, Va. 22314

- 1) Director
  - 2) Technical Advisor
  - 3) Chief, Intelligence Div.
  - 4) Chief, C<sup>3</sup> Div.
  - 5) Chief, Firepower Div.
- Development Center  
MCDEC  
Quantico, Va. 22134



UNCLASSIFIED

SECURITY CLASSIFICATION OF THIS PAGE (When Data Entered)

REPORT DOCUMENTATION PAGE		READ INSTRUCTIONS BEFORE COMPLETING FORM
1. REPORT NUMBER 78002	2. GOVT ACCESSION NO.	3. RECIPIENT'S CATALOG NUMBER
4. TITLE (and Subtitle) SEISMIC LOCALIZATION OF HOSTILE ARTILLERY		5. TYPE OF REPORT & PERIOD COVERED Final Report
		6. PERFORMING ORG. REPORT NUMBER
7. AUTHOR(s) Dr. D.C. Fletcher Mr. Xavier Zabalgogezcoa Dr. James Dorman		8. CONTRACT OR GRANT NUMBER(s) N00014-77-C-0446
9. PERFORMING ORGANIZATION NAME AND ADDRESS Institute for Acoustical Research 615 S.W. 2nd Avenue Miami, Florida 33130		10. PROGRAM ELEMENT, PROJECT, TASK AREA & WORK UNIT NUMBERS
11. CONTROLLING OFFICE NAME AND ADDRESS Procuring Contracting Officer Office of Naval Research, Dept. of the Navy, Arlington, Va. 22217		12. REPORT DATE July 1978
		13. NUMBER OF PAGES 139
14. MONITORING AGENCY NAME & ADDRESS (if different from Controlling Office) Office of Naval Research Resident Rep. Columbia University Lamont Doherty Geological Observatory Torrey Cliff, Palisades, New York 10913		15. SECURITY CLASS. (of this report) Unclassified
16. DISTRIBUTION STATEMENT (of this Report) Distribution of this Document is unlimited		18a. DECLASSIFICATION/DOWNGRADING SCHEDULE
17. DISTRIBUTION STATEMENT (of the abstract entered in Block 20, if different from Report)		
18. SUPPLEMENTARY NOTES		
19. KEY WORDS (Continue on reverse side if necessary and identify by block number)  Seismic wave Artillery localization Signal processing Simulation		
20. ABSTRACT (Continue on reverse side if necessary and identify by block number)  This report comprises the final statement regarding some initial exploratory research done by the Institute for Acoustical Research (IAR) on the Hostile Artillery Location (HAL) project. The objective of this research was to re-examine experimental data collected by Honeywell, Inc. and the Environmental Research Institute of Michigan (ERIM) during December 1975. The data collected comprised a series of digital tapes recording the		

DD FORM 1 JAN 73 1473

EDITION OF 1 NOV 63 IS OBSOLETE  
5/N 0102-014-6801

UNCLASSIFIED

SECURITY CLASSIFICATION OF THIS PAGE (When Data Entered)

**UNCLASSIFIED**

SECURITY CLASSIFICATION OF THIS PAGE (When Data Entered)

response of a seismometer array to the firing of various howitzers at various ranges.

IAR's analysis of this data, though not considered technically complete, nevertheless is considered very successful at least with respect to bearing estimates at 5 km. The composite IAR estimate on three firings is within a few hundredths degree of true and the standard deviation is  $1\frac{1}{2}$  degrees. Range estimates can be improved with a larger array and a more sophisticated second stage.

**UNCLASSIFIED**

SECURITY CLASSIFICATION OF THIS PAGE (When Data Entered)